이학박사 학위논문

Geology, mineralogy and stable isotope geochemistry of the Erdenetiin Ovoo porphyry Cu-Mo deposit and the Dzuunmod orogenic gold deposits in northern Mongolia: Implications for ore genesis and sources

몽골 북부에 위치한 에르데넷 오보 반암 동-몰리브덴 광상과 준모드 지역 조산형 금 광상의 지질학, 광물학 및 안정동위원소 지구화학 연구

2019년 2월

서울대학교 대학원

지구환경과학부

김 영 민

Ph.D. Thesis

Geology, mineralogy and stable isotope geochemistry of the Erdenetiin Ovoo porphyry Cu-Mo deposit and the Dzuunmod orogenic gold deposits in northern Mongolia: Implications for ore genesis and sources

몽골 북부에 위치한 에르데넷 오보 반암 동–몰리브덴 광상과 준모드 지역 조산형 금 광상의 지질학, 광물학 및 안정동위원소 지구화학 연구

February 2019

School of Earth and Environmental Sciences

Graduate School

Seoul National University

YEONGMIN KIM

Geology, mineralogy and stable isotope geochemistry of the Erdenetiin Ovoo porphyry Cu-Mo deposit and the Dzuunmod orogenic gold deposits in northern Mongolia: Implications for ore genesis and sources

지도 교수 이 인 성

이 논문을 이학박사 학위논문으로 제출함
2018년 12월

서울대학교 대학원
자연과학대학 지구환경과학부
김 영 민

김영민의 이학박사 학위논문을 인준함

2018년 12월

위 원 장 정 해 명 (인)
부위원장 이 인 성 (인)
위 원 허 영 숙 (인)
위 원 박 정 우 (인)
위 원 류 충 식 (인)

Abstract

Geology, mineralogy and stable isotope geochemistry of the Erdenetiin Ovoo porphyry Cu-Mo deposit and the Dzuunmod orogenic gold deposits in northern Mongolia: Implications for ore genesis and sources

YEONGMIN KIM

School of Earth and Environmental Sciences

Graduate School

Seoul National University

This study reports geological, mineralogical and stable isotope geochemical results of porphyry Cu-Mo deposit and orogenic gold deposit in northern Mongolia. The former is the Erdenetiin Ovoo deposit located in Orkhon province and the latter is the Dzuunmod gold area deposit in Selenge province. Both deposits have large tonnage of Cu, Mo and Au, and been mined for a long time. Compared to many geological studies about petrographic and mineralogical characteristic of both deposits, few researches have been conducted for ore genesis and material sources. Based on geological, mineralogical and stable isotope geochemical measurements, therefore, this study focuses on the ore genesis and sources of metal and sulfur, implying for deposit origin and mineral exploration.

The copper ($\delta^{65}Cu$) and sulfur ($\delta^{34}S$) isotope compositions of ore minerals from the Erdenetiin Ovoo porphyry Cu-Mo deposit in northern Mongolia were measured. The $\delta^{65}Cu$ values of Cu (I) sulfide minerals ranged from 0.14 ‰ to 2.69 ‰, suggesting that Cu predominantly originated from magmatic sources, whereas Cu (II) minerals such as chrysocolla, malachite and azurite presented much larger

variations of $\delta^{65}Cu$ values from -1.01 ‰ to 10.0 ‰. The small difference between the primary and secondary Cu sulfide minerals indicates an insignificant influence of Cu isotope fractionation processes during their formation, which may be explained by large mass transport and/or the involvement of biogenic activities. The $\delta^{65}Cu$ values of primary chalcopyrite suggest source heterogeneity and/or the occurrence of isotope fractionation under a high-temperature environment. The positive $\Delta_{Cu\ (II)\ mineral\ -\ Cu\ (I)\ mineral}$ values imply little transport of Cu in the deposit, with a rough mass balance and fast redox reaction.

The $\delta^{34}S$ values of the primary sulfide minerals (pyrite, molybdenite and chalcopyrite) clustered near 0 ‰, indicating that the sulfur is mainly derived from a homogeneous magmatic source. By contrast, the $\delta^{34}S$ values of secondary Cu sulfide minerals ranged from -3.2 ‰ to -0.3 ‰, with an average of -1.6 ‰. The lower $\delta^{34}S$ values are likely influenced by either S isotope fractionation processes or input of sulfur with different S isotope compositions during their formation.

The measured $\delta^{65}Cu$ and $\delta^{34}S$ values of these ore minerals suggest a large mass transportation of Cu to an adjacent location, indicating little possibility of a hidden Cu occurrence in the Erdenetiin Ovoo deposit area.

The Dzuunmod gold area located in the North Khentii Gold belt (NKGB) of Central Northern Mongolia includes lode gold deposits such as Gatsuurt, Boroo, Sujigtei, Ereen and Ulaanbulag with several gold occurrences. These show similar alteration types and ore mineral assemblages, where sericite, siliceous and potassic alteration assemblages are major hydrothermal alteration types. Pyrite and arsenopyrite are main sulfide minerals with minor amount of galena, sphalerite and chalcopyrite. Gold occurs as native form and invisible gold in pyrite and arsenopyrite. The major sulfide minerals are separated into earlier non-auriferous stage and later

auriferous grains containing invisible gold. Native gold postdates the major sulfide mineralization.

Gold and arsenic content of pyrite grains indicates that gold exists mainly as solid solution form (Au^{+1}) in the Gatsuurt and Boroo deposit whereas gold nanoparticle (Au^{0}) is present in the Sujigtei deposit. High Co/Ni and Mo/Ni ratios of pyrite grain suggest a post-sedimentary or hydrothermal origin and the ore-forming fluid was significantly affected by fluid-rock interaction during mineralization processes.

Large variation of $\delta^{34}S$ values of pyrite and arsenopyrite from -2.6 ‰ to 17.2 ‰ indicates that sulfur seems to be mainly derived from a source with heterogeneous sulfur isotope composition, which is the pyrite-bearing sediment mainly produced by the reduction of seawater sulfate. Consistent with geological evidence, relatively positive $\delta^{34}S$ values suggest that sulfidation plays an important role for gold and sulfide precipitation. The calculated $\delta^{18}O$ values of hydrothermal fluid from the measured $\delta^{18}O$ values of quartz samples (from 14.7 ‰ to 17.7 ‰) indicate that a metamorphic derivation of ore-forming fluid.

Based on the observation and analytical results in this study, gold mineralization processes seem to occur several times by multiple input of hydrothermal fluid, fluid-rock interactions and mixing of ore-forming fluids. Therefore, the gold deposits in the Dzuunmod area is considered to be orogenic gold type influenced by fluid-rock interactions in the deposit area.

Keywords: Ore deposits, Geology, Mineralogy, Stable isotope geochemistry, Mongolia

Student Number: 2011-23264

초 록

이 논문은 몽골 북부에 위치한 에르데넷틴 오보 반암 동-몰리브덴 광상과 준 모드 지역 조산형 금 광상의 지질학, 광물학 및 안정동위원소 지구화학 연구이다. 두 광상 모두 많은 구리, 몰리브덴 및 금 매장량을 갖고 있으며, 오랜 기간 동안 개발되어 왔다. 그러나 암석학 및 광물학적 특징을 파악하기 위한 연구에 비해 광상의 성인과 물질들의 기원에 대한 연구는 거의 수행되지 못하였다. 따라서 이번 연구에서는 지질학, 광물학 및 안정동위원소 지구화학 연구결과를 바탕으로 광상의 성인과 금속 및 황의 기원 추적을 통해 광상의 기원과 광물 탐사에 대해 초점을 맞추고자 한다.

몽골 북부의 에르데넷틴 오보 반암 동-몰리브덴 광상에서 산출되는 광석 광물의 구리(δ^{65}Cu) 및 황(δ^{34}S) 동위원소 조성을 측정하였다. 1가 구리(Cu (I))를 함유한 구리 황화물의 δ^{65}Cu 값은 0.14 ~ 2.69‰의 범위를 보이며, 이는 구리가 마그마에서 기원하였음을 지시한다. 반면에 2가 구리(Cu (II))를 함유한 크리소콜라, 공작석 및 남동석과 같은 구리 광물들의 δ^{65}Cu 값은 −1.01 ~ 10.0‰의 더 큰 범위를 보인다. 1차 및 2차 구리 황화물 간의 작은 구리 동위원소 값의 차이는 2차 구리 황화물이 생성되는 동안 구리 동위원소 분별 작용이 크지 않았음을 지시한다. 이러한 작은 분별 작용은 대규모의 구리 이동이 일어났거나 생물학적 활동에 의한 것으로 생각된다. 황동석의 δ^{65}Cu 값은 기원 물질의 비균질한 구리 동위원소 조성 또는 고온에서 일어난 구리 동위원소 분별 작용에 의한 것으로 여겨진다. 또한 양의 $\Delta_{\text{Cu (II) mineral - Cu (I) mineral}}$ 값은 광상에서 구리의 이동이 먼 곳까지 이뤄지지 않아 대략적인 물질 수지와 빠른 산화환원 반응이 일어났음을 지시한다.

1차 황화물(황철석, 황동석 및 휘수연석)의 δ^{34}S 값은 0‰ 근처에 모여 있으며, 이는 황이 균질한 마그마에서 기원하였음을 지시한다. 반면에 2차 황화물들의 δ^{34}S 값은 −3.2 ~ −0.3‰의 범위를 갖으며, −

1.6‰의 평균값을 갖는다. 이러한 더 낮은 황 동위원소 조성은 황 동위원소 분별 작용 또는 다른 황 동위원소 조성을 갖는 황의 유입에 의한 것으로 여겨진다.

광석 광물의 이러한 구리 및 황 동위원소 값은 근처 지역으로 대규모의 구리 물질이 이동하여, 연구 지역에서 다른 숨겨진 광체가 발견될 가능성은 매우 작음을 지시한다.

몽골 중북부의 겐티 금 광화대에 위치한 준모드 지역에는 갓쭈르트(Gatsuurt), 보루(Boroo), 수지테이(Sujigtei), 에린(Ereen) 및 울란불라그(Ulaanbulag)와 같은 금 광상들이 나타난다. 이들은 비슷한 변질 및 광석 광물 조합을 보여주며, 주로 견운모질, 규산질 및 K-장석질의 변질 광물 조합이 금 광화작용과 연관되어 나타난다. 황철석과 황비철석이 주요 광석 광물이며, 적은 양의 방연석, 섬아연석 및 황동석이 함께 산출된다. 금은 자연금과 황화물 내에 포함된 육안으로 관찰되지 않은 금의 형태로 모두 나타난다. 주요 황화물들은 초기의 금을 함유하지 않은 광화 단계와 후기의 금을 함유한 광화 단계로 나뉘며, 자연금은 이후에 형성된 것으로 여겨진다.

황비철석 내의 금과 비소 함량은 금이 갓쭈르트와 보루 광상에서는 고용체 형태의 1가 금으로 존재하는데 반해, 수지테이 광상에서는 나노입자 형태로 존재함을 보여준다. 황철석 내의 높은 Co/Ni과 Mo/Ni 비는 이들이 퇴적작용 이후에 생성되었으며, 광화 유체가 광화 작용 동안에 유체-암석 작용에 많은 영향을 받았음을 지시한다.

황철석과 황비철석의 $\delta^{34}S$ 값은 -2.6 ~ 17.2‰의 넓은 범위를 갖으며, 이는 황이 비균질한 황 동위원소 조성을 갖는 물질에서 기원하였음을 지시한다. 주로 해수 내 황산염의 환원에 의해 생성된 황철석이 포함된 퇴적물이 가장 주요한 황의 기원 물질이라 여겨진다. 지질학적 증거들과 일치하여 상대적으로 양의 값을 보이는 $\delta^{34}S$ 값은 황화작용이 금과 황화물의 침전에 중요한 역할을 하였음을 지시한다. 석영 맥 시료들의 $\delta^{18}O$ 값(14.7 ~ 17.7‰)을 통해 계산된 열수의 $\delta^{18}O$ 값은 광화 유체가 변성 기원을 갖음을 보여준다.

이번 연구를 통해 얻어진 관찰 및 측정 결과들은 금 광화작용이 여러 차례의 열수 유입, 유체-암석 반응과 광화 유체 간의 혼합에 의해 일어났음을 가리킨다. 따라서 연구 지역의 금 광상은 유체-암석 상호 작용에 영향을 받은 조산형 금 광상 유형으로 여겨진다.

주요어 : 광상, 지질학, 광물학, 안정동위원소 지구화학, 몽골

학 번 : 2011-23264

Preface

The vast area of Mongolia lies in the Central Asian Orogenic Belt (CAOB) bounded on the north by the Precambrian Siberian Craton and fringed by the Tarim and Sino-Korean Cratons in the south. It has been considered as a representative example of long-lasting continental growth and formed by multiple collision of intra-oceanic volcanic arcs, accretion and subduction events associated with magmatism on the continental margin. With the complex tectonic evolution, the CAOB hosts important and giant mineral deposits of gold, silver, copper, molybdenum, lead, zinc and nickel from Late Proterozoic to Early Mesozoic age.

The tectonic evolution of Mongolia has also been explained by the growth of the CAOB involving the subduction of small ocean basin, accretion of island arcs and formation of suture zones. These tectonic events were attributed to the closure of the Paleo-Asian Ocean including the Mongol-Okhotsk Ocean, which existed between the Siberian Craton and Sino-Korean Craton from Late Paleozoic to Early Mesozoic. The formation of the Mogol-Okhotsk Ocean and related complexes played an important role on metal endowment as well as the tectonic development of Mongolia even though the exact opening and closing time of the Mongol-Okhotsk Basin is still under debate.

Mongolia is separated into a northern and southern domain by the Main Mongolian Lineament (MML). The former is composed of Precambrian and Early Paleozoic rocks, whereas Middle to Late Paleozoic rocks occur in the latter. These domains are subdivided into forty-four terranes, three basins (Hovsgul basin, Tsagaanolom basin and Khangai-Khentii basin) and two belt (Selenge belt and Middle Gobi belt). Terranes are subdivided into Precambrian craton, high-grade

metamorphic rocks, passive continental margins, island arc, forearc/backarc basin, accretionary complex and ophiolitic types. Vast amount of mineral resources, especially gold, copper and molybdenum, are distributed in these various geological settings of Mongolia.

Copper (Cu) is one of base metals with great economic importance and shows affinity to sulfur as chalcophile element. Both Cu^{+} and Cu^{2+} cations exists and the redox-sensitive characteristics with high mobility in oxidizing condition allows many copper deposits to high grades by supergene enrichment processes. because copper ore deposits can be formed in all major systems such as magmatic, hydrothermal, diagenetic and metamorphic processes, primary copper deposit types include porphyry Cu (-Mo-Au), magmatic Ni-Cu, skarn and replacement Cu, iron-oxide-copper-gold (IOCG), volcanic-hosted massive sulfide (VMS), stratabound sediment-hosted and supergene ore deposits. Among these, porphyry Cu systems supply about 75 % of the world's Cu and half the Mo and most Re.

Gold (Au) shows strong siderophile characteristics and occurs as coarse-grained native gold or invisible form in sulfide grains. Although gold is one of the rarest elements, gold deposits are common owing to the crustal fluid which is able to transport the gold. Therefore, numerous gold deposits are associated with magmatic and metamorphic systems. Major gold deposit types are orogenic gold, porphyry, IOCG, Carlin type, epithermal and placer deposits. Especially, orogenic gold deposits formed by crustal-scale massive fluid flows of aqueous carbonic metamorphic and local magmatic water in orogenic belts are one of primary gold deposits.

Therefore, it is greatly important to identify the geological characteristics and understand the ore genesis for the exploration of deposit because of various deposit

types and geological settings. Based on the geological, mineralogical and petrological observations, stable isotope geochemical studies are able to provide a valuable information on formation and sources of the ore deposit. Not only sulfur and oxygen isotope analysis utilized from several decades ago, but non-conventional isotope analysis for Cu developed since 2000s can elucidate the source of metal itself, sulfur complexing with metals as sulfide minerals and hydrothermal fluid where metals and its complexes are transported. The development of Multi Collector-Induced Coupled Plasma Mass Spectrometer (MC-ICPMS) has enabled the measurement of transition metal isotopes including Cu isotopes with a great precision better than 0.2 ‰. Because Cu is utilized in both biotic and abiotic mechanisms, an exact measurement of Cu isotopes expands the application of Cu isotopes on various research field. The Cu isotope composition of ore deposits particularly provides a direct evidence for metal sources and supergene enrichment process, enabling to understand deposit origin.

In contrast, sulfur and oxygen isotope analysis has been researched for several decades and widely used to trace the sulfur and fluid sources in the porphyry Cu system and orogenic Au deposits. Most major Cu minerals are present as sulfide minerals such as chalcopyrite ($CuFeS_2$), chalcocite (Cu_2S) and covellite (CuS) whereas Cu is transported as a chloride complex (e.g., $CuCl_2$) in hydrothermal fluid. It means that the derivation of sulfur from its sources and the input to precipitation site is necessary to form Cu ore minerals. Because major sulfur sources have distinct range of sulfur isotope composition, the measurement of sulfur isotope composition of Cu ore minerals is helpful to constrain the sulfur sources. The oxygen isotope measurement of quartz veins in orogenic Au deposit can offer an information for the possible sources of hydrothermal fluid associated with ore-forming processes. Based

on the assumption that hydrothermal fluid and precipitated quartz are in equilibrium state, the oxygen isotope composition of ore-forming fluid can be calculated using an isotope fractionation factor between them controlled by temperature. Similar to sulfur sources, major fluid sources (magmatic, metamorphic and meteoric water) shows different range of oxygen isotope composition, indicating that the oxygen isotope measurement of quartz samples is a great pathway to trace the origination of ore-forming fluid in orogenic Au deposit.

In this study for Ph.D. thesis, two different deposits, the Erednetiin-Ovoo and Dzuunmod gold deposit, were chosen because (1) they are representative deposit type for Cu and Au, respectively in Mongolia as well as in the world, (2) there are many interesting geological issues in these deposits such as ore genesis and sources which can provide a valuable information for mineral exploration in the region and (3) they have large tonnage indicating a high potential for Cu and Au resources.

The Erdenetiin-Ovoo deposit is porphyry Cu-Mo type formed in Middle Triassic period, which was the largest porphyry Cu deposit in Mongolia before the discovery of Oyu Tolgoi deposit in southern Mongolia. The deposit was first discovered in 1964 and has been mined since 1978. According to a USGS report, the deposit has 1780 million metric tons of ore at 0.62 wt% Cu and 0.015 wt% Mo, with metal reserves of 11 Mt Cu and 0.162 Mt Mo. The Erdenentiin-Ovoo deposit is classified into giant porphyry Cu deposit containing more than 10 Mt Cu reserves.

Many placer and lode gold deposits are distributed in the Dzuunmod gold area in the North Khentii Gold Belt (NKGB) in central northern Mongolia. Potential gold resources in NKGB have varied depending on the researches from 250 t to more than 600 t. Most lode gold deposits contain Boroo, Gatsuurt, Sujigtei, Ereen, Ulaanbulag, Kharnaga with Biluut and Balj occurrence. These deposits formed from Late Triassic

to Early Jurassic and show similar host rocks (metasedimentary rocks, volcanic rocks and granitoid complex), alteration assemblage (sericitic, potassic, siliceous) and ore mineralogy (pyrite, arsenopyrite and gold), which is corresponding to the geological characteristics of orogenic gold deposit.

In this study for Ph.D. dissertation divided into two parts, I report geological, geochemical and stable isotopic characteristics of these two deposit types, the Erdenetiin-Ovoo porphyry Cu-Mo deposit and orogenic gold deposits distributed in the Dzuunmod gold area. In chapter 1, I report the Cu and S isotope data of major ore minerals in the Erdenetiin Ovoo porphyry Cu-Mo deposit to (1) determine the Cu and sulfur sources from the isotopic characteristics of ore minerals, (2) understand the isotope fractionation processes during the mineralization event, and (3) discuss the implications of Cu isotope data for mineral exploration and the deposit environment in the study area. In chapter 2, the trace element composition of auriferous pyrite and arsenopyrite, sulfur isotope composition of sulfide minerals are discussed with mineralogical and petrological characteristics of ore and gangue minerals by field-, macro- and micro-scale observation results, to (1) identify the geological and (stable isotope) geochemical features of the deposit, (2) constrain the fluid and metal sources related to the gold mineralization, and (3) understand the ore-forming processes in the Dzuunmod area.

Contents

List of Figure

List of Table

*Chapter 1. Cu and S isotopic signatures of the Erdenetiin Ovoo porphyry Cu-Mo deposit, northern Mongolia: Implications for their origin and mineral exploration

* Parts of this chapter has been published in *Ore Geology Reviews* as a research article by Yeongmin Kim, Insung Lee, Sodnom Oyungerel, Luvsanchultem Jargal and Tserenjav Tsedenbal.

Abstract

The copper ($\delta^{65}Cu$) and sulfur ($\delta^{34}S$) isotope compositions of ore minerals from the Erdenetiin Ovoo porphyry Cu-Mo deposit in northern Mongolia were measured. The $\delta^{65}Cu$ values of Cu (I) sulfide minerals ranged from 0.14 ‰ to 2.69 ‰, suggesting that Cu predominantly originated from magmatic sources, whereas Cu (II) minerals such as chrysocolla, malachite and azurite presented much larger variations of $\delta^{65}Cu$ values from -1.01 ‰ to 10.0 ‰. The small difference between the primary and secondary Cu sulfide minerals indicates an insignificant influence of Cu isotope fractionation processes during their formation, which may be explained by large mass transport and/or the involvement of biogenic activities. The $\delta^{65}Cu$ values of primary chalcopyrite suggest source heterogeneity and/or the occurrence of isotope fractionation under a high-temperature environment. The positive $\Delta_{Cu\ (II)\ mineral\ -\ Cu\ (I)\ mineral}$ values imply little transport of Cu in the deposit, with a rough mass balance and fast redox reaction.

The $\delta^{34}S$ values of the primary sulfide minerals (pyrite, molybdenite and chalcopyrite) clustered near 0 ‰, indicating that the sulfur is mainly derived from a homogeneous magmatic source. By contrast, the $\delta^{34}S$ values of secondary Cu sulfide minerals ranged from -3.2 ‰ to -0.3 ‰, with an average of -1.6 ‰. The lower $\delta^{34}S$ values are likely influenced by either S isotope fractionation processes or input of sulfur with different S isotope compositions during their formation.

The measured $\delta^{65}Cu$ and $\delta^{34}S$ values of these ore minerals suggest a large mass transportation of Cu to an adjacent location, indicating little possibility of a hidden Cu occurrence in the Erdenetiin Ovoo deposit area

Keywords: Erdenetiin Ovoo deposit, Cu isotope, S isotope, Porphyry Cu-Mo deposit, Mongolia

1. Introduction

The transition metal copper (Cu) has two stable isotopes, ^{63}Cu (69.15%) and ^{65}Cu (30.85%) (de Laeter et al., 2003). Cu is widely utilized in both abiotic and biotic mechanisms in natural systems (e.g., Beard et al., 2004; Stürup et al., 2008; Weiss et al., 2008), but early works measuring Cu isotope composition reported a large analytical error of up to 1.5 ‰ by Thermal Ionization Mass Spectrometry (TIMS) due to its high ionization energy (Walker et al., 1958; Shields et al., 1965). This poor analytical precision has restricted the application of Cu isotope analysis in many research fields for several decades. However, improvements in analytical instruments have enabled the measurement of Cu isotopes with greater precision better than 0.2 ‰ by Multi Collector-Induced Coupled Plasma-Mass Spectrometry (MC-ICP-MS) (Maréchal et al., 1999; Zhu et al., 2000).

Because the Cu isotope composition in the ore-forming environment may provide direct evidence of its sources and fluid movement, the Cu isotope ratios ($^{65}Cu/^{63}Cu$) of Cu minerals in various ore deposits have been increasingly studied to understand Cu isotope fractionation processes and determine the origin of Cu as well as ore deposits (Larson et al., 2003; Ehrlich et al., 2004; Graham et al., 2004; Rouxel et al., 2004; Mathur et al., 2005; Markl et al., 2006; Asael et al., 2007; Maher & Larson, 2007; Wall et al., 2007; Mathur et al., 2009; Li et al., 2010; Berkenbosch et al., 2015; Ripley et al., 2015; Duan et al., 2016; Wang et al., 2017; Wu et al., 2017a; Wu et al., 2017b; Luczaj & Huang, 2018). Especially, porphyry Cu systems exhibit a much larger range of $^{65}Cu/^{63}Cu$ ratios than other Cu deposit types, mainly due to the relatively large Cu isotope fractionation during redox reactions in low-temperature environments and therefore provide valuable information on deposit origins and the ore-forming environment (Larson et al., 2003; Graham et al., 2004;

Mathur et al., 2009; Li et al., 2010; Palacios et al., 2011; Wu et al., 2017b).

Differences in Cu isotope composition among Cu ore minerals may be a useful indicator for identifying the type (primary and secondary) of Cu ore minerals (Mathur et al., 2012; Mathur et al., 2013; Duan et al., 2016; Wu et al., 2017b; Mathur et al., 2018). Recently, Mathur et al. (2018) insisted that the classification of chalcocite based on Cu isotope composition could help to improve the mineralization models. Furthermore, several studies have suggested that the Cu isotopic gap between Cu (I) and Cu (II) mineral pairs can be used to evaluate the significance of Cu transport at the deposit scale and, in turn explore unrevealed Cu occurrence (Markl et al., 2006; Asael et al., 2007; Mathur et al., 2009).

The sulfur (S) isotope composition ($^{34}S/^{32}S$) of sulfide minerals in ore deposits has been used to constrain sulfur sources and evaluate the evolution of sulfur species in hydrothermal fluids (Ohmoto, 1972, 1979; Taylor, 1987; Seal et al., 2000; Seal, 2006). The $^{34}S/^{32}S$ ratio of sulfide minerals in porphyry Cu systems usually shows a signature of mantle-derived sulfur sources (e.g., Taylor, 1987; Seal, 2006; Wilson et al., 2007 and references therein), whereas the increase in oxidized sulfur species in the hydrothermal fluid lowers the $^{34}S/^{32}S$ ratio due to isotope fractionation between the oxidized and reduced species (Rye, 1993; Seal et al., 2000; Rye, 2005; Seal, 2006). For example, Khashgerel et al. (2006) suggested that the low $^{34}S/^{32}S$ ratio of sulfide minerals in the Oyu Tolgoi porphyry Cu systems is attributable to the oxidizing condition of the hydrothermal fluid.

The Erdenetiin Ovoo deposit, one of the largest porphyry Cu-Mo deposits in Mongolia, is located in northern Mongolia near the city of Erdenet in the central part of Orkhon Province and 384 km northwest of Ulaanbaatar. The deposit was first discovered in 1964 and started to be mined in 1978 (Gerel et al., 2005; Gerel &

Munkhtsengel, 2005). According to a United States Geological Survey (USGS) report, the Erdenetiin Ovoo deposit has 1780 million metric tons (Mt) of ore at 0.62 wt % Cu and 0.015 wt % Mo, with metal reserves of 11 Mt Cu and 0.162 Mt Mo (Singer et al., 2008). Based on the suggested classification of Cu deposits by Yakubchuk et al. (2012), the Erdenetiin Ovoo deposit is defined as a giant Cu deposit containing more than 10 Mt Cu.

Due to its large deposit size and tonnage and economical importance to Mongolian industry, many studies of its geological characteristics, geochemical features, ore-forming processes and formation age have been conducted since the discovery and exploitation of the deposit (Khasin et al., 1977; Koval et al., 1982; Gavrilova et al., 1984, 1990; Sotnikov et al., 1995; Dejidmaa & Naito, 1998; Gerel, 1998; Watanabe & Stein, 2000; Gerel et al., 2005; Gerel & Munkhtsengel, 2005; Berzina & Sotnikov, 2007; Kavalieris et al., 2017). Several radiogenic isotopic analyses were also conducted to identify the age of magmatic intrusion and mineralization of the deposit (Sotnikov et al., 1995; Berzina et al., 1999; Watanabe & Stein, 2000; Kavalieris et al., 2017), but few stable isotopic studies of ore minerals, which can provide direct evidence of metal sources and formation processes as well as the potential presence of hidden Cu occurrences, have been performed.

In this study, we report the Cu and S isotope data of ore minerals in the Erdenetiin Ovoo porphyry Cu-Mo deposit to (1) determine the Cu and sulfur sources from the isotopic characteristics of ore minerals, (2) understand the isotope fractionation processes during the mineralization event, and (3) discuss the implications of Cu isotope data for mineral exploration and the deposit environment in the study area.

2. Geological setting

2.1 Regional Geology

The Late Permian to Early Triassic Orkhon-Selenge trough included in the Mongolian subprovince, one of seven Cu belts in Central Asia, is part of the active margin of the Siberian craton (Yakubchuk et al., 2012). It is located between the Siberian craton, where Late Paleozoic to Mesozoic subduction-related volcanism was recorded (Watanabe & Stein, 2000; Yakubchuk et al., 2012), and the central Mongolian blocks consisting of three massifs with different Precambrian rocks (Fig. 1.1). The single large Amurian Massif was constructed by the amalgamation of these massifs during the Mesozoic and separation from the Siberian craton by the Mongol-Okhotsk Ocean (Gerel & Munkhtsengel, 2005). During the Late Paleozoic to Mesozoic, the Mongol-Okhotsk Ocean was closed and subducted northward beneath the Siberian craton (Watanabe & Stein, 2000; Gerel & Munkhtsengel, 2005; Windley et al., 2007b). They suggested that this collision and subduction was terminated in the Middle Jurassic within Mongolia and caused uplift of the Khangai-Khentii highlands, including the Orkhon-Selenge trough. The Erdenetiin Ovoo deposit is located 320 km from the subduction zone and occupies the southern boundary of the Khangai-Khentii highlands.

The Orkhon-Selenge trough is filled with Permian to early Mesozoic volcanogenic sedimentary rocks and mid to upper Triassic and Jurassic volcanic rocks as shown in Fig. 1.2. The Permian volcanic rocks, which belong to the Khanui Group, overlie the basement rocks consisting of Neoproterozoic metamorphic rocks, a Paleozoic sedimentary sequence, Devonian granitoids and non-intrusive rocks (Gerel & Munkhtsengel, 2005). The Khanui Group is composed of an upper Permian mafic and intermediate volcanic formation and a lower Permian felsic volcanic

formation overlain by volcaniclastics and mafic volcanics (Fig. 1.2).

The Erdenetiin Ovoo deposit is hosted by a Late Permian Selenge intrusive complex consisting of granite, gabbro and diorite (Gerel, 1998; Watanabe & Stein, 2000; Gerel & Munkhtsengel, 2005; Berzina & Sotnikov, 2007) (Fig. 1.3). Gerel and Munkhtsengel (2005) divided the Selenge intrusive complex into three (early, main and last) phases. The early phase ranges from diorite to monzonite, including gabbrodiorite, diorite, syenodiorite, monzonite and quartz-monzonite. The main phase comprises granitoids such as granosyenite, granodiorite and leucocratic granite, whereas the last phase is dominated by leucogranite and granite. The Selenge complex was subsequently intruded by the Late Permian to Early Triassic Erdenet porphyry complex, which is mainly composed of diorite and granodiorite ranging from gabbrodiorite to granodiorite and granite (Dejidmaa & Naito, 1998; Watanabe & Stein, 2000; Gerel & Munkhtsengel, 2005). Dejidmaa and Naito (1998) divided the Erdenet porphyry complex into three stages: the diorite porphyry complex, granodiorite porphyry complex and granodiorite associated with breccia. Gerel and Munkhtsengel (2005) also reported that the Erdenet porphyry complex associated with mineralization consists of subvolcanic and explosive stocks, including porphyritic quartz-diorite, diorite, quartz-syenite, granodiorite, granite and leucogranite. The syenite porphyry dikes and the porphyries associated with trachyte-trachyandesite-alkaline basalt series intrude the Selenge intrusive and Erdenet porphyry complex (Watanabe & Stein, 2000; Gerel & Munkhtsengel, 2005).

2.2 Deposit Geology

The Erdenetiin Ovoo ore district occurs within a 20–25-km-diameter structure embracing numerous intrusive centers with dykes and altered granodiorite stocks,

and the ore body of the deposit is located in an area of 2 × 1 km (Fig. 1.3). The Cu-Mo mineralization in the Erdenetiin Ovoo ore district is associated with the Erdenet porphyry complex consisting of quartz-diorite, granodiorite porphyry and granite porphyry, and the ore-bearing stockwork intrudes the Selenge intrusive complex, including granodiorite, granite and quartz-syenite (Watanabe & Stein, 2000; Gerel & Munkhtsengel, 2005). The mineralization of the deposit is related to the subvertical and pipe-like late Triassic granodiorite porphyry, where disseminated and vein-controlled mineralization developed (Gerel & Munkhtsengel, 2005). The weak potassic alteration zone with feldspar veins occurs in the host rocks, whereas the subsequent quartz-sericite alteration overprints the vein assemblages and appears to be responsible for the Cu-Mo mineralization (Watanabe & Stein, 2000; Gerel & Munkhtsengel, 2005). The widespread quartz-sericite alteration shows the replacement of feldspar by white mica (Gerel et al., 2005). The major ore minerals are pyrite, molybdenite, chalcopyrite, chalcocite and bornite occurring in veinlets and/or disseminated within the host rocks (Watanabe & Stein, 2000).

Zonation of both the major ore minerals and alteration is well-developed within the deposit (Gerel et al., 2005; Gerel & Munkhtsengel, 2005). Pyrite occurs mainly on the periphery and high-grade chalcopyrite-chalcocite-bornite ores are present in the core (Gerel & Munkhtsengel, 2005). Sericitic (quartz-sericite), intermediate argillic (chlorite-sericite) and prophylitic (chlorite and epidote-chlorite) alteration zones occur from the core to the periphery in the deposit (Gerel et al., 2005). A 30- to 300-m-thick secondary Cu enrichment blanket of a bornite-chalcocite-covellite assemblage is developed in the supergene zone at the top and overlain by native Cu and Cu oxides such as malachite, azurite and cuprite (Watanabe & Stein, 2000; Gerel & Munkhtsengel, 2005).

The mineralization and alteration stages of the Erdenetiin Ovoo deposit have been investigated by several researchers. Watanabe and Stein (2000) introduced the successive mineralization stages of the deposit from the study of Jargalsaihan (1996) as follows: (1) magnetite, (2) pyrite-quartz, (3) molybdenite-quartz, (4) chalcopyrite-pyrite-quartz, (5) pyrite, (6) pyrrhotite-chalcopyrite ± cubanite, (7) chalcocite-bornite and (8) galena-sphalerite-tennantite. In addition, Gerel and Munkhtsengel (2005) incorporated the paragenetic sequence of ore minerals of the Erdenetiin Ovoo deposit from previous studies (Khasin et al., 1977; Gavrilova et al., 1984, 1990) and described the integrated mineralization stages: (1) quartz-sericite, (2) quartz-chalcopyrite-pyrite, (3) quartz-pyrite-molybdenite-chalcopyrite, (4) quartz-chalcopyrite-tennantite, (5) quartz-pyrite-galena-sphalerite, (6) bornite-chalcocite-covellite, and (7) gypsum-calcite-pyrite. They classified it as the first pre-ore stage, followed by four ore stages, one Cu-enriched secondary stage and the last post-ore stage.

Despite slight differences among these studies, the paragenetic mineral association is usually divided into five mineralization stages as follows: quartz-pyrite, quartz-molybdenite, (quartz)-chalcopyrite, quartz-sphalerite-galena (polymetallic), and bornite-chalcocite-covellite (secondary enrichment zone) (Khasin et al., 1977; Gavrilova et al., 1984; Gerel & Munkhtsengel, 2005). The paragenetic sequences of the major ore and gangue minerals are presented in Fig. 1.4.

2.3 Age of the Deposit

Age dating results of both complexes have been reported in several studies, primarily the study of Sotnikov et al. (1995). The K-Ar age of the Selenge intrusive complex ranges from 290 to 260 Ma, and the biotite from the Erdenet porphyry

complex shows K-Ar age results of approximately 250 Ma and 230 Ma (Sotnikov et al., 1995). They suggested that these results represent the occurrence of two-stage magmatism. The similar age dating results obtained by the Rb-Sr method also indicated two-stage magmatism, with ages of 253 ± 18 Ma, 252 ± 11 Ma and 248 ±17 Ma for the first stage and 229 ± 14 Ma, 223 ±9 Ma and 220 ±7 Ma for the second stage (Sotnikov et al., 1995; Berzina et al., 1999). Gerel and Munkhtsengel (2005) introduced other age dating results for the K-Ar method of the granite from the Erdenet porphyry complex ranging from 245 to 226 Ma and from 226 to 221 Ma. $^{40}Ar/^{39}Ar$ age dating studies were conducted on the plagioclase (225 ± 7 Ma by Berzina et al. (1999)) and on the sericite (207 ± 5 Ma by Lamb and Cox (1998). Watanabe and Stein (2000) reported Re-Os ages of the molybdenite from the Erdenetiin Ovoo deposit of 240.7 ± 0.8 and 240.4 ± 0.8 Ma for the primary mineralization processes. They insisted that these results were significantly older than the $^{40}Ar/^{39}Ar$ ages, which might be attributed to a reset of the $^{40}Ar/^{39}Ar$ ages during hydrothermal events. A recent study by Kavalieris et al. (2017), however, reported new $^{40}Ar/^{39}Ar$ age dating results for muscovite of 239.7 ±1.6 and 240 ± 2.0 Ma, very close to the previous Re-Os ages.

3. Sample descriptions

Representative rock and ore samples were collected from the open pit of the Erdenetiin Ovoo deposit, including various ore minerals within the veinlet or disseminated (Fig. 1.5A). Most of the sampling positions are composed of granodiorite, granodiorite porphyry and silicified diorite porphyry associated with major mineralization processes (Fig. 1.5B). The collected granodiorite porphyry samples are composed of altered granodiorite with quartz veins and ore-bearing

stockwork associated with the Erdenet porphyry complex (Fig. 1.5C). Cu-oxide minerals such as malachite, azurite and chrysocolla are also well-developed (Fig. 1.5D). Feldspar with distinct albite twinning occurs, and quartz shows an isometric and anhedral texture. (Fig. 1.6-A). Due to the secondary alteration, polysynthetic twinning of plagioclase is not clear where intensive alteration to sericite occurs (Fig. 1.6B). Plagioclase with andesine composition is widely tabular and prismatic in shape and changes slightly to sericite (Fig. 1.6C). Chlorite seems to be intensively altered from mafic minerals such as hornblende and biotite (Fig. 1.6C-E). A pervasive quartz-sericite alteration composed of quartz, sericite and pyrite is well-developed (Fig. 1.6F) and overprints the previous potassium alteration.

The oxidized leach cap zone has already been eroded, and mining processes are in progress at the secondary sulfide enrichment zone in most areas of the deposit. This zone develops from 1325 m to 1310 m and from 1250 m to 1235 m where the rocks samples were collected.

Pyrite, the most common sulfide mineral, is isometric with sizes up to several millimeter scale and is associated with other ore and silicate minerals such as quartz and sericite (Fig. 1.7A). The dominant hypogene Cu sulfide mineral in the deposit is a chalcopyrite accompanied by quartz-pyrite or chalcocite-bornite-covellite (Fig. 1.7A-C). Other Cu sulfide minerals, such as bornite and covellite, are widespread. A supergene enrichment zone is a high-grade zone up to 300 m thick and dominated by secondary chalcocite replacing the other sulfide minerals. It is superimposed on pyrite and chalcopyrite (Fig. 1.7A-C). Bornite and covellite also overprint the pyrite and chalcopyrite intergrowth with chalcocite. Sphalerite and galena occur with quartz-pyrite-chalcopyrite or quartz-molybdenite (Fig. 1.7C-E). Another major sulfide ore mineral, molybdenite, is associated with quartz-molybdenite veins or

quartz-pyrite (Fig. 1.7F) prior to the dominant Cu mineralization processes. Molybdenite occurs rarely in association with chalcopyrite.

4. Analytical methods

Polished sections of rock and ore samples were prepared for microscopic observation of silicate and ore minerals. Pyrite, molybdenite and Cu ore minerals for Cu and S isotope analysis were separated manually under a binocular microscope after crushing the ore-bearing rocks.

4.1 Cu isotope analysis

All chemical procedures to pretreat and purify the Cu ore samples we report below were performed in a clean room (Class 100) at the Korea Basic Science Institute (KBSI) in Ochang, South Korea. Double-distilled MQ water and reagents including nitric acid (HNO_3), hydrochloric acid (HCl) and hydrofluoric acid (HF) were used.

4.1.1 Pretreatment processes for Cu isotopes

Approximately 0.1 g of manually separated Cu ore minerals were placed in a Teflon beaker and digested with 8 mL of a mixture of HNO_3 and HF in a ratio of 3:5 (v/v) at 180–200 °C. After completing the dissolution of the samples, 5 mL of 6 N HCl was added to eliminate the precipitated silicon tetrafluoride (SiF_4). Then, the solution was dried and diluted with 5% HNO_3 to analyze the Cu concentration by Inductively Coupled Plasma-Optical Emission Spectrometry (ICP-OES, PerkinElmer Optima 8300).

4.1.2 Ion exchange chromatography for separation of Cu

We followed the protocol of Cu separation by anion exchange chromatography outlined by Maréchal et al. (1999). To separate Cu from solution, chromatography columns (Poly-Prep® from Bio-rad company, 0.8 x 4 cm) with anion exchange resin (AG® MP-1M, 100-200 mesh) were used. The column was cleaned with 10 % HCl and filled with 2 mL (approximately 1.2 g) of anion exchange resin. The resin was cleaned 3 times with 7 mL of 0.5 N HNO_3, 5 mL of 7 N HCl and 2 mL of distilled water sequentially to remove fine particles within the resin. Then, the resin was conditioned with 6 mL of 7 N HCl + 0.001 % hydrogen peroxide (H_2O_2). After loading on the resin with a mixture of 0.5 mL of 7 N HCl + 0.001 % H_2O_2, the sample was adsorbed onto the resin by adding another mixture of 0.5 mL of 7 N HCl + 0.001 % H_2O_2. The matrix was removed in 10 mL of 7 N HCl + 0.001 % H_2O_2, and then Cu was eluted with 24 mL of 7 N HCl + 0.001 % H_2O_2. The procedures for column chromatography separation are described in Table 1.

To identify the efficiency of Cu separation by ion exchange chromatography, an ICP multi-elements standard solution (AccuTrace™ reference standard) and two United States Geological Survey (USGS) geological reference materials with relatively high Cu concentrations (BHVO-2 and BIR-1a) were tested. The recovery rates of the materials were higher than 95 % and the total procedural blank was 0.93 ng, which is typically less than 0.1% of loaded Cu (approximately 1 μg) in the measured samples.

4.1.3 Cu isotope analysis

The Cu isotope composition of the ore samples was measured on the MC-ICP-MS (Neptune, Thermo Scientific) at KBSI in Ochang. A sample-standard bracketing

(SSB) method was utilized to constrain and correct the instrumental mass fractionation. The Cu isotopic ratios of the measured samples were reported in δ notation relative to the international Cu standard material (ERM®-AE647) used as an operating standard material as follows:

$$\delta^{65}Cu_{(ERM®\text{-}AE647)} = [(^{65}Cu/^{63}Cu)_{sample} - (^{65}Cu/^{63}Cu)_{(ERM®\text{-}AE647)}]/(^{65}Cu/^{63}Cu)_{(ERM®\text{-}AE647)}$$

Typically, $\delta^{65}Cu_{(ERM®\text{-}AE647)}$ values are reported in per mil (‰, parts per thousand) which means that δ-value obtained by above equation are then multiplied by 1000.

Most previously reported Cu isotope values ($\delta^{65}Cu$) have been relative to another international Cu standard material (NIST SRM976), and $\delta^{65}Cu_{(SRM\ 976)}$ differs from $\delta^{65}Cu_{(ERM®\text{-}AE647)}$ by approximately 0.21 ‰ (Moeller et al., 2012). The measured $\delta^{65}Cu_{(ERM®\text{-}AE647)}$ value was calibrated to the $\delta^{65}Cu_{(SRM\ 976)}$ value using the following equation:

$$\delta^{65}Cu_{(NIST\ SRM976)}\ (‰) = \delta^{65}Cu_{(ERM®\text{-}AE647)}\ (‰) + 0.21\ ‰$$

4.2 S isotope analysis

The manually selected sulfide minerals were prepared as a powder within an agate cleaned with acetone and distilled water. The powder was placed into a 3.5 × 5 mm tin-foil cup and combusted within a combustion tube packed with reagent materials at 1030 °C in the Elemental Analyzer (EA). The reagent column was composed of 0-1 cm quartz wool, 1-7 cm quartz chips, 7-7.5 cm quartz wool, 7.5-14 cm 0.5-mm ultrahigh purity Cu wire, 14-14.5 cm quartz wool, 14.5-16.5 cm quartz chips, 16.5-17 cm quartz wool, 17-18.5 cm quartz chips and 18.5-19.5 cm quartz wool. The S isotopic ratio was measured by Continuous Flow (CF)-EA-IRMS (IsoPrime-EA) at the School of Earth and Environmental Sciences, Seoul National

University. The standard material, IAEA Ag_2S standard S-1, was bracketed within the samples and analyzed with the same procedure. The results were calculated by linear regression of the standards, and the S isotope composition of the samples is reported using δ-notation relative to the Vienna-Canyon Diablo Troilite (V-CDT) as follows:

$$\delta^{34}S_{(V\text{-}CDT)} = [(^{34}S/^{32}S)_{sample} - (^{34}S/^{32}S)_{(V\text{-}CDT)}]/(^{34}S/^{32}S)_{(V\text{-}CDT)}$$

Typically, $\delta^{34}S_{(V\text{-}CDT)}$ values are reported in per mil (‰, parts per thousand) which means that δ-value obtained by above equation are then multiplied by 1000.

All samples and standards were analyzed in duplicate, and the external reproducibility for long-term analyses was better than ± 0.2 ‰.

5. Results

The measured Cu isotope compositions ($\delta^{65}Cu$) of major Cu minerals from the Erdenetiin Ovoo porphyry Cu-Mo deposit are given in Table 2. The $\delta^{65}Cu$ values of Cu ore minerals range from -1.01 ‰ to 10.0 ‰. The $\delta^{65}Cu$ values of Cu (I) sulfide minerals have an average value of 0.82 ‰, with an overall variation of 2.55 ‰. Cu (II) minerals such as malachite and azurite show higher average values (6.88 ‰ and 6.29 ‰, respectively), whereas chrysocolla has a relatively low $\delta^{65}Cu$ value of 0.04 ‰. The $\delta^{65}Cu$ values of chalcopyrite range from 0.14 ‰ to 2.69 ‰, with a slightly higher average value (1.35 ‰), and other Cu (I) sulfide minerals, such as bornite, chalcocite and covellite, have lower and narrow $\delta^{65}Cu$ ranges clustering near 0.6 ‰ (Table 2).

The S isotope compositions ($\delta^{34}S$) of sulfide minerals range from -3.2 ‰ to 1.3 ‰, with an average of -0.8 ‰ (Table 2). The Cu sulfide minerals show slightly lower $\delta^{34}S$ values, including -0.5 ‰ for chalcopyrite, -1.1 ‰ for covellite, -1.7 ‰ for

chalcocite and -2.0 ‰ for bornite on average, whereas pyrite and molybdenite have average values of -0.1 ‰ and 0.5 ‰, respectively.

6. Discussion

6.1. The δ^{65}Cu values of ore deposits and igneous rocks

Cu isotope compositions of Cu ore minerals have been reported since the 2000s, revealing distinct δ^{65}Cu values depending on the deposit types, which are in turn related to the origin of Cu and the formation processes. The δ^{65}Cu values of Cu sulfide minerals from magmatic and hydrothermal deposits where Cu is considered to be derived from mantle sources and preserve its magmatic signature cluster around 0 ‰, similar to the δ^{65}Cu values of mantle sources of 0.06±0.20 ‰ (2SD), which has been suggested as the δ^{65}Cu value of bulk silicate Earth (BSE) by Liu et al. (2015). The hypogene Cu minerals from the porphyry deposit show δ^{65}Cu values ranging from -3.31 ‰ to 2.28 ‰ but mostly clustering from -1 ‰ to 1‰, as shown in Fig. 1.8 (Maréchal et al., 1999; Larson et al., 2003; Mathur et al., 2009; Li et al., 2010; Mirnejad et al., 2010; Braxton & Mathur, 2011; Palacios et al., 2011; Mathur et al., 2012; Mathur et al., 2013; Wu et al., 2017b; Mathur et al., 2018). The Cu minerals from Ni-Cu-PGE deposits and volcanic-associated massive sulfide (VMS) deposits have δ^{65}Cu values ranging from -5.26 ‰ to 3.98 ‰ (Zhu et al., 2000; Larson et al., 2003; Malitch et al., 2014; Ripley et al., 2015; Zhao et al., 2017) and from -0.34 ‰ to 2.97 ‰, respectively (Mason et al., 2005; Ikehata et al., 2011).

The Cu isotope composition of magma has been researched by measuring the δ^{65}Cu values of ordinary chondrite, native Cu and igneous rocks such as granite, volcanic rocks and ultramafic/mafic rocks (Luck et al., 2003; Li et al., 2009; Ikehata & Hirata, 2012; Dekov et al., 2013; Liu et al., 2015; Savage et al., 2015; Huang et

al., 2016; Baggio et al., 2018). These rocks present a very narrow range of δ^{65}Cu values from -0.51 ‰ to 0.10 ‰ in ordinary chondrite (Luck et al., 2003), from -1.07 ‰ to 1.18 ‰ in native Cu (Dekov et al., 2013; Baggio et al., 2018), from -0.46 ‰ to 1.51 ‰ in granite (Li et al., 2009), from -0.22 ‰ to 0.51 ‰ in volcanic rocks (Liu et al., 2015; Huang et al., 2016) and from -0.64 ‰ to 1.82 ‰ in ultramafic/mafic rocks (Ikehata & Hirata, 2012; Liu et al., 2015). In particular, MORBs and OIBs exhibit a narrow δ^{65}Cu range from -0.18 ‰ to 0.21 ‰ (Liu et al., 2015; Savage et al., 2015; Huang et al., 2016). The non-metasomatized peridotites have an overlapping range with MORBs and OIBs from -0.15 ‰ to 0.18 ‰ (Liu et al., 2015), representing a homogeneous Cu isotope composition of the mantle source.

Several studies have shown insignificant Cu isotope fractionation during magmatic processes such as mantle partial melting, magma differentiation and fractional crystallization under high-temperature conditions (Li et al., 2009; Ikehata & Hirata, 2012; Huang et al., 2016), indicating that the Cu isotope of fresh igneous rocks maintains its homogeneous magmatic signature during their formation. Li et al. (2009) reported tight clustering of δ^{65}Cu values near 0 ‰ for I-type granites (0.03±0.15 ‰, 2SD) and suggested a homogeneous mantle source and insignificant fractionation processes for the Cu isotope. By contrast, the S-type granites span more variable δ^{65}Cu values (-0.03±0.42 ‰, 2SD), reflecting the heterogeneous Cu isotope composition of sedimentary sources (Li et al., 2009). Similarly, the δ^{65}Cu values of the arc and continental basalts and the metasomatized peridotites range from -0.19 ‰ to 0.47 ‰ and from -0.64 ‰ to 1.82 ‰, respectively (Liu et al., 2015). This wider variation of δ^{65}Cu values was considered to reflect the involvement of crustal materials with their Cu isotopic heterogeneity due to redox and hydrothermal processes (Li et al., 2009; Liu et al., 2015). The heterogeneous Cu isotope

composition of sedimentary reservoirs is considered to be attributable to the variable $\delta^{65}Cu$ values of the sediment-hosted stratiform copper (SSC) deposit from -3.44 ‰ to 1.85 ‰ (Fig. 1.8), although other conditions, such as redox reactions, variation of Eh and pH can also affect the $\delta^{65}Cu$ values of Cu minerals in this deposit type (Asael et al., 2007; Asael et al., 2009; Asael et al., 2012; Mathur et al., 2018).

Some previous studies of hypogene ore deposits have revealed distinct $\delta^{65}Cu$ variations under high-temperature magmatic and hydrothermal processes, especially the Cu isotope fractionation process due to its partitioning into vapor and liquid phases during phase separation or fluid boiling (Seo et al., 2007; Li et al., 2010; Maher et al., 2011; Yao et al., 2016; Wu et al., 2017a). Quantum chemical calculations (Seo et al., 2007) and experimental (Li et al., 2010; Maher et al., 2011) studies, however, indicated opposite Cu isotope fractionation pathways. The former suggested preferential partitioning of the heavier Cu isotope (^{65}Cu) into the vapor phases, such as Cu_3Cl_3, whereas the latter indicated that the light Cu isotope (^{63}Cu) is enriched in the vapor controlled by the kinetic isotope fractionation processes under pH and salinity variation.

The $\delta^{65}Cu$ values of Cu minerals in the ore deposit where low-temperature mineralization events occur show much larger variations (Fig. 1.8), mostly related to the redox reactions. In the porphyry deposit, the Cu minerals from the supergene enrichment and leach cap zone present a much larger variation of $\delta^{65}Cu$ values from -16.5 ‰ to 8.30 ‰ (Fig. 1.8), whereas the $\delta^{65}Cu$ values of hypogene sulfide minerals, mostly chalcopyrite, span a narrow range clustering near 0 ‰ (Maréchal et al., 1999; Larson et al., 2003; Mathur et al., 2009; Li et al., 2010; Mirnejad et al., 2010; Braxton & Mathur, 2011; Palacios et al., 2011; Mathur et al., 2012; Mathur et al., 2013; Wu et al., 2017b; Mathur et al., 2018). The $\delta^{65}Cu$ data from the high-sulfidation Cu

deposit show a similar pattern, with a large range of overall δ^{65}Cu values from -4.76 ‰ to 2.84‰ (Fig. 1.8), but most of the δ^{65}Cu values within a small variation of 1 ‰ have hypogene origin (Duan et al., 2016; Wu et al., 2017a). These studies suggested that the δ^{65}Cu sign of hypogene Cu is altered by the change in redox conditions under the supergene environment, similar to the porphyry system. A distinctly wider variation of δ^{65}Cu values from -4.82 ‰ to 11.5 ‰ was observed in sea-floor hydrothermal deposits (Maréchal et al., 1999; Zhu et al., 2000; Rouxel et al., 2004; Berkenbosch et al., 2015) and was suggested to be mainly attributable to the oxidation of primary Cu sulfide, but other complex processes, such as hydrothermal reworking and fluid mixing between seawater and hydrothermal fluids, may play an important role in Cu isotope fractionation (Rouxel et al., 2004). The native Cu from volcanic lavas (Baggio et al., 2018) and mantle rock (Ikehata & Hirata, 2012) shows a range from -0.9 ‰ to 2.9 ‰ and from -0.67 ‰ to 0.14 ‰, respectively (Fig. 1.8). Both studies suggested that the primary native Cu retains its original δ^{65}Cu signature of magmatic origin and that the δ^{65}Cu values of secondary Cu have a larger range due to hydrothermal alterations, such as oxidation and leaching under supergene conditions.

The range of δ^{65}Cu values from the skarn-type deposit seems to be influenced by the occurrence of redox reactions. An early Cu isotope study by Graham et al. (2004) reported a wide δ^{65}Cu range of chalcopyrite of 1.26 ‰ to 13.4 ‰. By contrast, several studies have reported relatively narrow ranges of -0.15 ‰ to 0.77 ‰ for chalcopyrite (Wang et al., 2017) and -1.29 ‰ to 3.07 ‰ for chalcopyrite and bornite (Maher & Larson, 2007), indicating a lack of evidence for redox reaction occurrence in the skarn system. The former study presented the typical δ^{65}Cu signature of hypogene Cu in the skarn deposit, and the latter suggested that the measured δ^{65}Cu

variation is due to equilibrium isotope fractionation between fluid and mineral and other isotope fractionation mechanisms rather than redox reactions. The carbonate-hosted Mississippi Valley-type (MVT) deposit also yielded limited δ^{65}Cu values (0 ± 0.5 ‰) for chalcopyrite (Fig. 1.8), indicating a homogeneous Cu source of magmatic origin and little effect of redox reactions and subsequent modification of δ^{65}Cu values (Luczaj & Huang, 2018).

6.2. Cu isotope data

6.2.1. The δ^{65}Cu values of Cu sulfide minerals

The measured δ^{65}Cu values of Cu sulfide minerals in the Erdenetiin Ovoo porphyry Cu-Mo deposits, which range from 0.14 ‰ to 2.69 ‰, reveal little difference in the average δ^{65}Cu value of each Cu sulfide mineral (1.35 ‰ for chalcopyrite, 0.69 ‰ for chalcocite, 0.61 ‰ for bornite and 0.68 ‰ for covellite), indicating that the Cu source in the Erdenetiin Ovoo deposit has a mantle origin and retains its magmatic signature. The δ^{65}Cu values of chalcopyrite appear to be large and somewhat scattered compared to other Cu sulfide minerals (Fig. 1.9), which is attributable to the two high-δ^{65}Cu-samples. Excluding these two samples, the average δ^{65}Cu value of the other chalcopyrite is 0.20 ‰, which is close to that of the BSE (0.06±0.20 ‰).

As mentioned above, the recent study by Mathur et al. (2018) suggested that the origin of chalcocite can be classified into three groups depending on its δ^{65}Cu value. δ^{65}Cu values of chalcocite ranging from -1 ‰ to 1 ‰ indicate hypogene mineralization under high-temperature conditions, where equilibrium fractionation predominates. By contrast, the chalcocites from the sedimentary Cu bed and supergene enrichment zone show δ^{65}Cu values of less than -1 ‰ and greater than 1

‰, respectively, due to redox reactions of primary Cu minerals. Based on these criteria, the measured δ^{65}Cu values of chalcocite in the Erdenetiin Ovoo deposit may indicate a hypogene origin.

The difference in δ^{65}Cu values between the primary and secondary minerals, however, varies depending on the δ^{65}Cu value of the starting primary Cu sulfide minerals and the degree of redox reactions (Larson et al., 2003; Markl et al., 2006; Asael et al., 2007; Asael et al., 2009; Mathur et al., 2009; Mathur et al., 2018). Although abundant data support origin classification by the Cu isotope composition, the averages and ranges of δ^{65}Cu values from primary and secondary chalcocite may overlap in some cases (Mathur et al., 2018), thus interfering with the identification of the origin based on the δ^{65}Cu values. Mathur et al. (2009), for example, measured both primary (chalcocite and covellite) and secondary (chalcocite) Cu sulfide minerals from Butte, Montana. The mean δ^{65}Cu value of the former is 0.06 ‰, whereas the latter has a slightly higher average δ^{65}Cu value (0.40 ‰), indicating small enrichment of the heavier Cu isotope during the supergene processes.

The microscopic observation results (Fig. 1.7) and paragenetic sequences of minerals (Fig. 1.4) represent the characteristics of the secondary chalcocite under the supergene enrichment environment in the Erdenetiin Ovoo deposit. Chalcocite usually occurs as an overprinted or superimposed form on pyrite and chalcopyrite minerals (Fig. 1.7B-E). Macro-scale observation also reveals that the chalcocite is mainly coating the other sulfide grains rather than occurring itself as a massive form. The covellite and bornite grains, like the chalcocite grain, form by replacing other sulfide grains. Most studies of the Erdenetiin Ovoo deposit, therefore, have divided the Cu-sulfide minerals assemblage (chalcocite-bornite-covellite) into the secondary phase, where a high-grade supergene enrichment blanket develops with a thickness

of up to 300 m (e.g., Khasin et al., 1977; Gavrilova et al., 1984; Gerel & Munkhtsengel, 2005).

Compared to the typical $\delta^{65}Cu$ values of Cu sulfide minerals in porphyry deposits (Fig. 1.8), the relatively small difference in $\delta^{65}Cu$ values between the primary chalcopyrite and secondary Cu sulfide minerals is considered to indicate an insignificant influence of Cu isotope fractionation by redox reactions during their formation. Many studies have reported the enrichment of the heavier Cu isotope (^{65}Cu) in the secondary Cu sulfide minerals in the porphyry deposit, mainly induced by the redox state change of Cu during the dissolution of the primary Cu sulfide and precipitation of the secondary mineral from the solution (Larson et al., 2003; Markl et al., 2006; Mathur et al., 2009; Palacios et al., 2011; Mathur et al., 2018). Several studies have demonstrated that the heavier Cu isotope (^{65}Cu) is preferentially removed from primary Cu sulfide minerals by reaction with the low-pH solution, and its valance state changes to cupric ion (Cu^{2+}), causing Cu isotope fractionation of up to 3 ‰ (Zhu et al., 2002; Mathur et al., 2005; Kimball et al., 2009; Wall et al., 2011). Ehrlich et al. (2004) reported the lighter Cu isotope (^{63}Cu) enrichment up to approximately 3 ‰ into covellite during reduction processes at 20 °C, which is similar with the degree of Cu isotope fractionation by dissolution processes. The secondary Cu sulfide minerals, however, can preserve the ^{65}Cu-enriched signature of oxidized fluids, mainly due to the successive reworking of previous supergene minerals and the occurrence of complete reduction processes at water table (Chávez, 2000; Mathur et al., 2005; Braxton & Mathur, 2011; Mathur et al., 2018).

There are two possible explanations for the small Cu isotope fractionation during the development of the thick enrichment zone in the Erdenetiin Ovoo porphyry Cu-Mo deposit. First, less Cu isotope fractionation can be observed when

a large mass is transported from aqueous solution to mineral phase during the precipitation of secondary Cu sulfide minerals (Ehrlich et al., 2004). Several studies have reported that the magnitude of Cu isotope fractionation between solution and the mineral phase is gradually reduced as the redox reaction proceeds (Mathur et al., 2005; Fernandez & Borrok, 2009; Kimball et al., 2009; Wall et al., 2011). Second, the involvement of biogenic mechanisms could lead to a decrease in Cu isotope fractionation during the redox reactions (Zhu et al., 2002; Ehrlich et al., 2004). Zhu et al. (2002), in an experimental study performed under low-temperature conditions, suggested that distinctly smaller Cu isotope fractionation is found in bacterially involved redox fractionation processes than in abiogenic systems.

Chalcopyrite, the primary Cu sulfide mineral in the Erdenetiin Ovoo deposit, shows distinctly separated δ^{65}Cu values into near 0 ‰ and 2.5 ‰ (Fig. 1.9). This separation may indicate heterogeneity of the magmatic Cu source and/or the Cu isotope fractionation processes under high-temperature conditions. The variation of δ^{65}Cu values in high-temperature minerals due to source heterogeneity is mainly attributed to the input of crustal materials (Liu et al., 2015; Ripley et al., 2015) or metasomatism by hydrothermal fluid from the altered lithosphere (Huang et al., 2016). Although Cu isotope fractionation in high-temperature magmatic and hydrothermal processes is much smaller than that in the supergene environment via the redox reactions, the δ^{65}Cu values of hypogene minerals in high-temperature deposits vary up to 2.6 ‰ (Larson et al., 2003; Markl et al., 2006; Asael et al., 2009; Li et al., 2010; Maher et al., 2011; Berkenbosch et al., 2015; Yao et al., 2016; Wu et al., 2017b). The potential processes for the high-temperature Cu isotope fractionation, excluding redox-driven reactions, include isotope fractionation between complexing species, physicochemical variation such as pH and Eh, equilibrium isotope

fractionation, phase separation among vapor, brine and sulfide, and partitioning of Cu isotopes between fluid and mineral during sulfide precipitation (Graham et al., 2004; Markl et al., 2006; Seo et al., 2007; Li et al., 2010; Maher et al., 2011; Berkenbosch et al., 2015; Savage et al., 2015).

Gerel and Munkhtsengel (2005) proposed a genetic model for the Erdenetiin Ovoo deposit including multiple partial melting of the upper mantle to produce the wide span of composition of host rocks from diorite to granite. They suggested that multiple partial melting and intrusion led to at least three distinguishable intrusive rocks with variable compositions, textures and ages (Koval et al., 1982). Therefore, the δ^{65}Cu values of chalcopyrite in the Erdenetiin Ovoo deposit may be interpreted to be affected by different magma or hydrothermal fluid sources with different Cu isotope compositions. However, it is unclear whether the variable δ^{65}Cu values of chalcopyrite in the Erdenetiin Ovoo deposit are controlled by heterogeneous Cu sources due to a lack of distinct evidence. Maher et al. (2011) noted that the explanations for a larger δ^{65}Cu value range of hypogene minerals in some ore deposits vary slightly depending on the case study and deposit types, and the reason is not fully understood. Further research is needed to interpret this large variation of δ^{65}Cu values in chalcopyrite from the Erdenetiin Ovoo deposit.

6.2.2. The δ^{65}Cu values of Cu (II) minerals

The measured δ^{65}Cu values of Cu (II) minerals (chrysocolla, malachite and azurite) represent a distinctly separate range compared to those for Cu sulfide minerals (Fig. 1.9). The δ^{65}Cu values of chrysocolla have a lower range from -1.01 ‰ to 1.49 ‰, with an average of 0.04 ‰, whereas malachite and azurite show a much higher range and average, from 4.06 ‰ to 10.0 ‰ (avg. 6.29 ‰) and from

4.72 ‰ to 9.05 ‰ (avg. 6.88 ‰), respectively (Table 2). When secondary Cu minerals are produced from the mineralizing fluid under low-temperature conditions, the magnitude of Cu isotope fractionation varies depending on the mineral phase (Zhu et al., 2002; Ehrlich et al., 2004). As mentioned above, the lighter Cu isotope can be enriched in the secondary Cu sulfide minerals by up to 3 ‰ compared to the solution from which precipitate (Larson et al., 2003; Ehrlich et al., 2004; Mathur et al., 2005; Braxton & Mathur, 2011). By contrast, the secondary Cu (II) minerals where Cu exists as Cu^{2+} show much smaller Cu isotope fractionation (Maréchal & Sheppard, 2002; Ehrlich et al., 2004). In an experimental study, Maréchal and Sheppard (2002) reported that the Cu isotope fractionation between Cu^{2+} ion in solution and malachite is 0.20 ‰ to 0.38 ‰ at 30 °C.

The characteristics of the $\delta^{65}Cu$ values of Cu (II) minerals in the Erdenetiin Ovoo deposit indicate that they were precipitated from fluid with a different $\delta^{65}Cu$ value and/or at different timing in the supergene environment. Because of the small Cu isotope fractionation during the precipitation of Cu (II) minerals, they appear to reflect the $\delta^{65}Cu$ value of the mineralizing solution. These results imply that chrysocolla might be precipitated from the solution with lower $\delta^{65}Cu$ values, whereas malachite and azurite formed from the ^{65}Cu-enriched solution.

As the secondary Cu sulfide minerals precipitate from the fluid in the supergene environment, the $\delta^{65}Cu$ value of the fluid becomes heavier due to the preferential partitioning of the lighter Cu isotope (^{63}Cu) into the mineral phase. If secondary Cu (II) minerals are precipitated from single solution, the deposition of chrysocolla with a lower $\delta^{65}Cu$ value could occur at relatively early stage of fluid evolution, when the value of $\delta^{65}Cu$ is sufficiently low. Then, malachite and azurite would be precipitated from the fluid with increasing $\delta^{65}Cu$ value due to the partitioning of the lighter Cu

isotope into secondary Cu (I) minerals.

However, it is not plausible that the δ^{65}Cu values of secondary Cu (II) minerals in the Erdenetiin Ovoo deposit could be affected by the evolution of a single mineralizing fluid. The natural variation of Cu isotope composition in supergene ore minerals has been reported to range from -16.5 ‰ to 12 ‰, much larger than the measured Cu isotope fractionation factors in experimental studies (e.g., Larson et al., 2003; Mathur et al., 2005; Mathur et al., 2009). The greater variation of δ^{65}Cu values observed in natural ore minerals has been attributed to various factors, such as multiple cycles of redox reactions, fractionation processes among dissolved species within a fluid and between dissolved and solid phases during precipitation, Rayleigh fractionation in a closed system, fractionation behavior in an open system and ligand-bonding characteristics (Markl et al., 2006; Asael et al., 2009; Sherman, 2013; Moynier et al., 2017).

The δ^{65}Cu values of Cu (I) and Cu (II) mineral pairs can be helpful for tracing the signature of Cu transport at the deposit scale (Markl et al., 2006; Asael et al., 2007; Mathur et al., 2009). Mathur et al. (2009) suggested that the significance of Cu transport in the supergene environment can be examined by measuring the δ^{65}Cu values of Cu (I) and Cu (II) mineral pairs. If the difference between the δ^{65}Cu values between Cu (II) and Cu (I) minerals is positive ($\Delta_{\text{Cu (II) mineral – Cu (I) mineral}} > 0$), there is an insignificant mobilization of Cu. This indicates an occurrence of a rough mass balance during the reactions, and the products exist near the reaction site (Mathur et al., 2009). By contrast, no mass balance occurs and most Cu is transported laterally when the $\Delta_{\text{Cu (II) mineral – Cu (I) mineral}}$ value is negative (Mathur et al., 2009).

The positive difference in δ^{65}Cu values between Cu (II) and Cu (I) minerals (Table 2) therefore suggests an insignificant transport of Cu in the Erdenetiin Ovoo

deposit, implying that the precipitation of Cu (II) minerals by the redox reactions occurs adjacent to the site where the reactions occur. Thus, the redox reactions occur very quickly, and there is insufficient time for the transport of Cu toward the distant area. In this case, the border between the leach cap and enrichment zone tends to vary slightly (Mathur et al., 2009). However, it is hard to identify this relationship because the leach cap zone has been already eroded in the Erdenetiin Ovoo deposit.

6.3 S isotope data

The average $\delta^{34}S$ value of sulfide minerals in the Erdenetiin Ovoo deposit, -0.8 ‰, implies that sulfur is mostly derived from deep sources and preserves its magmatic signature. The narrow range of $\delta^{34}S$ values from -3.2 ‰ to 1.3 ‰ is very similar to the typical $\delta^{34}S$ values from porphyry Cu deposits worldwide of -3 ‰ to 1 ‰ (Wilson et al., 2007 and references therein), indicating a homogeneous sulfur source and an insignificant crustal contamination of magma. Due to the wide variation of $\delta^{34}S$ values from crustal sulfur, the involvement of sulfur derived from crustal materials can affect the $\delta^{34}S$ value of magmatic sulfur and then alter the $\delta^{34}S$ value of sulfide minerals in magmatic-hydrothermal deposits (Ripley & Li, 2003; Seal, 2006).

Primary sulfide minerals (pyrite, chalcopyrite and molybdenite) show very close average $\delta^{34}S$ values and ranges (Fig. 1.10), indicating that the S isotope composition of magmatic sources retains its homogeneity during their precipitation processes under high-temperature conditions. In addition, there is no distinct variation of $\delta^{34}S$ values between the primary sulfide minerals occurring as the disseminated form and within the quartz vein type. According to the paragenetic sequences of major ore minerals (Fig. 1.4), these types have different main stages of

mineralization. This indicates that even though multiple intrusion and hydrothermal mineralization occur in the Erdenetiin Ovoo deposit (Koval et al., 1982; Gerel & Munkhtsengel, 2005), the homogeneous S isotope composition in the magma and hydrothermal fluids appears to be preserved in the hypogene environment.

Compared to the $\delta^{34}S$ values of primary sulfide minerals, which cluster near 0 ‰, the secondary Cu sulfide minerals show lower range of $\delta^{34}S$ values, with an average of -1.6 ‰ (Fig. 1.10), which can be interpreted as a result of either isotope fractionation during their formation in the low-temperature condition or the involvement of sulfur species with different $\delta^{34}S$ values. Since the formation of secondary Cu sulfide minerals includes the dissolution of the existing sulfide minerals under the oxidized condition and precipitation from solution, the S isotope fractionation may affect their $\delta^{34}S$ values. When the oxidized species increase in the hydrothermal fluid, the $\delta^{34}S$ value can be lowered due to isotope fractionation (Rye, 1993; Seal et al., 2000). For example, the $\delta^{34}S$ value of the produced sulfate ion (SO_4^{2-}) can be up to 2 ‰ lower the dissolution from sulfide minerals (Balci et al., 2007; Heidel et al., 2013). By contrast, the lighter S isotope (^{32}S) is enriched in the product, the reduced sulfur form, during the sulfate reduction process (e.g., Strebel et al., 1990; Krouse & Mayer, 2000; Seal, 2006).

If the sulfur combined as the secondary Cu sulfide in the Erdenetiin Ovoo deposit is derived from the dissolution of primary sulfide minerals to sulfate and/or its reduction by abiotic or biotic reaction, the product should reflect the variation of S isotope composition via a change in valance state and have a lower $\delta^{34}S$ value than the primary sulfide mineral. In particular, the involvement of microorganisms such as sulfate-reducing bacteria can amplify the degree of S isotope fractionation during the sulfate reduction process (e.g., Aharon & Fu, 2003; Brunner et al., 2005). The

existence of biological activity in the Erdenetiin Ovoo deposit has been proposed as one possible explanation for the smaller Cu isotope fractionation in the supergene enrichment zone. However, it is unclear if the lower $\delta^{34}S$ value of the secondary Cu sulfide minerals is due to a redox change of sulfur because direct evidence is lacking.

Another explanation for the lower $\delta^{34}S$ value of the secondary Cu sulfide mineral is that the sulfur originated from the input of sulfur species in the hydrothermal fluid with lower $\delta^{34}S$ value. As mentioned above, there were multiple magmatic intrusions and hydrothermal mineralization events in the Erdenetiin Ovoo deposit ore district (Koval et al., 1982; Gavrilova et al., 1984; Gerel & Munkhtsengel, 2005). Since the secondary Cu sulfide minerals were formed when most of the primary sulfide minerals already existed (Fig. 1.4), there seems to be a possibility that the fluid related to the production of secondary Cu sulfide minerals has a different S isotope composition. The $\delta^{34}S$ values of magma and hydrothermal fluid can vary depending on the S isotope fractionation processes in the high-temperature condition, which is influenced by several parameters, such as temperature, pressure, the chemical composition of magma and sulfur species (e.g., O'Neil, 1986). This variation implies that the S isotope composition of magma and hydrothermal fluid can evolve during the development of the deposit and finally affect the $\delta^{34}S$ value of the sulfide minerals where they formed.

Potential relationship between the Cu and S isotope data may provide some information on their sources and mineralization processes by plotting the Cu and S isotope data together. Unfortunately, there was no distinct systemic relationship between them and very poor linear correlation (R^2=0.15) between them in this study makes it difficult to grasp the meaningful information (Fig. 1.11). The Cu and S isotope signals of primary sulfide minerals indicate their magmatic source in the

Erdenetiin-Ovoo deposit. However, the distinct difference of Cu and S isotope fractionation are observed in secondary Cu sulfide minerals. The small difference of δ^{65}Cu values and relatively larger gap of δ^{34}S values imply that the Cu and S isotopes show the different geochemical behavior in the hydrothermal fluid. In addition, to the best of our knowledge, there is few researches reporting the distinct relationship of Cu and S isotope data in porphyry Cu system.

6.4 Implications for mineral exploration and deposit environment

Several recent studies have suggested the application of Cu isotope values from Cu minerals in the exploration of hidden Cu occurrence in porphyry Cu systems (Mathur et al., 2012; Mathur et al., 2013; Wu et al., 2017b) and high-sulfidation Cu deposits (Duan et al., 2016). Either the absence of a heavier Cu-enriched zone (Mathur et al., 2012; Duan et al., 2016) or the relationship between the δ^{65}Cu values and silicate alteration assemblages (Mathur et al., 2013; Wu et al., 2017b) could be used as an indicator of an unrevealed enrichment zone of Cu minerals. The former case is related to the development of the supergene enrichment zone from the mass balance perspective, whereas the latter example can be applied to high-temperature mineralization processes where the center of hydrothermal systems occurs. In particular, Duan et al. (2016) measured the δ^{65}Cu values of Cu sulfide minerals in the Tiegelongnan high-sulfidation deposits and found a large variation of δ^{65}Cu values in only two of four drill holes. They suggested that the absence of an isotopically light or heavy zone in the two drill holes might be used to trace a possible undiscovered mineralized zone in a porphyry Cu system.

The measured δ^{65}Cu values in this study are dominantly positive (Table 2), which can be a signal for the presence of a Cu-enriched zone elsewhere. Considering

mass balance, the absence of either an isotopically heavier or lighter zone in the porphyry system may suggest the existence of an undiscovered Cu-enriched occurrence (Mathur et al., 2012; Duan et al., 2016). Because the leach cap zone has already been eroded, it is difficult to determine the Cu isotope composition of this zone in the Erdenetiin Ovoo deposit. Therefore, it is unclear if the lighter Cu isotope either remained in the leach cap zone or was transported and formed a hidden mineralized zone.

The signatures of an insignificant Cu mobilization in the Erdenetiin Ovoo porphyry Cu-Mo deposit, however, suggest that there is little possibility of the formation of an exotic Cu deposit in the study area. In this study, the measured $\delta^{65}Cu$ values in the Erdenetiin Ovoo deposit show a large variation of overall Cu minerals (up to 11.0 ‰), which is usually attributed to the difference in $\delta^{65}Cu$ values between Cu (II) and Cu (I) minerals. As discussed above, the calculated $\Delta_{Cu\ (II)\ mineral\ -\ Cu\ (I)\ mineral}$ values are mostly positive, implying trivial transport of Cu during their formation. In addition, the $\delta^{65}Cu$ values of the primary and secondary Cu sulfide minerals have a relatively small difference, indicating apparent satisfaction of an approximate mass balance. Both characteristics of the $\delta^{65}Cu$ values seem to indicate a large mass but short-distance transportation of Cu occurred under the supergene environment in the Erdenetiin Ovoo ore district. That is, most of the Cu was transformed from primary to secondary Cu minerals during the redox reaction in the low-temperature environment and moved to an adjacent location where the reaction took place.

7. Conclusions

The $\delta^{65}Cu$ values of the Cu sulfide minerals from the Erdenetiin Ovoo porphyry Cu-Mo deposit (0.14 ‰ to 2.69 ‰) indicate a magmatic source as the Cu origin and

little effect of Cu isotope fractionation during formation of secondary Cu sulfide minerals, caused by large mass transportation and/or the involvement of biological activities. In contrast, the values of Cu (II)-bearing minerals (chrysocolla, malachite and azurite) show a much larger variation of $\delta^{65}Cu$ from -1.01 ‰ to 10 ‰. The positive $\Delta_{Cu\ (II)\ mineral\ -\ Cu\ (I)\ mineral}$ values in the study area indicate that insignificant transport of Cu occurred, thus satisfying an approximate mass balance, and that quick redox reactions did not allow sufficient time for Cu transport.

The $\delta^{34}S$ values of the primary sulfide minerals show a narrow range clustering near 0 ‰ from -2 ‰ to 1.3 ‰, with an average value of -0.1 ‰, implying that sulfur is mainly derived from the homogeneous magmatic source. By contrast, the slightly lower $\delta^{34}S$ values of the secondary sulfide minerals, from -3.2 ‰ to -0.3 ‰ with an average of -1.6 ‰, are regarded as the result of either S isotope fractionation processes or input of sulfur species with different S isotope compositions.

The little difference of $\delta^{65}Cu$ values between primary and secondary Cu sulfide minerals and the positive $\Delta_{Cu\ (II)\ mineral\ -\ Cu\ (I)\ mineral}$ values indicate the signals of insignificant Cu transport in the study area. In turn, this indicates little possibility of the formation of an exotic Cu occurrence in the Erdenetiin Ovoo porphyry Cu-Mo deposit.

References

Aharon, P., & Fu, B. (2003). Sulfur and oxygen isotopes of coeval sulfate–sulfide in pore fluids of cold seep sediments with sharp redox gradients. *Chemical Geology, 195*(1), 201-218.

Asadi, S., Mathur, R., Moore, F., & Zarasvandi, A. (2015). Copper isotope fractionation in the Meiduk porphyry copper deposit, Northwest of Kerman

Cenozoic magmatic arc, Iran. *Terra Nova, 27*(1), 36-41.

Asael, D., Matthews, A., Bar-Matthews, M., & Halicz, L. (2007). Copper isotope fractionation in sedimentary copper mineralization (Timna Valley, Israel). *Chemical Geology, 243*(3-4), 238-254.

Asael, D., Matthews, A., Bar-Matthews, M., Harlavan, Y., & Segal, I. (2012). Tracking redox controls and sources of sedimentary mineralization using copper and lead isotopes. *Chemical Geology, 310*, 23-35.

Asael, D., Matthews, A., Oszczepalski, S., Bar-Matthews, M., & Halicz, L. (2009). Fluid speciation controls of low temperature copper isotope fractionation applied to the Kupferschiefer and Timna ore deposits. *Chemical Geology, 262*(3-4), 147-158.

Baggio, S. B., Hartmann, L. A., Lazarov, M., Massonne, H.-J., Opitz, J., Theye, T., & Viefhaus, T. (2018). Origin of native copper in the Paraná volcanic province, Brazil, integrating Cu stable isotopes in a multi-analytical approach. *Mineralium Deposita, 53*(3), 417-434.

Balci, N., Shanks III, W. C., Mayer, B., & Mandernack, K. W. (2007). Oxygen and sulfur isotope systematics of sulfate produced by bacterial and abiotic oxidation of pyrite. *Geochimica et Cosmochimica Acta, 71*(15), 3796-3811.

Beard, B. L., Johnson, C. M., & Albarede, F. (2004). *Geochemistry of non-traditional stable isotopes*: Mineralogical Society of Amer.

Berkenbosch, H., de Ronde, C., Paul, B., & Gemmell, J. (2015). Characteristics of Cu isotopes from chalcopyrite-rich black smoker chimneys at Brothers volcano, Kermadec arc, and Niuatahi volcano, Lau basin. *Mineralium Deposita, 50*(7), 811-824.

Berzina, A., & Sotnikov, V. (2007). Character of formation of the Erdenet-Ovoo

porphyry Cu-Mo magmatic center (northern Mongolia) in the zone of influence of a Permo-Triassic plume. *Russian Geology and Geophysics, 48*(2), 141-156.

Berzina, A., Sotnikov, V., Ponomarchuk, V., Berzina, A., & Kiseleva, V. (1999). Temporal periods of formation of Cu-Mo porphyry deposits, Siberia and Mongolia. *Mineral deposits: Processes to processing: Rotterdam, Balkema*, 321-324.

Braxton, D., & Mathur, R. (2011). Exploration applications of copper isotopes in the supergene environment: A case study of the Bayugo porphyry copper-gold Deposit, southern Philippines. *Economic Geology, 106*(8), 1447-1463.

Brunner, B., Bernasconi, S. M., Kleikemper, J., & Schroth, M. H. (2005). A model for oxygen and sulfur isotope fractionation in sulfate during bacterial sulfate reduction processes. *Geochimica et Cosmochimica Acta, 69*(20), 4773-4785.

Chávez, W. (2000). Supergene oxidation of copper deposits: zoning and distribution of copper oxide minerals. *SEG Newsletter, Society of Economic Geologists, 41*, 10-21.

de Laeter, J. R., Böhlke, J. K., De Bièvre, P., Hidaka, H., Peiser, H., Rosman, K., & Taylor, P. (2003). Atomic weights of the elements. Review 2000 (IUPAC Technical Report). *Pure and applied chemistry, 75*(6), 683-800.

Dejidmaa, G., & Naito, K. (1998). Previous studies on the Erdenetiin ovoo porphyry copper-molybdenum deposit, Mongolia. *Bulletin of the Geological Survey of Japan, 49*(6), 299-308.

Dekov, V. M., Rouxel, O., Asael, D., Hålenius, U., & Munnik, F. (2013). Native Cu from the oceanic crust: Isotopic insights into native metal origin. *Chemical Geology, 359*, 136-149.

Duan, J., Tang, J., Li, Y., Liu, S.-A., Wang, Q., Yang, C., & Wang, Y. (2016). Copper

isotopic signature of the Tiegelongnan high-sulfidation copper deposit, Tibet: implications for its origin and mineral exploration. *Mineralium Deposita, 51*(5), 591-602.

Ehrlich, S., Butler, I., Halicz, L., Rickard, D., Oldroyd, A., & Matthews, A. (2004). Experimental study of the copper isotope fractionation between aqueous Cu (II) and covellite, CuS. *Chemical Geology, 209*(3-4), 259-269.

Fernandez, A., & Borrok, D. M. (2009). Fractionation of Cu, Fe, and Zn isotopes during the oxidative weathering of sulfide-rich rocks. *Chemical Geology, 264*(1-4), 1-12.

Gavrilova, S., Maksimyuk, I., & Orolmaa, D. (1984). Features of magmatism and composition of ore of the copper-molybdenum deposit at Erdenetiin Ovoo [G]. *Endogenic ore formations of Mongolia. Nauka*, 101-105.

Gavrilova, S., Maksimyuk, I., & Orolmaa, D. (1990). Stages of formation of the Erdenet molybdenum-copper porphyry deposit (Mongolia). *Geologiya Rudnych Mestorozhdenii,(6)*, 3-17.

Gerel, O. (1998). Phanerozoic felsic magmatism and related mineralization in Mongolia. *Bulletin of the Geological Survey of Japan, 49*(6), 239-248.

Gerel, O., Dandar, S., Amar-Amgalan, S., Javkhlanbold, D., Myagamarsuren, S., Myagmarsuren, S., Munkhtsengel, B., & Soyolmaa, B. (2005). *Geochemistry of granitoids and altered rocks of the Erdenet porphyry copper-molybdenum deposit, central Mongolia.* Paper presented at the Mineral Deposit Research: Meeting the Global Challenge.

Gerel, O., & Munkhtsengel, B. (2005). Erdenetiin Ovoo porphyry copper–molybdenum deposit in northern Mongolia. *Geodynamics and Metallogeny of Mongolia with a Special Emphasis on Copper and Gold Deposits. CERCAMS,*

Natural History Museum, London, 85-103.

Graham, S., Pearson, N., Jackson, S., Griffin, W., & O'reilly, S. (2004). Tracing Cu and Fe from source to porphyry: in situ determination of Cu and Fe isotope ratios in sulfides from the Grasberg Cu–Au deposit. *Chemical Geology, 207*(3-4), 147-169.

Haest, M., Muchez, P., Petit, J. C., & Vanhaecke, F. (2009). Cu isotope ratio variations in the Dikulushi Cu-Ag deposit, DRC: Of primary origin or induced by supergene reworking? *Economic Geology, 104*(7), 1055-1064.

Heidel, C., Tichomirowa, M., & Junghans, M. (2013). Oxygen and sulfur isotope investigations of the oxidation of sulfide mixtures containing pyrite, galena, and sphalerite. *Chemical Geology, 342*, 29-43.

Huang, J., Liu, S.-A., Wörner, G., Yu, H., & Xiao, Y. (2016). Copper isotope behavior during extreme magma differentiation and degassing: a case study on Laacher See phonolite tephra (East Eifel, Germany). *Contributions to Mineralogy and Petrology, 171*(8-9), 76.

Ikehata, K., & Hirata, T. (2012). Copper isotope characteristics of copper-rich minerals from the Horoman peridotite complex, Hokkaido, northern Japan. *Economic Geology, 107*(7), 1489-1497.

Ikehata, K., Notsu, K., & Hirata, T. (2011). Copper isotope characteristics of copper-rich minerals from Besshi-type volcanogenic massive sulfide deposits, Japan, determined using a femtosecond LA-MC-ICP-MS. *Economic Geology, 106*(2), 307-316.

Jargalsaihan, D. (1996). Mineral resources of Mongolia in Jargalsaihan, D., Kázmér, M., Baras, Z., and Sanjaadorj, D., eds., Guide to the geology and mineral resources of Mongolia: Ulaanbaatar, Mongolia:. *Geological Exploration,*

Consulting and Services, p. 111-221.

Jiang, S., Woodhead, J., Yu, J., Pan, J., Liao, Q., & Wu, N. (2002). A reconnaissance of Cu isotopic compositions of hydrothermal vein-type copper deposit Jinman, Yunnan, China. *Chinese Science Bulletin, 47*(3), 249-251.

Kavalieris, I., Khashgerel, B.-E., E. Morgan, L., Undrakhtamir, A., & Borohul, A. (2017). Characteristics and 40Ar/39Ar geochronology of the Erdenet Cu-Mo deposit, Mongolia. *Economic Geology, 112*(5), 1033-1053.

Khashgerel, B.-E., Rye, R. O., Hedenquist, J. W., & Kavalieris, I. (2006). Geology and reconnaissance stable isotope study of the Oyu Tolgoi porphyry Cu-Au system, South Gobi, Mongolia. *Economic Geology, 101*(3), 503-522.

Khasin, R., Marinov, N., Khurtz, C., & Yakimov, L. (1977). The copper–molybdenum deposit at Erdenetiin Ovoo in northern Mongolia. *Geology of ore deposits, 6*, 3-15.

Kimball, B. E., Mathur, R., Dohnalkova, A., Wall, A., Runkel, R., & Brantley, S. L. (2009). Copper isotope fractionation in acid mine drainage. *Geochimica et Cosmochimica Acta, 73*(5), 1247-1263.

Koval, P., Gerel, O., & Smirnov, V. (1982). *Association of porphyritic intrusions in the Erdenet area.* Paper presented at the Problems of Geology and Mineral Resources of Central and Eastern Mongolia. Thesis of IV Kherlen Expedition Symposium. Ulaanbaatar.

Krouse, H. R., & Mayer, B. (2000). Sulphur and oxygen isotopes in sulphate *Environmental tracers in subsurface hydrology* (pp. 195-231): Springer.

Lamb, M. A., & Cox, D. (1998). New 40 Ar/39 Ar age data and implications for porphyry copper deposits of Mongolia. *Economic Geology, 93*(4), 524-529.

Larson, P. B., Maher, K., Ramos, F. C., Chang, Z., Gaspar, M., & Meinert, L. D.

(2003). Copper isotope ratios in magmatic and hydrothermal ore-forming environments. *Chemical Geology, 201*(3-4), 337-350.

Li, W., Jackson, S. E., Pearson, N. J., Alard, O., & Chappell, B. W. (2009). The Cu isotopic signature of granites from the Lachlan Fold Belt, SE Australia. *Chemical Geology, 258*(1-2), 38-49.

Li, W., Jackson, S. E., Pearson, N. J., & Graham, S. (2010). Copper isotopic zonation in the Northparkes porphyry Cu–Au deposit, SE Australia. *Geochimica et Cosmochimica Acta, 74*(14), 4078-4096.

Liu, S.-A., Huang, J., Liu, J., Wörner, G., Yang, W., Tang, Y.-J., Chen, Y., Tang, L., Zheng, J., & Li, S. (2015). Copper isotopic composition of the silicate Earth. *Earth and Planetary Science Letters, 427*, 95-103.

Luck, J., Othman, D. B., Barrat, J., & Albarède, F. (2003). Coupled 63Cu and 16O excesses in chondrites. *Geochimica et Cosmochimica Acta, 67*(1), 143-151.

Luczaj, J., & Huang, H. (2018). Copper and sulfur isotope ratios in Paleozoic-hosted Mississippi Valley-type mineralization in Wisconsin, USA. *Applied Geochemistry, 89*, 173-179.

Maher, K. C., Jackson, S., & Mountain, B. (2011). Experimental evaluation of the fluid–mineral fractionation of Cu isotopes at 250° C and 300° C. *Chemical Geology, 286*(3-4), 229-239.

Maher, K. C., & Larson, P. B. (2007). Variation in copper isotope ratios and controls on fractionation in hypogene skarn mineralization at Coroccohuayco and Tintaya, Peru. *Economic Geology, 102*(2), 225-237.

Malitch, K. N., Latypov, R. M., Badanina, I. Y., & Sluzhenikin, S. F. (2014). Insights into ore genesis of Ni-Cu-PGE sulfide deposits of the Noril'sk Province (Russia): Evidence from copper and sulfur isotopes. *Lithos, 204*, 172-187.

Maréchal, C., & Sheppard, S. (2002). *Isotopic fractionation of Cu and Zn between chloride and nitrate solutions and malachite or smithsonite at 30 degrees and 50 degrees C.* Paper presented at the Geochimica et Cosmochimica Acta.

Maréchal, C. N., Télouk, P., & Albarède, F. (1999). Precise analysis of copper and zinc isotopic compositions by plasma-source mass spectrometry. *Chemical Geology, 156*(1), 251-273.

Markl, G., Lahaye, Y., & Schwinn, G. (2006). Copper isotopes as monitors of redox processes in hydrothermal mineralization. *Geochimica et Cosmochimica Acta, 70*(16), 4215-4228.

Mason, T. F., Weiss, D. J., Chapman, J. B., Wilkinson, J. J., Tessalina, S. G., Spiro, B., Horstwood, M. S., Spratt, J., & Coles, B. J. (2005). Zn and Cu isotopic variability in the Alexandrinka volcanic-hosted massive sulphide (VHMS) ore deposit, Urals, Russia. *Chemical Geology, 221*(3-4), 170-187.

Mathur, R., Dendas, M., Titley, S., & Phillips, A. (2010). Patterns in the copper isotope composition of minerals in porphyry copper deposits in southwestern United States. *Economic Geology, 105*(8), 1457-1467.

Mathur, R., Falck, H., Belogub, E., Milton, J., Wilson, M., Rose, A., & Powell, W. (2018). Origins of Chalcocite Defined by Copper Isotope Values. *Geofluids, 2018*.

Mathur, R., Munk, L., Nguyen, M., Gregory, M., Annell, H., & Lang, J. (2013). Modern and paleofluid pathways revealed by Cu isotope compositions in surface waters and ores of the Pebble porphyry Cu-Au-Mo deposit, Alaska. *Economic Geology, 108*(3), 529-541.

Mathur, R., Ruiz, J., Casselman, M. J., Megaw, P., & van Egmond, R. (2012). Use of Cu isotopes to distinguish primary and secondary Cu mineralization in the

Cañariaco Norte porphyry copper deposit, Northern Peru. *Mineralium Deposita, 47*(7), 755-762.

Mathur, R., Ruiz, J., Titley, S., Liermann, L., Buss, H., & Brantley, S. (2005). Cu isotopic fractionation in the supergene environment with and without bacteria. *Geochimica et Cosmochimica Acta, 69*(22), 5233-5246.

Mathur, R., Titley, S., Barra, F., Brantley, S., Wilson, M., Phillips, A., Munizaga, F., Maksaev, V., Vervoort, J., & Hart, G. (2009). Exploration potential of Cu isotope fractionation in porphyry copper deposits. *Journal of Geochemical Exploration, 102*(1), 1-6.

Mirnejad, H., Mathur, R., Einali, M., Dendas, M., & Alirezaei, S. (2010). A comparative copper isotope study of porphyry copper deposits in Iran. *Geochemistry: Exploration, Environment, Analysis, 10*(4), 413-418.

Moeller, K., Schoenberg, R., Pedersen, R. B., Weiss, D., & Dong, S. (2012). Calibration of the New Certified Reference Materials ERM-AE633 and ERM-AE647 for Copper and IRMM-3702 for Zinc Isotope Amount Ratio Determinations. *Geostandards and Geoanalytical Research, 36*(2), 177-199.

Molnár, F., Mänttäri, I., O'Brien, H., Lahaye, Y., Pakkanen, L., Johanson, B., Käpyaho, A., Sorjonen-Ward, P., Whitehouse, M., & Sakellaris, G. (2016). Boron, sulphur and copper isotope systematics in the orogenic gold deposits of the Archaean Hattu schist belt, eastern Finland. *Ore Geology Reviews, 77*, 133-162.

Moynier, F., Vance, D., Fujii, T., & Savage, P. (2017). The isotope geochemistry of zinc and copper. *Reviews in Mineralogy and Geochemistry, 82*(1), 543-600.

O'Neil, J. R. (1986). Theoretical and experimental aspects of isotopic fractionation. *Reviews in mineralogy, 16*, 1-40.

Ohmoto, H. (1972). Systematics of sulfur and carbon isotopes in hydrothermal ore deposits. *Economic Geology, 67*(5), 551-578.

Ohmoto, H. (1979). Isotopes of sulfur and carbon. *Geochemistry of hydrothermal ore deposits*, 509-567.

Palacios, C., Rouxel, O., Reich, M., Cameron, E. M., & Leybourne, M. I. (2011). Pleistocene recycling of copper at a porphyry system, Atacama Desert, Chile: Cu isotope evidence. *Mineralium Deposita, 46*(1), 1-7.

Ripley, E. M., Dong, S., Li, C., & Wasylenki, L. E. (2015). Cu isotope variations between conduit and sheet-style Ni–Cu–PGE sulfide mineralization in the Midcontinent Rift System, North America. *Chemical Geology, 414*, 59-68.

Ripley, E. M., & Li, C. (2003). Sulfur isotope exchange and metal enrichment in the formation of magmatic Cu-Ni-(PGE) deposits. *Economic Geology, 98*(3), 635-641.

Rouxel, O., Fouquet, Y., & Ludden, J. N. (2004). Copper isotope systematics of the Lucky Strike, Rainbow, and Logatchev sea-floor hydrothermal fields on the Mid-Atlantic Ridge. *Economic Geology, 99*(3), 585-600.

Rye, R. O. (1993). The evolution of magmatic fluids in the epithermal environment; the stable isotope perspective. *Economic Geology, 88*(3), 733-752.

Rye, R. O. (2005). A review of the stable-isotope geochemistry of sulfate minerals in selected igneous environments and related hydrothermal systems. *Chemical Geology, 215*(1-4), 5-36.

Savage, P. S., Moynier, F., Chen, H., Shofner, G., Siebert, J., Badro, J., & Puchtel, I. (2015). Copper isotope evidence for large-scale sulphide fractionation during Earth's differentiation. *Geochemical Perspectives Letters*.

Seal, R. R. (2006). Sulfur isotope geochemistry of sulfide minerals. *Reviews in*

Mineralogy and Geochemistry, 61(1), 633-677.

Seal, R. R., Alpers, C. N., & Rye, R. O. (2000). Stable isotope systematics of sulfate minerals. *Reviews in Mineralogy and Geochemistry, 40*(1), 541-602.

Seo, J. H., Lee, S. K., & Lee, I. (2007). Quantum chemical calculations of equilibrium copper (I) isotope fractionations in ore-forming fluids. *Chemical Geology, 243*(3-4), 225-237.

Sherman, D. M. (2013). Equilibrium isotopic fractionation of copper during oxidation/reduction, aqueous complexation and ore-forming processes: Predictions from hybrid density functional theory. *Geochimica et Cosmochimica Acta, 118*, 85-97.

Shields, W., Goldich, S., Garner, E., & Murphy, T. (1965). Natural variations in the abundance ratio and the atomic weight of copper. *Journal of Geophysical Research, 70*(2), 479-491.

Singer, D., Berger, V., & Moring, B. (2008). *Porphyry copper deposits of the world: Database and grade and tonnage.* US department of the Interior, US Geological Survey.

Sotnikov, V., Ponomarchuk, V., Berzina, A., & Travin, A. (1995). Geochronological borders of magmatism of Cu-Mo-porphyry Erdenetuin-Obo deposit (Mongolia). *Geologiya i Geofizika, 36*(3), 78-89.

Strebel, O., Böttcher, J., & Fritz, P. (1990). Use of isotope fractionation of sulfate-sulfur and sulfate-oxygen to assess bacterial desulfurication in a sandy aquifer. *Journal of Hydrology, 121*(1-4), 155-172.

Stürup, S., Hansen, H. R., & Gammelgaard, B. (2008). Application of enriched stable isotopes as tracers in biological systems: a critical review. *Analytical and bioanalytical chemistry, 390*(2), 541-554.

Taylor, B. (1987). Stable isotope geochemistry of oreforming fluids. *Short course in stable isotope geochemistry of low temperature fluids*, 337-445.

Walker, E. C., Cuttitta, F., & Senftle, F. E. (1958). Some natural variations in the relative abundance of copper isotopes. *Geochimica et Cosmochimica Acta, 15*(3), 183-194.

Wall, A., Heaney, P., Mathur, R., & Post, J. (2007). Insights into copper isotope fractionation during the oxidative phase transition of chalcocite, using time-resolved synchrotron X-ray diffraction. *Geochimica et Cosmochimica Acta, 71*(15), A1081-A1081.

Wall, A. J., Mathur, R., Post, J. E., & Heaney, P. J. (2011). Cu isotope fractionation during bornite dissolution: an in situ X-ray diffraction analysis. *Ore Geology Reviews, 42*(1), 62-70.

Wang, C., Bagas, L., Chen, J., Yang, L., Zhang, D., Du, B., & Shi, K. (2018). The genesis of the Liancheng Cu–Mo deposit in the Lanping Basin of SW China: Constraints from geology, fluid inclusions, and Cu–S–H–O isotopes. *Ore Geology Reviews, 92*, 113-128.

Wang, P., Dong, G., Santosh, M., Liu, K., & Li, X. (2017). Copper isotopes trace the evolution of skarn ores: A case study from the Hongshan-Hongniu Cu deposit, southwest China. *Ore Geology Reviews, 88*, 822-831.

Watanabe, Y., & Stein, H. J. (2000). Re-Os ages for the Erdenet and Tsagaan Suvarga porphyry Cu-Mo deposits, Mongolia, and tectonic implications. *Economic Geology, 95*(7), 1537-1542.

Weiss, D. J., Rehkdmper, M., Schoenberg, R., McLaughlin, M., Kirby, J., Campbell, P. G., Arnold, T., Chapman, J., Peel, K., Gioia, & Simone. (2008). Application of nontraditional stable-isotope systems to the study of sources and fate of

metals in the environment: ACS Publications.

Wilson, A. J., Cooke, D. R., Harper, B. J., & Deyell, C. L. (2007). Sulfur isotopic zonation in the Cadia district, southeastern Australia: exploration significance and implications for the genesis of alkalic porphyry gold–copper deposits. *Mineralium Deposita, 42*(5), 465-487.

Windley, B. F., Alexeiev, D., Xiao, W., Kröner, A., & Badarch, G. (2007). Tectonic models for accretion of the Central Asian Orogenic Belt. *Journal of the Geological Society, 164*(1), 31-47.

Wu, L.-Y., Hu, R.-Z., Li, X.-F., Liu, S.-A., Tang, Y.-W., & Tang, Y.-Y. (2017a). Copper isotopic compositions of the Zijinshan high-sulfidation epithermal Cu–Au deposit, South China: Implications for deposit origin. *Ore Geology Reviews, 83*, 191-199.

Wu, S., Zheng, Y. Y., Wang, D., Chang, H. F., & Tan, M. (2017b). Variation of copper isotopes in chalcopyrite from Dabu porphyry Cu-Mo deposit in Tibet and implications for mineral exploration. *Ore Geology Reviews, 90*, 14-24. doi:10.1016/j.oregeorev.2017.10.001

Yakubchuk, A., Degtyarev, K., Maslennikov, V., Wurst, A., Stekhin, A., & Lobanov, K. (2012). Tectonomagmatic settings, architecture, and metallogeny of the Central Asian copper province. *Soc. Econ. Geol., Inc. Spec. Publ, 16*, 403-432.

Yao, J., Mathur, R., Sun, W., Song, W., Chen, H., Mutti, L., Xiang, X., & Luo, X. (2016). Fractionation of Cu and Mo isotopes caused by vapor-liquid partitioning, evidence from the Dahutang W-Cu-Mo ore field. *Geochemistry, Geophysics, Geosystems, 17*(5), 1725-1739.

Zhao, Y., Xue, C., Liu, S.-A., Symons, D. T., Zhao, X., Yang, Y., & Ke, J. (2017). Copper isotope fractionation during sulfide-magma differentiation in the

Tulaergen magmatic Ni–Cu deposit, NW China. *Lithos, 286*, 206-215.

Zhu, X., Guo, Y., Williams, R., O'nions, R., Matthews, A., Belshaw, N., Canters, G., De Waal, E., Weser, U., & Burgess, B. (2002). Mass fractionation processes of transition metal isotopes. *Earth and Planetary Science Letters, 200*(1-2), 47-62.

Zhu, X., O'nions, R., Guo, Y., Belshaw, N., & Rickard, D. (2000). Determination of natural Cu-isotope variation by plasma-source mass spectrometry: implications for use as geochemical tracers. *Chemical Geology, 163*(1-4), 139-149.

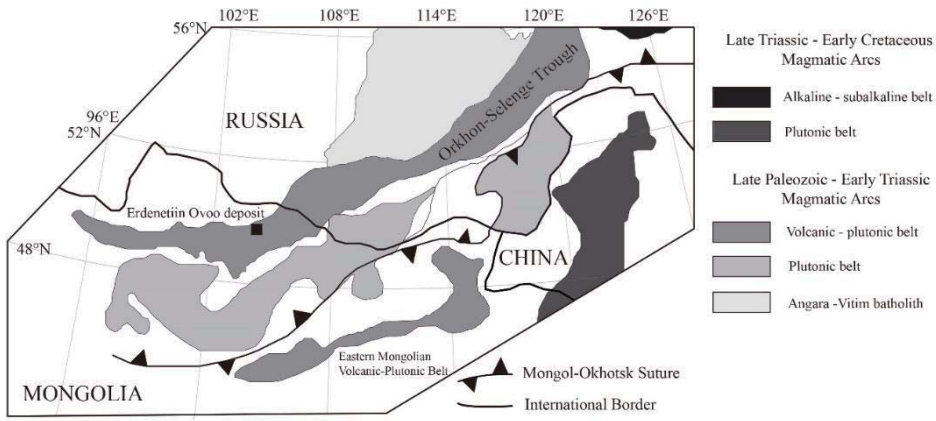

Figure 1.1. Schematic map of the Mongol-Okhotsk fold belt in northern Mongolia, southern Siberia and northern China (modified from Gerel & Munkhtsengel, 2005).

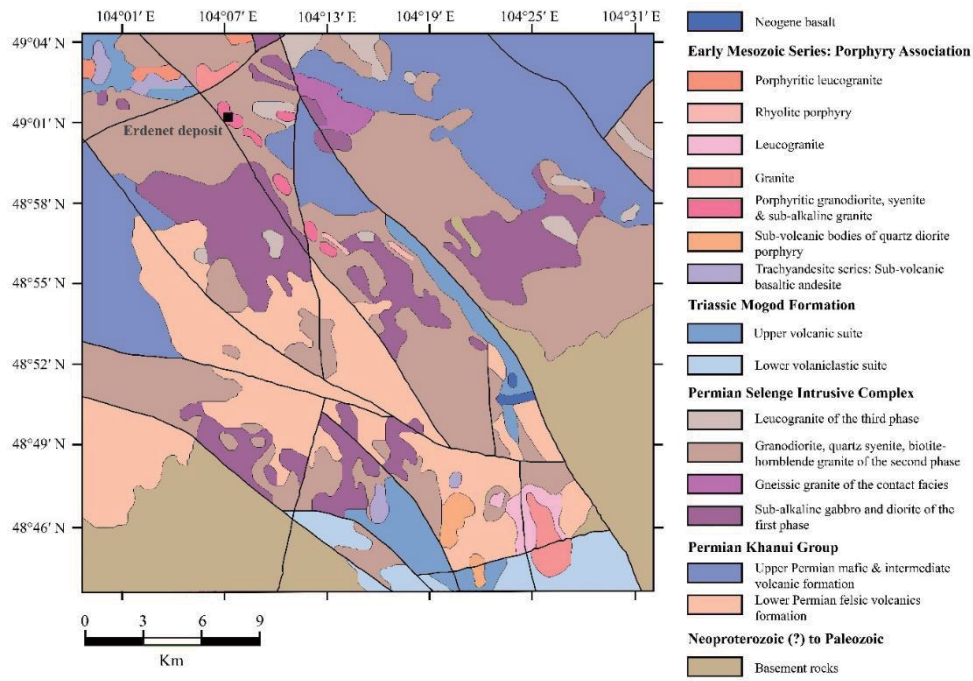

Figure 1.2. Geological map of the Erdenetiin Ovoo porphyry Cu-Mo deposit area (modified from Gerel & Munkhtsengel, 2005).

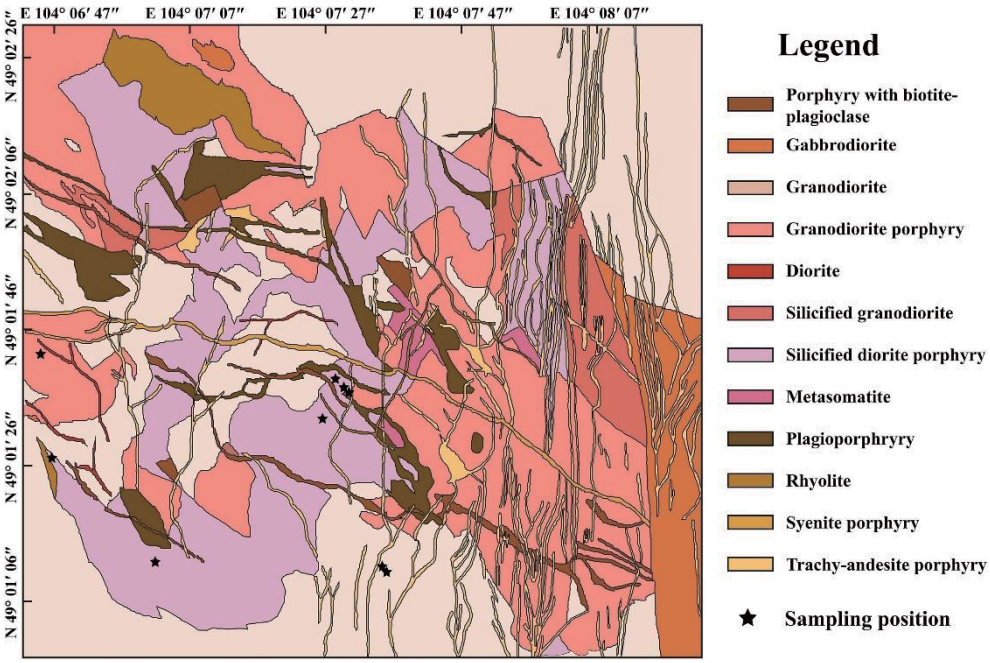

Figure 1.3. Geological map of the open-pit mine in the Erdenetiin Ovoo deposit and the sampling locations in this study.

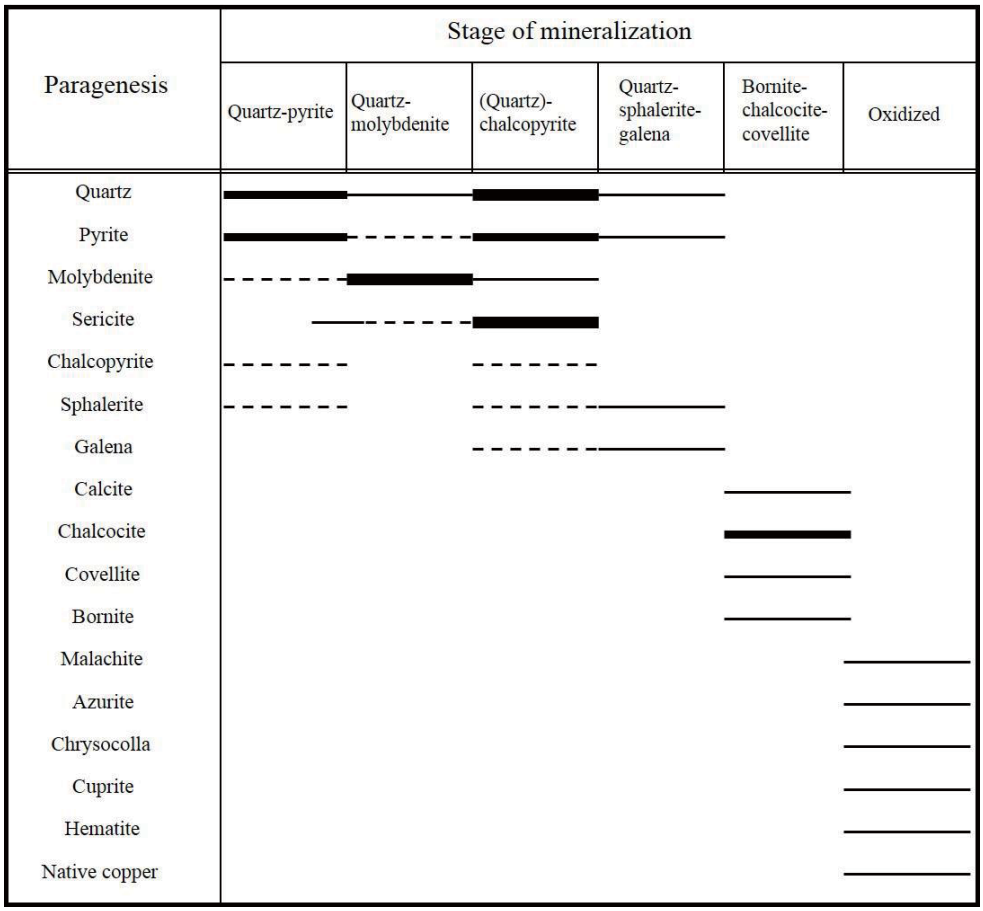

Figure 1.4. Paragenetic sequences of the major ore and gangue minerals in the Erdenetiin Ovoo deposit (modified from Gavrilova et al., 1984).

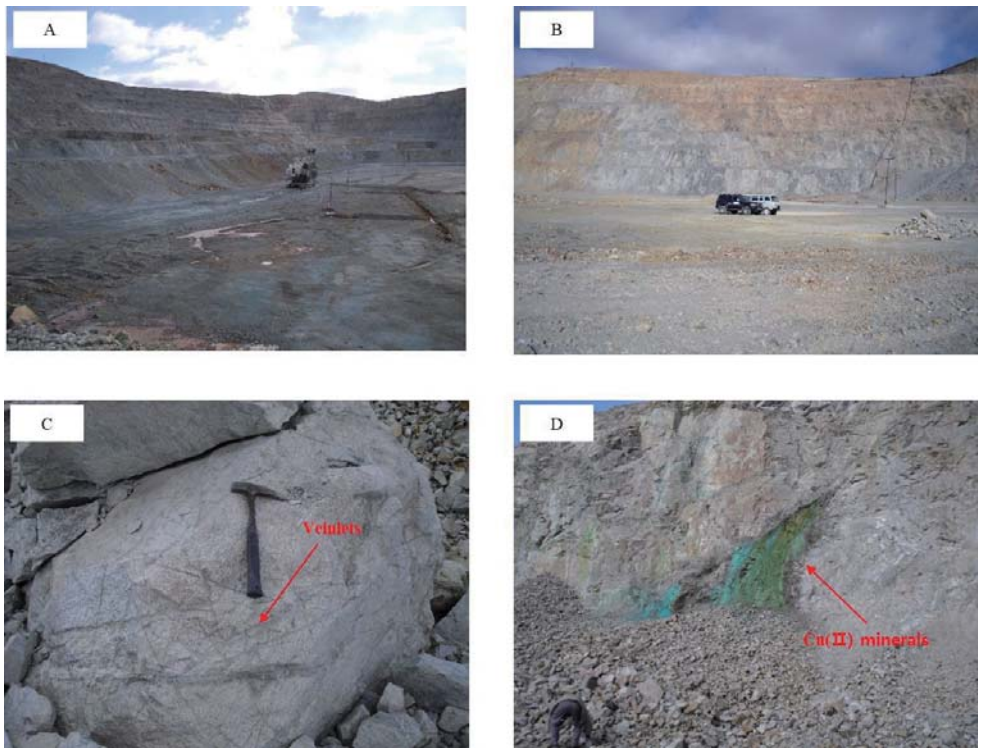

Figure 1.5. (A) & (B) General view of the open-pit mine in the Erdenetiin Ovoo deposit, (C) the vein-let developed in the host rocks and (D) the occurrence of Cu (II) minerals.

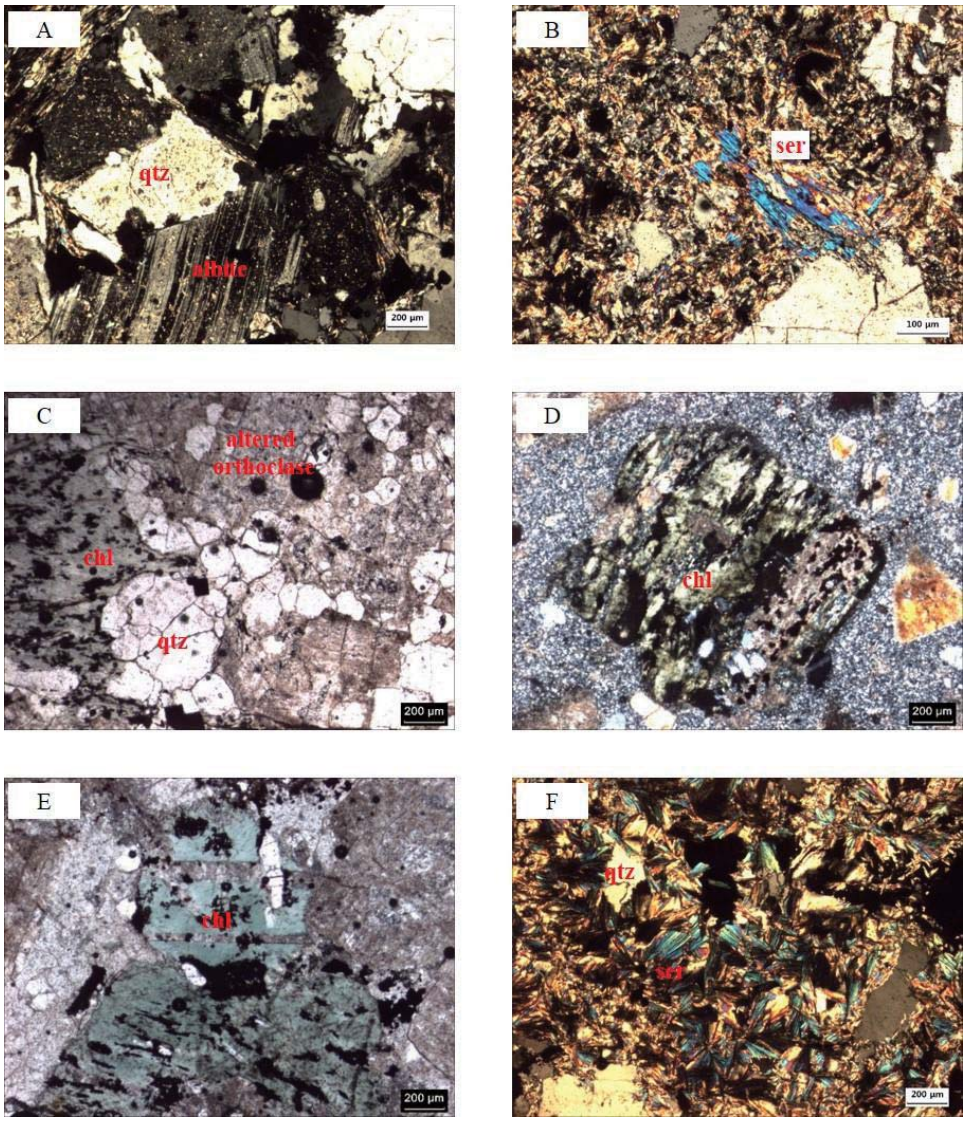

Figure 1.6. Representative photos of micrographs of the host rocks in the Erdenetiin Ovoo deposit. (A) Feldspar with distinct albite twinning and quartz with isometric texture; (B) plagioclase altered to sericite; (C) chlorite, quartz and altered orthoclase; (D) & (E) chlorite altered from mafic minerals and (F) a pervasive quartz-sericite alteration assemblage. Chl: chlorite, qtz: quartz, ser: sericite.

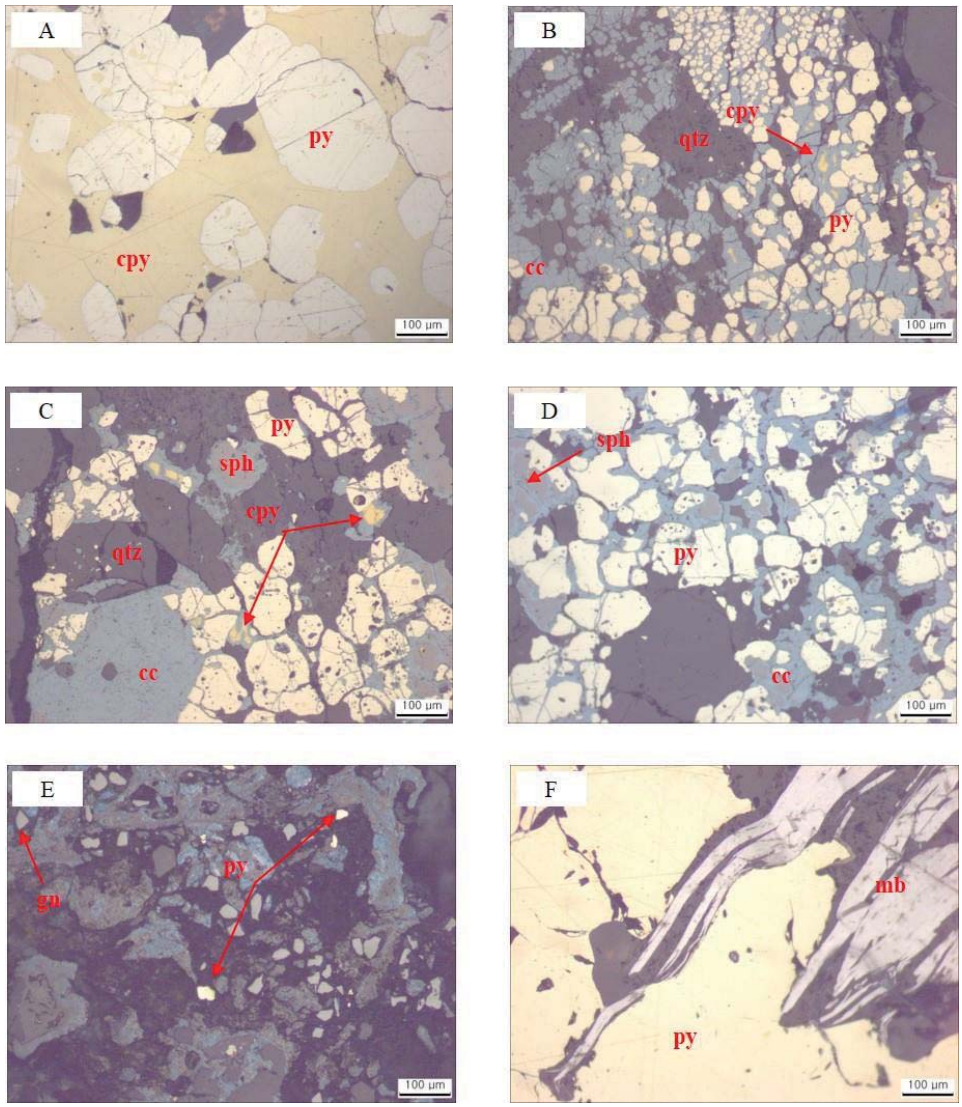

Figure 1.7. Representative photos of micrographs of the ore minerals in the Erdenetiin Ovoo deposit. (A) Dominant hypogene minerals such as chalcopyrite and pyrite; (B) the dominant secondary mineral, chalcocite, replacing other primary minerals; (C) hypogene minerals accompanied by sphalerite; (D) & (E) sphalerite and galena occurring with pyrite; and (F) molybdenite with quartz-molybdenite veins or quartz-pyrite veins. cc chalcocite, cpy: chalcopyrite, gn: galena, mb: molybdenite, py: pyrite, qtz: quartz, sph: sphalerite.

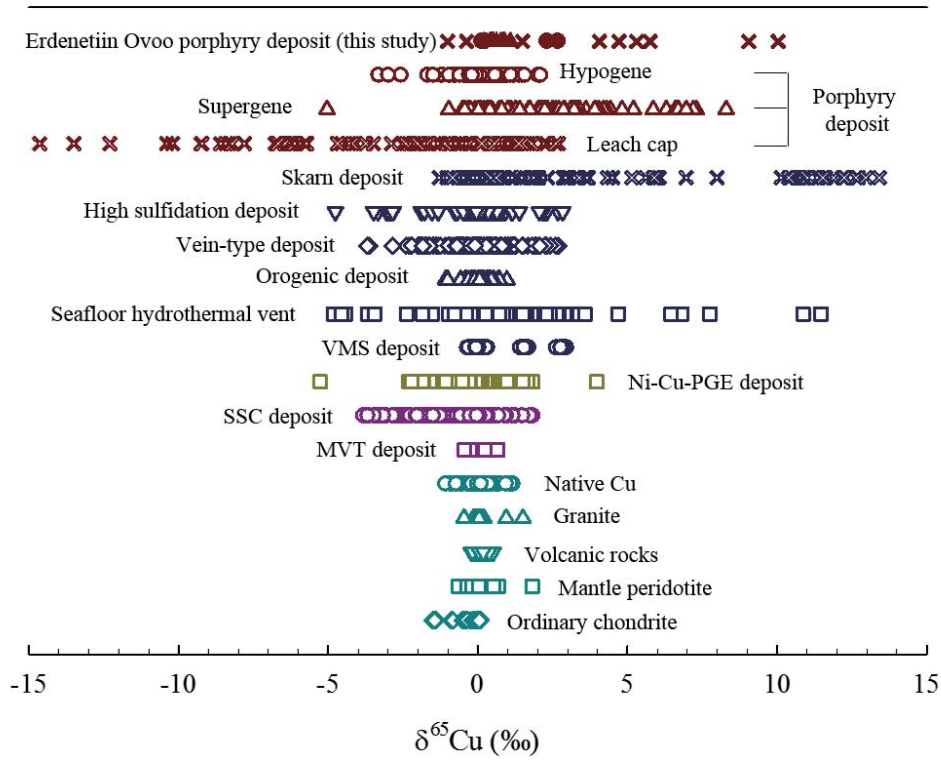

Figure 1.8. The range of $\delta^{65}Cu$ values in this study and various ore deposits from porphyry Cu deposits (Maréchal et al., 1999; Larson et al., 2003; Graham et al., 2004; Mathur et al., 2009; Li et al., 2010; Mathur et al., 2010; Mirnejad et al., 2010; Braxton & Mathur, 2011; Palacios et al., 2011; Mathur et al., 2012; Mathur et al., 2013; Asadi et al., 2015; Wu et al., 2017b), skarn deposits (Larson et al., 2003; Graham et al., 2004; Maher & Larson, 2007; Wang et al., 2017), high sulfidation epithermal deposits (Duan et al., 2016; Wu et al., 2017a), vein-type deposits (Jiang et al., 2002; Markl et al., 2006; Haest et al., 2009; Yao et al., 2016), orogenic deposits (Molnár et al., 2016; Wang et al., 2018), seafloor hydrothermal vents (Maréchal et al., 1999; Zhu et al., 2000; Rouxel et al., 2004; Berkenbosch et al., 2015), VMS

deposits (Mason et al., 2005; Ikehata et al., 2011), Ni-Cu-PGE deposits (Zhu et al., 2000; Larson et al., 2003; Malitch et al., 2014; Ripley et al., 2015; Zhao et al., 2017), SSC deposits (Asael et al., 2007; Asael et al., 2009; Li et al., 2010; Asael et al., 2012; Mathur et al., 2018), MVT deposits (Luczaj & Huang, 2018), and various igneous rocks such as native Cu, granite, volcanic rocks, mantle peridotite and ordinary chondrite (Luck et al., 2003; Li et al., 2009; Ikehata & Hirata, 2012; Liu et al., 2015; Huang et al., 2016).

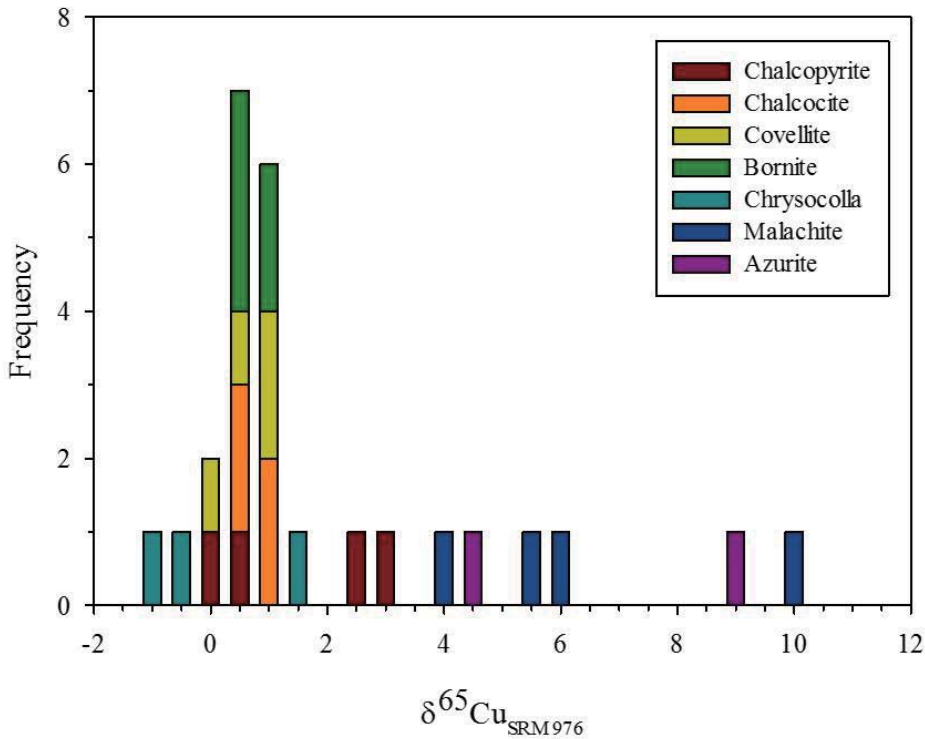

Figure 1.9. Histogram of the $\delta^{65}Cu$ values from the Cu ore minerals in the Erdenetiin Ovoo deposit.

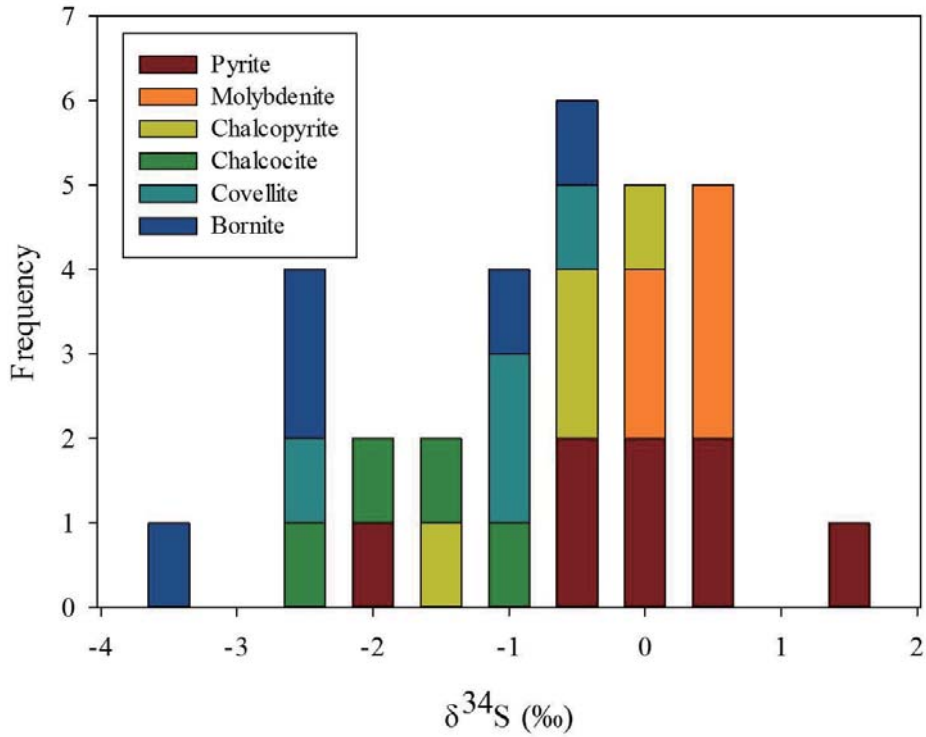

Figure 1.10. Histogram of the $\delta^{34}S$ values from sulfide minerals in the Erdenetiin Ovoo deposit.

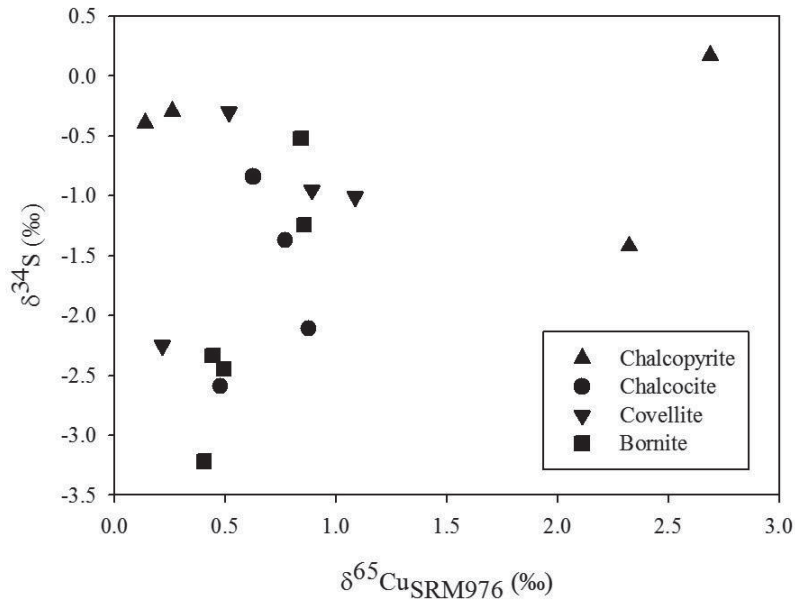

Fig. 1.11. The plot of Cu and S isotope data of major sulfide minerals in the Erdenetiin-Ovoo porphyry Cu-Mo deposit.

Table 1. 1. Column chromatography separation procedure for Cu isotope analysis.

Process	Medium	Volume (mL)
Resin loading	AG® MP-1M, 100-200 mesh	2
Resin cleaning*	0.5 N HNO_3	7
	7 N HCl	5
	H_2O	2
Conditioning	7 N HCl + 0.001% H_2O_2	6
Sample loading		0.5
		0.5
Na, Mg elution		10
Cu elution		2 × 12

* Repeat three times

Table 1. 2. Cu and S isotope compositions of ore minerals from the Erdenetiin Ovoo porphyry Cu-Mo deposit. AZ: azurite, BN: bornite, CC: chalcocite, CH: chrysocolla, CPY: chalcopyrite, CV: covellite, MC: malachite, MB: molybdenite, PY: pyrite.

Sample	Mineral	δ^{65}Cu	2SD	*n*	δ^{34}S			Altitude (m)
					I	II	mean	
ER01	CPY	2.69	0.03	6	0.2	0.2	0.2	1280
ER02	CPY	0.26	0.04	3	-0.3	-0.3	-0.3	1280
ER03	CPY	0.14	0.05	3	-0.4	-0.4	-0.4	1275
ER04	CC	0.77	0.02	3	-1.4	-	-1.4	1352
ER05	CC	0.48	0.05	3	-2.6	-	-2.6	1274
ER06	CH	-1.01	0.01	3	-	-	-	1332
ER07	CH	1.49	0.05	3	-	-	-	1332
ER08	CH	-0.37	0.02	3	-	-	-	1332
ER09	AZ	4.72	0.04	3	-	-	-	1332
ER10	MC	5.76	0.01	3	-	-	-	1332
ER11	CV	0.51	0.06	3	-0.5	-0.1	-0.3	1352
ER12	MC	10.0	0.07	2	-	-	-	1320
ER13	AZ	9.05	0.09	3	-	-	-	1310
ER14	CV+PY	0.21	0.14	2	-2.3	-	-2.3	1250
ER15	BN+PY	0.44	0.02	2	-2.3	-2.4	-2.3	1250
ER16	MB	-	-	-	0.1	0.2	0.2	1250
ER17	BN+PY	0.40	0.06	2	-3.2	-	-3.2	1250
ER18	CV+PY	1.09	0.06	3	-1.0	-1.0	-1.0	1310
ER19	PY	-	-		-0.5	-0.4	-0.5	1310
ER20	BN	0.86	0.03	3	-1.1	-1.4	-1.2	1265
ER21	CC	0.88	0.03	2	-2.1	-2.1	-2.1	1265
ER22	CV+PY	0.89	0.08	3	-1.1	-0.8	-1.0	1265
ER23	BN+PY	0.84	0.06	3	-1.9	0.9	-0.5	1265
ER24	PY	-	-		-0.4	-	-0.4	1265
ER25	CC+PY	0.63	0.07	2	-0.9	-0.8	-0.8	1280
ER26	BN+PY	0.49	0.09	3	-2.6	-2.3	-2.5	1335
ER27	PY	-	-		-2.0	-2.1	-2.0	1335
ER28	CPY	2.32	0.05	3	-1.4	-1.5	-1.4	1310
ER29	MC	5.31	0.03	3	-	-	-	1332
ER30	MC	4.06	0.06	2	-	-	-	1293
ER31	PY	-	-		0.4	0.4	0.4	1293
ER32	PY	-	-		0.4	0.2	0.3	1274
ER33	PY	-	-		-0.1	-0.3	-0.2	1280
ER34	MB	-	-		-0.2	-0.1	-0.2	1332
ER35	MB	-	-		0.3	0.5	0.4	1332
ER36	MB	-	-		0.4	0.5	0.5	1310
ER37	PY	-	-		1.3	1.2	1.3	1332
ER38	PY	-	-		-0.2	0.0	-0.1	1275
ER39	MB	-	-		0.4	0.4	0.4	1275

Chapter 2. Geology, mineralogy and stable isotope geochemistry of the Dzuunmod orogenic gold area in northern Mongolia: Constraints for ore genesis and sources

Abstract

The Dzuunmod gold area located in the North Khentii Gold belt (NKGB) of Central Northern Mongolia includes lode gold deposits such as Gatsuurt, Sujigtei, Ereen, Boroo and Ulaanbulag with several gold occurrences. These show similar alteration types and ore mineral assemblages, where sericite, siliceous and potassic alteration assemblages are major hydrothermal alteration types associated with gold mineralization. Pyrite and arsenopyrite are main sulfide minerals with minor amount of galena, sphalerite and chalcopyrite. Gold occurs as native form and invisible gold in pyrite and arsenopyrite. The major sulfide minerals are separated into earlier non-auriferous stage and later auriferous grains containing invisible gold. Native gold postdates the major sulfide mineralization.

Gold and arsenic content of pyrite grains indicates that gold exists mainly as solid solution form (Au^{+1}) in the Gatsuurt and Boroo deposit whereas gold nanoparticle (Au^{0}) is present in the Sujigtei deposit. High Co/Ni and Mo/Ni ratios of pyrite grain suggest a post-sedimentary or hydrothermal origin and the ore-forming fluid was significantly affected by fluid-rock interaction during mineralization processes.

Large variation of $\delta^{34}S$ values of pyrite and arsenopyrite from -2.6 ‰ to 17.2 ‰ indicates that sulfur seems to be mainly derived from a source with heterogeneous sulfur isotope composition, which is pyrite-bearing sediment mainly produced by the seawater sulfate reduction processes. Consistent with geological evidence, relatively positive $\delta^{34}S$ values suggest that sulfidation plays an important role for gold and sulfide precipitation. The calculated $\delta^{18}O$ values of hydrothermal fluid from the measured $\delta^{18}O$ values of quartz samples (from 14.7 ‰ to 17.7 ‰) indicate a metamorphic derivation of ore-forming fluid.

Based on the observation and analytical results in this study, gold mineralization

processes seem to occur several times by multiple input of hydrothermal fluid, fluid-rock interactions and mixing of ore-forming fluids. The Dzuunmod gold deposits are considered to be orogenic gold type influenced by fluid-rock interactions in the deposit area.

Keywords: Dzuunmod orogenic gold deposit, Geology, Stable isotope geochemistry, Ore genesis, Mongolia

1. Introduction

Orogenic gold deposit is one of main gold sources in the world and widely distributed in a long time range from Phanerozoic orogenic belts to Precambrian cratons (Goldfarb et al., 2001). It had been considered that they show consistent geological and geochemical characteristics including host rocks, alteration assemblages, fluid inclusion composition and oxygen isotope composition (Goldfarb et al., 2001 and references therein). Alteration assemblage of sericite, quartz, sulfide ± carbonate in greenschist-facies host rocks, low-salinity, CO_2-rich fluid and restricted range of $\delta^{18}O$ values (see the Samples and analytical method section for definition of notation) had been regarded as typical characteristics of this deposit type (Goldfarb et al., 2001; Goldfarb et al., 2005). However, with an accumulation of recent studies on the orogenic gold deposits, there seem to be many uncertainties to interpret the fluid and metal sources mainly attributed to complicate geological settings of the orogenic gold deposit (Goldfarb & Groves, 2015 and references therein).

The trace element geochemistry of sulfide grains such as pyrite and arsenopyrite from various ore deposits is able to provide a valuable information about fluid and metal sources in the deposit area as well as in the source area (e.g., Clark et al., 2004; Koglin et al., 2010; Zhu et al., 2011; Li et al., 2014; Niu et al., 2016; Yuan et al., 2018; Zhang et al., 2018). Trace element contents such as arsenic (As), cobalt (Co), Nickel (Ni) and molybdenum (Mo) and their ratios like Co/Ni and Mo/Ni have been utilized to constrain the source characteristics and change of fluid composition during ore-forming processes in the gold deposit (Su et al., 2008; Sung et al., 2009; Yuan et al., 2018; Zhang et al., 2018). Especially, the As and gold (Au) content in the auriferous pyrite and arsenopyrite can be an useful indicator of gold occurrence

form, estimated by an empirical gold solubility line as a function of As content (Reich et al., 2005).

Stable isotope measurement such as sulfur and oxygen has been pervasively used to constrain the fluid and sulfur sources and to understand the ore-forming processes in orogenic gold deposits for many decades (e.g., Goldfarb & Groves, 2015; Ding et al., 2016; LaFlamme et al., 2018a; Zhang et al., 2018). Most studies reported a narrow $\delta^{18}O$ range of auriferous hydrothermal fluids from 5 ‰ to 15 ‰ in the orogenic gold deposits (Kerrich, 1987; Bierlein & Crowe, 2000; Ding et al., 2016; Zhang et al., 2018). The $\delta^{18}O$ values of ore-forming fluid can be calculated from the $\delta^{18}O$ values of auriferous quartz vein and mineralization temperature estimated by fluid inclusion data (Vallance et al., 2004; Goldfarb & Groves, 2015; Wen et al., 2015; Hoefs, 2018) and/or arsenopyirte geothermometry (e.g., Koh et al., 1992; Zoheir, 2008; Deng et al., 2017). The uniform oxygen isotope composition of fluid favorably suggests the origination of ore-forming fluid from metamorphic devolatilization at depth (Goldfarb et al., 2005).

The S isotope ratio ($^{34}S/^{32}S$) of sulfide minerals in various ore deposits has been widely utilized to trace the sulfur sources and constrain the ore-forming processes (Ohmoto & Rye, 1979; Taylor, 1987; Rye, 2005; Seal, 2006). Especially, because it has been broadly accepted that gold is transported as bisulfide complexes in hydrothermal fluid under moderate salinities and temperature (e.g., Pokrovski et al., 2015), the $\delta^{34}S$ values accompanied with trace element composition of sulfides can be used to understand gold mineralization processes and to identify the sulfur sources in orogenic gold deposits (e.g., Hou et al., 2016; Ward et al., 2017; Yuan et al., 2018). The $\delta^{34}S$ values in in the orogenic gold deposit show an extremely large variation from -20 ‰ to 25 ‰ (Palin & Xu, 2000; Chang et al., 2008; Neumayr et al., 2008;

Hodkiewicz et al., 2009; Ward et al., 2017; Xu et al., 2017; LaFlamme et al., 2018b; Ma et al., 2018; Yuan et al., 2018; Zhang et al., 2018). Ridley and Diamond (2000) argued that the $\delta^{34}S$ values of sulfide minerals in orogenic gold deposits reflect the evolution of sulfur isotope composition of sulfur species during transportation within hydrothermal fluid. This implies that the broad range of the $\delta^{34}S$ values in the orogenic deposits has been caused by not only multiple sources (e.g., Goldfarb et al., 2005; Goldfarb & Groves, 2015), but gold precipitation mechanisms such as fluid-rock interaction (e.g., Palin & Xu, 2000; Evans et al., 2006; Ward et al., 2017), phase separation by rapid pressure changes (e.g., Hodkiewicz et al., 2009), fluid mixing (e.g., LaFlamme et al., 2018a) and/or input of granitic magma (e.g., Neumayr et al., 2008; Hou et al., 2016).

The North Khentii Gold Belt (NKGB) is located in the Khangai-Khentii basin, central northern Mongolia within the Mongol-Okhotsk orogenic belt and includes many lode and placer gold deposits with long history of gold production. The lode gold deposits contain Boroo, Gatsuurt, Sujigtei, Ereen, Ulaanbulag deposit and several gold occurrences such as Balj, Biluut, Urt and Baavgait (Dejidmaa, 1996), compiled to the Dzuunmod gold area. The Boroo and the Gatsuurt deposit have been estimated to have large tonnage, which is more than 50 Au tons, whereas the other deposits are lack of economic significance (Dejidmaa, 1996; Gerel et al., 1999). These deposits have been described to show similar geological and geochemical characteristics such as host rocks, alteration assemblages, mineralization types by several previous studies, classified as an orogenic gold deposit type (Cluer et al., 2005; Goldfarb et al., 2014; Khishgee et al., 2014; Khishgee & Akasaka, 2015). Cluer et al. (2005) reported the $^{40}Ar/^{39}Ar$ age dating result of hydrothermally altered minerals, suggesting that the gold mineralization in the study area occurred in early

Mesozoic. Compared to mineralogical and petrological studies conducted by several researchers mentioned above, there have been few researches about stable isotope compositions of the Dzuunmod gold area.

Here, we reported the trace element composition of auriferous pyrite and arsenopyrite, $\delta^{34}S$ values of sulfide minerals, and $\delta^{18}O$ values of the quartz grains with mineralogical and petrological observation of ore and gangue minerals to (1) identify the geological and geochemical features of the deposit, (2) constrain the fluid and sulfur sources related to the gold mineralization, and (3) understand the ore-forming processes in the Dzuunmod area.

2. Geological setting

2.1 Regional geological setting

Central Asian Orogenic Belt (CAOB) is one of the largest orogenic accretionary complexes on Earth, extending from the Siberian craton in the north to the Sino-Korean and the Tarim cratons in the south (Şengör et al., 1993; Sengor & Natal'In, 1996; Yakubchuk, 2001; Windley et al., 2007; Donskaya et al., 2013). It was formed by the accretion of island arcs, oceanic islands, back-arc basins, accretionary wedges, ophiolites and Precambrian microcontinents during the collisional event of the Siberian and Sino-Korean cratons from *c.* 1.0 Ga to *c.* 250 Ma (Zonenshain et al., 1990; Şengör et al., 1993; Khain et al., 2003; Xiao et al., 2003; Xiao et al., 2004; Windley et al., 2007; Donskaya et al., 2013). The Mongol-Okhotsk orogenic belt (or suture) is the youngest part of the CAOB and formed during the closure of the Mongol-Okhotsk ocean (or the Kangai-Khantii Ocean named by Şengör et al. (1993)) between the Siberian and Amurian blocks from the late Paleozoic to mid-late Mesozoic (Fig. 2.1), although its opening and closing time have been debated by

several researchers (Zonenshain et al., 1990; Şengör et al., 1993; Zorin, 1999; Parfenov et al., 2001; Khain et al., 2003; Xiao et al., 2003; Tomurtogoo et al., 2005; Windley et al., 2007; Donskaya et al., 2013).

The Khangai-Khentii basin in the north-central Mongolia was the part of the Mongol-Okhotsk ocean and separated by a northwest fault system into Khangai basin in the west and Khentii basin in the east (Fig. 2.2) (Zonenshain et al., 1990; Şengör et al., 1993; Sengor & Natal'In, 1996; Yin & Nie, 1996; Kelty et al., 2008). It mainly consists of Devonian to Carboniferous turbidite sequences intruded by Mesozoic and Cenozoic igneous rocks and is mixed with Ordovician and Silurian chert and basalt (Fig. 2.2) (Şengör et al., 1993; Zorin, 1999; Badarch et al., 2002; Kelty et al., 2008; Bussien et al., 2011; Hara et al., 2013). Several researchers suggested that the turbidite sequences were accumulated in an active continental margin, back-arc basin or forearc basin (Zorin, 1999; Badarch et al., 2002; Kelty et al., 2008; Bussien et al., 2011).

2.2 Deposit geological setting

The Dzuunmod gold area is located in the North Khentii Gold Belt (NKGB) within the Haraa terrane classified into the back-arc or forearc basin and suggested to be formed during the closure of the Mongol-Okhotsk Ocean (Fig. 2.2 & 2.3) (Badarch et al., 2002; Cluer et al., 2005; Goldfarb et al., 2014; Khishgee et al., 2014; Khishgee & Akasaka, 2015). The NKGB is bounded by two left-lateral fault systems, which is the Bayangol fault in the northwest and Yeroogol fault system in the southeast with SW-NE trending (Fig. 2.3). It is mostly composed of Cambrian to early Ordovician greenschist metasedimentary rocks such as sandstone, siltstone, argillite, phyllite, schist with minor amount of conglomerate and tuff, which is

intruded by Ordovician to Devonian igneous rocks (Fig. 2.3) (Badarch et al., 2002).

Three major lithological units comprise the NKGB (Tumur et al., 1995; Gerel et al., 1999; Badarch et al., 2002; Cluer et al., 2005; Hendry et al., 2006; Hou et al., 2010): (1) Late Proterozoic to Early Paleozoic metasedimentary rocks of the Yeroo series (greenschist metamorphic rocks) and Haraa series (sandstone, shale, siltstone, conglomerate, phyllite and schist) and late Ordovician Boroo granitoids complex; (2) Early Permian Dzuunmod felsic pluto-volcanic (phyolite porphyry, tuffaceous andesite lava and breccia) and sedimentary rocks (shale, sandstone and conglomerate); and (3) Late Mesozoic coal-bearing sedimentary rocks and conglomerates. The metasediment of the Early Cambrian to Early Ordovician Haraa group was intruded by multiple phases of the Middle to Late Ordovician Boroo granitoids complex (Cluer et al., 2005; Hendry et al., 2006). Volcanic rocks of Early Ordovician Ulaan-Under formation are located in north and north-west Dzuunmod gold area and intrusive bodies and dykes including unaltered medium-grained leucogranite, monzodiorite and diorite occur in the central part of the Dzuunmod gold area (Altanzul et al., manuscript in preparation).

The Dzuunmod gold area including Gatsuurt, Sujigtei and Khargana deposit is separated into the Dzuumnod massive volcanics and the Boroo complex granite plutons by the Yeroogol fault system (Hendry et al., 2006). The Sujigtei fault, high-angle fault (oriented 40°) with NE-trending, is a boundary between the Dzuunmod volcanic rocks and the Boroo granitoids complex. Displacement along the fault seems to be 800 meters with the left-lateral movement. Because tectonic clay (or fault gouge) and clay-mylonitic alteration zone is very narrow, the Sujigtei fault is suggestive to play a second or higher order role in the fault system relative to the Yeroogol fault (Hendry et al., 2006). However, the Sujigtei fault and parallel faults

are one of major structural elements controlling the distribution of gold mineralization in the Gatsuurt, Sujigtei and Khargana deposit.

2.3 Ages of the deposits

The U-Pb isotope compositions of zircon grains from 5 samples in Dzuunmod gold area were measured by SHIRMP (Altanzul et al., manuscript in preparation). A weighted mean of $^{206}Pb/^{238}U$ concordant age is 476.2 ± 3.0 Ma of DZ-GR-3, 473.1 ± 3.8 Ma of AZ-DZ-177, 471.4 ± 2.7 Ma of GT-425-4.0m, 467.0 ± 3.8 Ma of UB-60 and 464.6 ± 4.9 Ma of UB-78, where first three and the other ages are corresponding to early and middle Ordovician, respectively. These ages are interpreted to indicate an occurrence of the Boroo granitoids complex intrusion during Ordovician period. The U-Pb ages of the Gatsuurt deposit area are slightly older than those of the Ulaanbulag deposit area, although the error range (1σ) of them overlaps. This means that there is small but distinct difference of intrusion timing between the Gatsuurt and Ulaanbulag deposit area.

Previous study on the U-Pb age dating of ore-bearing granite in the Boroo deposit reported 452.2 ± 3.9 Ma and 441.9 ± 6.6 Ma U-Pb age of zircon, corresponding to the late Ordovician period (Hou et al., 2010). These slightly younger U-Pb ages indicate that the intrusion of the Boroo granitoid complex seems to occur about 20 – 30 Ma earlier in the Boroo deposit area than Gatsuurt and Ulaanbulag deposit area.

It is suggested that there was temporal variation of the intrusion timing of the Boroo granitoid complex in the Dzuunmod gold area. In the study area, the Gatsuurt and the Boroo deposit are located in the most southeastern and northwestern part, whereas the Ulaanbulag deposit is positioned in the middle of them (Fig. 2.3). The

U-Pb age of zircon grains is getting younger toward from the Gatsuurt deposit of the early Ordovician to the Boroo deposit area in the late Ordovician. This indicates that the Boroo granitoids complex intruded earlier in the Gatsuurt deposit area and occurred in the Ulaanbulag and the Boroo deposit area successively.

In contrast to the intrusion age of the Boroo granitoids complex, which is the host rock of gold mineralization in the Dzuunmod area, mineralization of gold seems to occur in Mesozoic period. Cluer et al. (2005) reported the $^{40}Ar/^{39}Ar$ age dating results of hydrothermal alteration minerals such as sericite and muscovite in the Gatsuurt and the Boroo deposit. The $^{40}Ar/^{39}Ar$ age of the Gatsuurt deposit is *ca.* 178 Ma corresponding to early Jurassic, while the mineralization age of the Boroo deposit range from 208.3 ± 1.9 Ma to 186.2 ± 1.6 Ma of late Triassic to early Jurassic period (Cluer et al., 2005). Because the mineralization of gold is related to the hydrothermal alteration (e.g., sericite alteration) in the study area, it seems to interpret that the hydrothermal alteration age represents the mineralization age. Therefore, the intrusion of the Boroo granitoid complex and gold mineralization event occurred in the significantly different period, indicating that the completely different tectonic or geological events were related to the intrusion and mineralization processes.

3. Samples and analytical methods

More than 100 ore and host rocks samples were collected from the drill core for microscopic observation, U-Pb age dating, trace element and stable isotope analysis. Representative polished ore sections and thin sections were made for mineral identification by microscope and Electron Probe Micro Analyzer (EPMA). Sulfide and quartz grains were separated from the crushed rock samples by hand-picking method for sulfur and oxygen isotope analysis.

Trace element composition of ore minerals was analyzed by EPMA (JEOL, JXA-8530F PLUS) in the Center for research facilities of Gyeongsang National University, Korea. Accelerating voltages were 15 kV and beam size was 5 μm.

The sulfide minerals were prepared as a powder and put into a 3.5 x 5 mm tin-foil cup. The combustion was conducted in the tube packed with reagent materials of quartz wool, quartz chips and ultrahigh purity Cu wire under the 1030 °C in the Elemental Analyzer (EA). The sulfur isotope composition (^{32}S and ^{34}S) was measured by Continuous Flow (CF)-EA-IRMS (IsoPrime-EA) at the School of Earth and Environmental Sciences (SEES), Seoul National University. The standard material (IAEA S-1) was bracketed within the samples. The data were calculated by linear regression of the standard and the sulfur isotope composition of the samples is expressed using δ-notation relative to the Vienna-Canyon Diablo Troilite (V-CDT) as follows:

$$\delta^{34}S_{(V\text{-}CDT)} = [(^{34}S/^{32}S)_{sample} - (^{34}S/^{32}S)_{(V\text{-}CDT)}]/(^{34}S/^{32}S)_{(V\text{-}CDT)}$$

Typically, $\delta^{34}S_{(V\text{-}CDT)}$ values are reported in per mil (‰, parts per thousand) which means that δ-value obtained by above equation are then multiplied by 1000. All samples and standards were analyzed in duplicate, and the external reproducibility for long-term analyses was better than ± 0.2 ‰.

The quartz grains were hand-picked from crushed ore samples and prepared as a fine-grain. The oxygen isotope composition of quartz grains was analyzed using a CO_2-laser BrF_5 fluorination system installed at Korea Polar Research Institute (KOPRI). The system is composed of four major parts: (1) reaction chamber, (2) 25W CO_2 laser, (3) purification line and (4) mass spectrometer (MAT 253 plus, Thermo Fisher Scientific) controlled by ISODAT 3.0 software. The detail explanation of method for oxygen isotope analysis is described in Ahn et al. (2012).

The external reproducibility of oxygen isotope analysis is better than ± 0.05 ‰ (2σ) for $\delta^{18}O$ based on repetitive analyses of obsidian in-house standard and expressed using δ-notation relative to the Vienna Standard Mean Ocean Water (V-SMOW) as follows:

$$\delta^{18}O_{(V\text{-}SMOW)} = [(^{18}O/^{16}O)_{sample} - (^{18}O/^{16}O)_{(V\text{-}SMOW)}]/ (^{18}O/^{16}O)_{(V\text{-}SMOW)}$$

Typically, $\delta^{18}O_{(V\text{-}SMOW)}$ values are reported in per mil (‰, parts per thousand) which means that δ-value obtained by above equation are then multiplied by 1000.

4. Characteristics of the Dzuunmod gold area

In the Dzuunmod gold area, six alteration types are distinctly observed including sericitic, siliceous, postassic, prrpylitic, carbonation and argillic alteration, indicating the multiple event of hydrothermal alteration. The gold mineralization is associated with first three alteration types. The sericitic alteration consists of sericite, quartz and pyrite assemblage and is mainly related to a mineralization of low-sulfide with gold-quartz vein style. This assemblage intensely occurs in rhyolite, granite and even metasedimentary rocks. The siliceous alteration mainly develops as quartz veinlets, stockwork and massive style. The potassic alteration is divided into massive core coincident with potential gold mineralization and peripheral alteration. The former is confined to the core of the Gatsuurt deposit and adjacent to the Sujigtei fault whereas the latter exists in volcanic rocks and makes the outer boundary of the Main zone.

There are three types of major gold mineralization in the Dzuunmod gold area: disseminated/stockwork, quartz vein and silica. First type occurs in granite and rhyolite porphyry with the sericitic and potassic alteration assemblages with pyrite and arsenopyrite as a major sulfide mineral. Gold exists as invisible form in the

sulfide grain. The quartz vein type includes major sulfide minerals and native gold with minor sphalerite and galena. The silica type is subdivided into pervasive quart silica zone (PQSZ), black quartz zone (BQZ) and normal silica. The PQSZ consists of medium to coarse-grained quartz with visible gold, fine-grained arsenopyrite and pyrite. The BQZ occurs only in the Central zone and contains very fine-grained quartz, pyrite, arsenopyrite and minor amount of chalcopyrite and tetrahedrite. The normal silica zone is composed of fine-grained quartz, sericite with few sulfide minerals. The geological characteristics of major gold deposits and occurrences in study area are summarized in Table 2.1.

4.1. Gatsuurt deposit

The Gatsuurt deposit (Fig. 2.4-a), first discovered in 1998, is mainly hosted by metasedimentary rocks (Haraa formation) and volcanic rocks of rhyolite and rhyolite porphyry (Fig. 2.5-a & b) bounded by the left-lateral Sujigtei fault (Fig. 2.4-b & c). The Gatsuurt deposit is composed of Main zone and Central zone, South Slope and GT60 (Fig. 2.4-a) and the style and magnitude of gold mineralization varies depending on the host rocks. The Main zone consists of sericitic and siliceous alteration in sulfidized rhyolite porphyry with disseminated/stockwork and quartz vein mineralization types (Fig. 2.5-b). Pyrite and arsenopyrite are major sulfide minerals with quartz, sericite and carbonate as a major gangue mineral. The Central zone, South Slope and GT60 is hosted by Boroo granitoids complex consisting of hornblende-biotite granite, granodiorite and diorite (Fig. 2.5-a & c) and metasedimentary rocks of Haraa formation (Fig. 2.5-d). The disseminated/stockwork type occurs in the Central zone in altered granite while silica mineralization along the fault and quartz vein type exist in the metasedimentary rocks. The South Slope

zone is located in Southeast side of the Central zone and the host rock is granite with siliceous, sericitic and potassic alteration. The GT60 is located in Northwest side of the Central zone along the Sujigtei fault (Fig. 2.4-a) with disseminated/stockwork mineralization in granite and diorite altered by siliceous, sericitic and potassic alteration.

Gold mineralization of the Gatsuurt deposit includes all three mineralization types. The disseminated/stockwork type is observed in granite with an assemblage of quartz, sericite and K-feld spar. The major sulfide minerals are pyrite and arsenopyrite (Fig. 2.6-a & b) and quartz, sericite and carbonate occur as a gangue mineral. Silica type including all three sub-classified types occurs only in the Central zone and consists of fine-grained quartz with minor sericite and disseminated sulfide minerals (Fig. 2.5-e). Especially, the BQZ is uniquely detected in the Central zone. Pyrite and arsenopyrite are major sulfide minerals and gold grain occurs both as native form (Fig. 2.6-c) and invisible gold in the sulfide minerals. Quartz vein type occurs in most volcanic rocks and granitoids such as rhyolite and granite (Fig. 2.5-f) altered by sericite alteration. Quartz veins contain major sulfide minerals and native gold with minor amount of sphalerite and galena (Fig. 2.6-c, d & e). Pyrite and arsenopyrite occur with minor amount of galena, sphalerite and native gold in quartz vein type ores (Fig. 2.6-d & e) whereas major and minor ore minerals occur separately in the other types, indicating that they formed at different mineralization stage.

4.2 Sujigtei deposit

The Sujigtei deposit, 7 km southwest away from the Gatsuurt deposit (Fig. 2.3), was first discovered in early 20th century and has been mined as several small

underground mines along the fault. The main host rock for gold-bearing quartz vein and disseminated/stockwork mineralization is granite whereas rhyolite and rhyolite porphyry are barren (Fig. 2.5-g). The NE-trending faults with N45E/85SE show no apparent displacement and the largest lode structure is referred to as 'vein-1'(Fig. 2.5-h). The main fault zone is composed of fault gouge and siliceous altered materials and important gold mineralization is associated with the fault. The major sulfide minerals are pyrite and arsenopyrite with minor galena and Cu-bearing minerals such as chalcopyrite, bornite, covellite and chalcocite (Fig. 2.6-f). Also, very tiny native gold grains are observed within pyrite grain (Fig. 2.6-g).

4.3 Ereen Deposit

The Ereen deposit is located in the central part of the Dzuunmod felsic pluto-volcanic rocks zone and about 3.4 km west away from the Gatsuurt deposit (Fig. 2-3). It was discovered in early 20th century and two quartz veins with NE-trending has been explored by ten trenches (Fig. 2.4-d). The main host rocks are volcanic rocks such as altered rhyolite (Fig. 2.5-i) and the gold-bearing veins are controlled by faults (Fig. 2.4-e). The alteration types of the Ereen deposit are very similar to those of the Gatsuurt deposit, which are quartz-sericite alteration, potassic alteration and quartz vein. The quartz-sericite alteration occurs in the vicinity of the quartz veins and ore minerals such as pyrite, arsenopyrite, gold, galena, sphalerite and chalcopyrite exist within quartz veins. The gold grains occur as both native form and invisible gold in the sulfide minerals.

4.4 Boroo deposit

The Boroo deposit (Fig. 2.4-f) is the largest gold deposit in the Dzuunmod area

and has been mined as an open-pit mine with four main ore zones from 2004 to 2010 (Cluer et al., 2005; Khishgee & Akasaka, 2015). The NE-trending thrust fault, which is the part of the Yeroogol fault system, develops and has been considered to control the gold mineralization in the deposit (Cluer et al., 2005). The fault separates the metasedimentary rocks of the Haraa formation and the Boroo granitoids complex. The altered sandstone and silicified granite contains the gold and sulfide grains as a disseminated form, stockwork and quartz veins (Fig. 2.5-j). The alteration assemblages are very similar to those of the Gatsuurt deposit and the most pervasive alteration represents a quartz-sericite-carbonate assemblage. Pyrite and arsenopyrite are the most abundant sulfide minerals with minor amount of sphalerite, galena and chalcopyrite (Fig. 2.6-h). Native gold grains are observed in the quartz veins and as a disseminated in the host rocks.

4.5 Ulaanbulag deposit

The Ulaanbulag deposit is located in the western part of the the Dzuunmod felsic pluto-volcanic rocks zone and 19 km away from the Gatsuurt deposit (Fig. 2.3). It was discovered in 2003 as a small deposit with low grade. The host rocks are the meta-sedimentary rocks (Haraa formation) and the Boroo granitoids complex intruding the Haraa formation. The Ulaanbulag thrust fault is major structural feature controlling the gold mineralization (Fig. 2.4-g). An alteration assemblage of quartz, sericite and pyrite occurs and the mineralization types consist of the quartz veins (Fig. 2.5-k) and the disseminated/stockwork. Pyrite, arsenopyrite, iron oxides and visible gold are present with minor amount of galena, chalcopyrite, sphalerite.

4.6 Khargana deposit

The Khargana deposit is located in the southern part of the Dzuunmod felsic pluto-volcanic rocks zone and 15 km away from the Gatsuurt deposit (Fig. 2.3). It has been developed as a small underground mine. The main host rock is rhyolite and the gold mineralization is composed of the disseminated/stockwork and the quartz vein type with an assemblage of quartz, sericite and K-feldspar. The major sulfide minerals are pyrite and arsenopyrite with few Cu-bearing sulfide minerals and galena. The quartz veins are parallel to the NE-trending Sujigtei fault with steep southeast dip.

4.7 Balj occurrence

The Balj occurrence is located 4.5 km away from the Gatsuurt deposit. It was explored and mined from 2010 to 2012 as both open pit and under-mining style, but could not be further mined due to low grade and tonnage of gold. The host rocks are the meta-sedimentary rocks (Haraa formation) and the Boroo granitoids complex (Fig. 2.4-h & i). The NE-trending fault in the Balj occurrence is considered to control the mineralization processes in this area (Fig. 2.4-h & i). The auriferous quartz veins occur in the sandstone (Fig. 2.5-l). The alteration type and ore mineralogy is very similar with the Gatsuurt deposit, which is pervasive quartz and sericite assemblage with pyrite and arsenopyrite as major sulfide minerals.

4.8 Biluut occurrence

The Biluut occurrence is located in the the Dzuunmod felsic pluto-volcanic rocks zone (Fig. 2.3) and hosted by rhyolite porphyry and rhyolite. The gold mineralization type is quartz vein controlled by fault and major sulfide minerals are pyrite and arsenopyrite within the quartz vein.

4.9 Paragenetic sequences

As mentioned above, gold deposits in the Dzuunmod area represent similar alteration assemblages and ore mineralogy usually controlled by NE-trending fault (Table 2.1). The Gatsuurt deposit are divided into three distinct ore types; disseminated and stockwork, quartz vein and silica type. Previous studies reported the mineralogical and petrological observation of the Gatsuurt and the Boroo deposit, which are the largest deposits in the study area (Khishgee et al., 2014; Khishgee & Akasaka, 2015). First two types of mineralization occur in the Boroo deposit without silica zone. They divided each mineralization type into four stages in disseminated and stockwork type, five stages in quartz vein type and two stages in silicified ore type.

Quartz is major gangue mineral pervasively developed in all deposits. Major ore minerals, pyrite and arsenopyrite, occur in all mineralization types, but are concentrated in early stages of each types. Both minerals are more abundant in disseminated and stockwork ores, and silicified ores than quartz vein ores. Interestingly, auriferous pyrite and arsenopyrite postdates the non-auriferous ones in both mineralization types and deposits. Then, native gold mineralization occurs after the major sulfide mineralization stages. Other minor sulfides including galena, sphalerite, chalcopyrite, tetrahedrite, tennantite and bournonite vary depending on the ore types and deposits. In the Gatsuurt deposit, these minerals occur after the precipitation of major sulfide minerals in the disseminated and stockwork ore types, whereas they exist with major ore minerals in the quartz vein ores. In contrast, they postdate the occurrence of major ore minerals in both ore types in the Boroo deposit. It, therefore, is considered that there are slightly different ore mineral assemblages

in sulfidized and quartz vein ore types. The paragenetic sequences of ore minerals and quartz are summarized in Fig. 2.7.

5. Trace element geochemistry

As mentioned above, pyrite and arsenopyrite are the most abundant sulfide minerals in the Dzuunmod gold area. Iron (Fe) content of pyrite grains (*n=137*) ranges from 43.64 wt.% to 46.59 wt.% with an average of 45.56 wt.% in the study area (Supplementary Table 2.1). S content of pyrite grains in these deposits ranges from 49.39 wt.% to 53.80 wt.% with an average of 52.25 wt.% (Supplementary Table 2.1).

Variation of sulfur (S) content of pyrite is closely related to As content in pyrite grains. Pyrite grains in the Sujigtei deposit show distinctly lower range and average value of As content ranging from 0.02 wt.% to 0.52 wt.% (avg. 0.20 wt.%), whereas S content ranges from 52.58 wt.% to 53.80 wt.% with an average of 53.17 wt.%. In contrast, higher As and lower S content are observed in the the Gatsuurt deposit (As: 0.09 ~ 5.87 wt.% (avg. 1.68 wt.%), S: 49.39 ~ 53.32 wt.% (avg. 51.86 wt.%)) and in the Boroo deposit (As: 0.73 ~ 2.70 wt.% (avg. 1.35 wt.%), S: 51.22 ~ 52.28 wt.% (avg. 51.77 wt.%)). This relationship between S content and As content indicates a substitution of As for S in pyrite grains (e.g., Blanchard et al., 2007).

Au and As content of the Au-bearing pyrite and arsenopyrite grains can be used to predict not only the saturation state, but the chemical state of Au incorporated into them (Reich et al., 2005; Su et al., 2008; Sung et al., 2009; Khishgee & Akasaka, 2015; Yuan et al., 2018). Reich et al. (2005) suggested an empirical solubility limit of Au in Au-bearing pyrite and arsenopyrite defined as a line with an equation of $C_{Au}=0.02xC_{As}+4x10^{-5}$ where C_{Au} and C_{As} indicates the mole % of Au and As,

respectively. As shown in Fig. 2.8, plots above the line indicates that gold occurs mainly as Au^0 nanoparticles whereas Au exists as Au^{+1} ion in solid solution in the plots below the line. In this study, all measured arsenopyrite grains and most pyrite grains except one grain from the Gatsuurt and Boroo deposit are plotted below the solubility line of Au while most plots of pyrite grains from the Sujigtei deposit are present above the line (Fig. 2.8). This suggests that gold exists mainly as Au^{+1} of solid solution in pyrite and arsenopyrite in the Gatsuurt and Boroo deposit. In contrast, gold was present as nanoparticles in pyrite grains at the Sujigtei deposit.

In contrast to the Gatsuurt and Boroo deposit where pyrite and arsenopyrite are most abundant sulfide minerals, few arsenopyrite is observed in the Sujigtei deposit. Considering the lower As content of pyrite grains in the Sujigtei deposit, this suggests the deficiency of As in hydrothermal fluid and/or unfavorable condition of As precipitation. When As substitutes S in pyrite structure during As pyrite formation, more As can enter into pyrite grain under an anoxic condition of its precipitation (Mango & Ryan, 2015) and Au positively related to As is more easily able to be incorporated into pyrite or arsenopyrite (Yuan et al., 2018). This indicates that if As is not deficient, the hydrothermal fluid of the Sujigtei deposit was under more oxic condition than the other deposit, restraining the precipitation of Au-bearing minerals.

This higher oxidation state of ore-forming fluid is consistent with the lack of disseminated and stockwork ore type in the Sujigtei deposit compared to two other deposits. Only a quartz vein type developed in the Sujigtei deposit, whereas both disseminated and stockwork type and quartz vein type formed in the Gatsuurt and Boroo deposit (Fig. 2.7). Because the disseminated and stockwork mineralization process accompanied with Fe-sulfidation leads to the reduction of ore-forming fluid (Palin & Xu, 2000), the absence of this ore type in the Sujigtei deposit indicates a

different oxidation state of ore-forming fluid. Therefore, the Sujigtei deposit underwent the single-type ore-forming process restricted to quartz vein type and the different oxidation state of ore-forming fluid led to lower As and Au contents. These results indicate that the conditions of hydrothermal fluid were variable and, in turn, this difference led to completely contrasting result of gold mineralization between the Gatsuurt and Boroo deposit where mining has been available, and Sujigtei deposit with low grade and tonnage.

Co and Ni content of pyrite grains in the study area ranges from 0.01 wt.% to 0.68 wt.% with an average of 0.05 wt.% and from 0.01 wt.% to 0.08 wt.% with an average of 0.02 wt.% (Supplementary Table 2.1). The Co content is generally higher than the Ni content showing larger variation and average value. Little difference of average value and total variation of both Co and Ni contents is observed among deposits, indicating that there is no spatial variation of these elements in the study area.

Both Co and Ni content in pyrite grains have been used to distinguish the sources of hydrothermal fluid because both elements are derived from mantle, but show different behavior (e.g., Li et al., 2014; Niu et al., 2016; Yuan et al., 2018). Ni represents more compatible behavior compared to Co, indicating that Ni is preferentially moved into solid phase during early stage of magma and hydrothermal fluid evolution. As an empirical parameter, the Co/Ni ratio greater than one in pyrite is considered to indicate the influence from hydrothermal fluid on the deposit (Clark et al., 2004; Li et al., 2014; Niu et al., 2016; Yuan et al., 2018).

Calculated Co/Ni ratio of pyrite grains (*n=63)* has an average value of 4.49 from 0.44 to 45.2. Considering the higher content of Co than Ni, most Co/Ni ratios greater than one suggests that the hydrothermal fluid in the Dzuunmod gold area was

greatly influenced by fluid-rock interaction during mineralization processes. Compared to Co and Ni, Mo shows more incompatible behavior causing an enrichment in differentiated igneous rocks. This indicates that the Mo/Ni ratios of pyrite grains are able to infer the relative strength of (ultra)-mafic rock over felsic rocks such as granite in the source region (Koglin et al., 2010; Yuan et al., 2018). The Mo content of pyrite grains in the study area shows one order greater value than Co and Ni, which is approximately 0.45 wt.% as an average value in each deposit (supplementary Table 2.1). This makes the extremely large (one order higher) Mo/Ni ratios of pyrite grains in the Dzuunmod gold area from 5.51 wt.% to 479 wt.% (avg. 34.7 wt.%), suggesting a felsic rock provenance for metal sources. Koglin et al. (2010) suggested that both high Co/Ni and Mo/Ni ratio are characteristics of post-sedimentary or hydrothermal origin of pyrite and the composition of hydrothermal fluid may be intensely affected by fluid-rock interaction.

6. Stable isotope systematics

6.1 Sulfur isotope data

Pyrite and arsenopyrite are the most abundant sulfide minerals with minor amount of chalcopyrite, galena and sphalerite in the Dzuunmod gold area. Even though changes of several physico-chemical factors such as temperature, pressure, oxygen fugacity and pH are able to influence the S isotope composition of both sulfide minerals and ore-forming fluid, the $\delta^{34}S$ value of sulfide minerals is generally corresponding to that of total sulfur species of hydrothermal fluid where they precipitated under a reduced fluid system such as the mineral association of pyrite-arsenopyrite-pyrrhotite (Ohmoto & Rye, 1979; Taylor, 1987; Seal, 2006; Hoefs, 2018). It means that the sulfide minerals seem to be precipitated from a reduce fluid

as a simple mineral assemblage and their $\delta^{34}S$ value reflects the $\delta^{34}S$ of fluid.

The sulfide minerals in the Dzuunmod area represent a wide variation of the $\delta^{34}S$ values from -2.6 ‰ to 17.2 ‰ with an average of 2.1 ‰ (Table 2.2). The arsenopyrite has a larger variation of $\delta^{34}S$ values from -2.6 ‰ to 17.2 ‰, whereas the $\delta^{34}S$ values of pyrite range from -0.7 ‰ to 9.3 ‰ (Fig. 2.9). However, the average $\delta^{34}S$ value of pyrite and arsenopyrite is 2.3 ‰ and 1.9 ‰ respectively, which is very similar to the $\delta^{34}S$ value of total sulfide as well as themselves. The paragenetic sequences of the ore minerals also show that pyrite and arsenopyrite were precipitated in the similar stages (Fig. 2.7). Therefore, it is considered that they were precipitated from the hydrothermal fluids with similar $\delta^{34}S$ values and did not undergo the S isotope fractionation between them during the precipitation event.

Relatively large range of $\delta^{34}S$ values enables to exclude a possibility that a magmatic sulfur plays a dominant role of sulfur source in the Dzuunmod area. The $\delta^{34}S$ value of magmatic sulfur is close to 0 ‰ and sulfide minerals in the various ore deposits where the sulfur is mainly derived from the deep magma show very restricted range of the $\delta^{34}S$ values near 0 ‰ (e.g., Ohmoto, 1972; Taylor, 1987; Seal, 2006). In orogenic gold deposits, the $\delta^{34}S$ values of major sulfide minerals where sulfur is derived from a deep-seated magmatic source show a relatively smaller variation (e.g., Ding et al., 2016; Ma et al., 2018; Yuan et al., 2018). Compared to the magmatic sulfur, the $\delta^{34}S$ values of sedimentary and metamorphic rocks show much wider variation approximately from -40 ‰ to 50 ‰ and from -20 ‰ to 20 ‰, respectively (Hoefs, 2018 and references therein).

The mixing of multiple sulfur sources or S isotope fractionation of sulfur species in ore-forming fluids driven by progressive oxidation of them can influence the $\delta^{34}S$ values of minerals in the orogenic gold deposit (Chang et al., 2008; Xu et

al., 2017; LaFlamme et al., 2018a; Ma et al., 2018), making it more difficult to constrain the sulfur sources. For example, Xu et al. (2017) and Zhang et al. (2018) proposed a slightly different sulfur sources in the orogenic gold deposit in Jiangnan orogeny region, south China. The former suggested a mixing of metamorphosed sulfur source and magma-derived sulfur, whereas the latter insisted of a single metamorphic sulfur source affected by S isotope fractionation processes during sulfide deposition. The absence of coeval magmatic intrusion with mineralization age, however, indicates little possibility of the involvement of magmatic activities as a major sulfur source in the study area (Fig. 2.3).

Many studies interpreted the decreasing trend of $\delta^{34}S$ values of sulfide minerals depending on the precipitation order as an effect of the isotopic fractionation by fluid oxidation during mineralization process such as sulfidation, carbonation and phase separation and/or fluid mixing (e.g., Uemoto et al., 2002; Evans et al., 2006; Neumayr et al., 2008; Hodkiewicz et al., 2009; Ward et al., 2017; LaFlamme et al., 2018b; Ma et al., 2018). Especially, host rock-fluid interaction such as carbonation and sulfidation has been suggested as a major gold precipitation process in orogenic gold deposits, causing the oxidation of ore-forming fluids (e.g., Phillips & Groves, 1983; Phillips et al., 1986; Palin & Xu, 2000; Ridley & Diamond, 2000; Evans et al., 2006; Neumayr et al., 2008). Both reactions include the formation of Fe-Ca-Mg carbonates and iron-bearing sulfides respectively within the host rocks, causing the oxidation of ore-forming fluids. The variation of fluid oxidation state and subsequent decrease of activity of the reduced sulfur species triggers the decrease of gold solubility by destabilizing the gold bisulfide complexes, leading to the gold precipitation. Geological evidences of the Dzuunmod gold area represent the presence of widespread wall-rock sulfidation and, to a lesser extent, carbonation

reactions during precipitation events. The occurrence of sulfidation and carbonation, therefore, indicates that these reactions played a significant role in gold precipitation in the study area.

The $\delta^{34}S$ values measured in this study suggest that the sulfidation, rather than carbonation, contributed more importantly to the formation of gold deposits in the study area. According to modelling result, both reactions resulted in the reduction of ore-forming fluid and decrease of activity of the reduced sulfur species, necessary for the decrease of gold solubility, but completely different evolutionary pathways of S isotope composition (Palin & Xu, 2000). The $\delta^{34}S$ value of ore-forming fluid shifts insignificantly during sulfidation reaction because it stays within pyrite-pyrrhotite stability field (Palin & Xu, 2000 and references therein). In contrast, substantial variation of $\delta^{34}S$ value accompanied with fluid oxidation and decrease of activity of reduced sulfur species within fluid during carbonation reaction occurs owing to the change of oxidized (HSO_4^-) and reduced (H_2S) sulfur species (Phillips & Groves, 1983; McCuaig & Kerrich, 1998; Palin & Xu, 2000; Evans et al., 2006). The fluid oxidation brings about the increase of HSO_4^- in fluid, leading to the rise of proportion of HSO_4^- to H_2S. Because the heavier S isotope (^{34}S) tends to be enriched in HSO_4^- rather than H_2S in the hydrothermal fluid, the H_2S species remained in the fluid and the products of sulfides become lighter (Ohmoto & Rye, 1979). The negative mean and range of $\delta^{34}S$ values of sulfide minerals in orogenic gold deposits is a diagnostic of the presence of carbonation reaction (e.g., Palin & Xu, 2000; Hodkiewicz et al., 2009). Therefore, relatively positive $\delta^{34}S$ values measured in this study cannot be explained by carbonation reactions.

Phase separation may be one of gold precipitation mechanisms accompanying the large shift of the $\delta^{34}S$ values of ore-forming fluid and products without rock-fluid

reaction. Preferential partitioning of the reduced species such as H_2, CO_2 and CH_4, and to a lesser extent, H_2S decreasing the activity of H_2 and H_2S (Palin & Xu, 2000). As similar to wall-rock carbonation, the oxidized fluid moved to HSO_4^--dominant field with increase of the proportion of HSO_4^- to H_2S and the decrease of gold solubility and $\delta^{34}S$ values (e.g., Ohmoto & Rye, 1979; Drummond & Ohmoto, 1985; Palin & Xu, 2000). However, the $\delta^{34}S$ values of sulfide samples within the quartz vein range from -0.2 ‰ to 17.2 ‰ in this study (Fig. 2.9) representing a positive deviation of S isotope composition, which is consistent with the lack of geological data for phase separation in the study area.

Even though some sulfide samples in this study show negative $\delta^{34}S$ values, most $\delta^{34}S$ values and mean value are positive (Table 2.2). This indicates that the sulfidation is a predominant host rock-fluid interaction for gold precipitation in the Dzuunmod gold deposits. Also, the measured $\delta^{34}S$ values are consistent with the geological observation, which is the occurrence of the widespread disseminated sulfides. This implies that the $\delta^{34}S$ values of sulfur species in the ore-forming fluid in the study area might be preserved during gold precipitation processes. Even though the influence of carbonation cannot be completely discounted because of the existence of carbonation alteration, the $\delta^{34}S$ values enable to exclude the carbonation and phase separation as a major mechanism for gold precipitation.

The heterogeneous S isotope composition of sulfur sources attributes to the observed large variation of $\delta^{34}S$ values rather than the changes of S isotope composition of fluid during fluid migration or sulfide deposition. This means that the possible sulfur sources have large range of $\delta^{34}S$ values in the study area. Several studies suggested that syngenetic and diagenetic pyrite produced by both bacterial and thermochemical seawater sulfate reduction processes could be possible sulfur

sources in the sediment-hosted orogenic gold deposit (e.g., Chang et al., 2008; Goldfarb & Groves, 2015; Zhang et al., 2018). Because both biotic and abiotic sulfate reduction can trigger a large S isotope fractionation up to 50 ‰, resulting in the depletion of the heavier isotope (^{34}S) in a reduced sulfur species (Krouse & Mayer, 2000; Seal, 2006; Hoefs, 2018 and references therein), the syngenetic and diagenetic pyrite in the marine sediment have a wide range of $\delta^{34}S$ values. During the metamorphic event of the pyrite-bearing sedimentary rocks, the sulfur seems to be put into the metamorphic fluid, possibly ore-forming fluid, and transported to the deposit site (Goldfarb, 1997; Goldfarb et al., 2005; Goldfarb & Groves, 2015).

6.2 Oxygen isotope data

The measured $\delta^{18}O_{quartz}$ values of the Dzuunmod area vary from 14.7 ‰ to 17.7 ‰ with a narrow range (3 ‰) indicating a homogeneous oxygen isotope composition of quartz vein samples (Table 2.3). These values can be converted into the oxygen isotope composition of hydrothermal fluid ($\delta^{18}O_{water}$) where quartz grains precipitate on the assumption that they are in equilibrium state. The $\delta^{18}O_{water}$ is calculated using an equation under the temperature condition between 200 and 500 °C as follows:

$$1000\ln\alpha_{water}^{quartz} = \delta^{18}O_{quartz} - \delta^{18}O_{water} = \frac{3.38 \times 10^6}{T^2} - 2.90$$

where α is the isotopic fractionation factor between quartz and hydrothermal fluid and T is the absolute temperature (K) (Friedman & O'Neil, 1977). This indicates that the higher mineralization temperature is, the smaller the isotopic fractionation factor becomes.

For the calculation of $\delta^{18}O_{water}$ values, the mineralization temperatures of the ore-forming fluids were obtained from the arsenpyrite geothermometry estimating

the T-fS_2 conditions of mineralization with atomic percentage of As in arsenopyrite (at. % As) in the Fe-As-S system where arsenopyrite and arsenic pyrite coexist (Clark, 1960; Barton Jr, 1969; Kretschmar & Scott, 1976). The measured As contents of arsenopyrite have an average of 29.2 at. % As (from 28.0 to 30.9 at. % As) in the study area (S. Table 2.2). As shown in Fig. 2.10, these values are corresponding to the estimated mineralization temperature of 275 ± 15 °C, which is included in the range of the homogenization temperatures for fluid inclusions in quartz of the Gatsuurt deposit from 194 to 355 °C reported by Khishgee et al. (2014). However, this previously reported range of homogenization temperatures seems to be unlikely to reflect the variation of mineralization temperatures. Goldfarb and Groves (2015) argued that when the measured $\delta^{18}O_{quartz}$ values are clustered within a few ‰ the mineralization temperature is also consistent and variable homogenization temperature results are attributed to the measurement of post-ore or modified inclusions.

Based on the measured $\delta^{18}O_{quartz}$ values and the temperature data obtained from the arsenopyrite geothermometry, the calculated $\delta^{18}O_{water}$ values vary from 6.3 to 9.3 ‰ (Table 2.3). These ranges are consistent with those of orogenic gold deposits, which is from 5 ‰ to 15 ‰, where hydrothermal fluids seem to be derived from metamorphic sources (Fig. 2.11) (Taylor, 1987; McCuaig & Kerrich, 1998; Goldfarb et al., 2005; Goldfarb & Groves, 2015; Zhang et al., 2018). The $\delta^{18}O$ values of metamorphic fluid show a wide and higher variation from 3 ‰ to 20 ‰, whereas primary magmatic fluid has a restricted $\delta^{18}O$ values from 5.5 ‰ to 9.5 ‰ (Sheppard, 1986). A meteoric water has generally negative $\delta^{18}O$ value satisfying the Meteoric Water Line, meaning that the input of the meteoric water shifts $\delta^{18}O$ value of hydrothermal fluid into lower range.

The calculated $\delta^{18}O_{water}$ values overlap with those of primary magmatic water as well as metamorphic fluid, implying that the magmatic water cannot be ruled out as the ore-forming fluid sources (Fig. 2.11). However, the absence of coeval magmatic intrusion near the Dzuunmod gold deposits area (Fig. 2.3) enables to exclude the magmatic water from major hydrothermal fluid sources. As mentioned above, the ages of host rocks are much older than mineralization ages in the Dzuunmod area indicating that there is no direct genetic relationship between the formation of host rocks and mineralization events. This implies that it is unlikely that the ore-forming fluid was derived from or mixed with a minor contribution of magmatic water in the study area. Considering that meteoric water will not reach the crustal depth where most orogenic gold deposits formed (Goldfarb & Groves, 2015), it is most likely that the ore-forming fluid in the Dzuunmod area was derived from metamorphic sources, consistent with their $\delta^{18}O$ values (Fig. 2.11).

7. Implications for ore genesis and sources and Conclusions

As described above, the mineralization types in the Dzuunmod gold area are divided into disseminated and stockwork, quartz vein and silicified ores hosted in Phanerozoic metasedimentary rocks (Haraa Formation) and granitoids complex (Boroo Complex). Gold occurs as native grain and invisible form in auriferous pyrite and arsenopyrite. Predominant alteration assemblage is sericite alteration dominated by quartz, sericite and carbonate. Major sulfide minerals are pyrite and arsenopyrite, which are divided into earlier non-auriferous stage and following auriferous stage. Then, native gold occurs in disseminated and stockwork, and auriferous quartz vein ore types. The trace element composition of pyrite and arsenopyrite shows high Co/Ni and Mo/Ni ratios, indicating that these sulfides have post-sedimentary or

hydrothermal origin and the ore-forming fluids were greatly affected by fluid-rock interaction during mineralization processes. The mineralization ages of late Triassic to early Jurassic estimated by $^{40}Ar/^{39}Ar$ age of hydrothermally altered minerals are much younger than intrusion ages of host rocks (Boroo granitoid complex), which range from 476.2 Ma to 464.6 Ma determined by U-Pb age dating of zircon grains. This means that a great time gap between the formation of host rocks and the occurrence of mineralization event.

Ore-mineral assemblages, paragenetic sequences, age dating results and trace element compositions in this study suggest the possible gold mineralization processes in the Dzuunmod gold area. First, the input of hydrothermal fluid without gold altered the host rocks causing the sulfidation of iron oxides or silicates within host rocks. The precipitation of non-auriferous major sulfides occurred during this period by fluid-rock interactions or physicochemical variations of hydrothermal fluid (Groves & Foster, 1991; Seward, 1993; Goldfarb et al., 2001; Phillips & Powell, 2010). Second, the influx of the auriferous hydrothermal fluid where gold is mainly transported by Au^{+1} ions with bisulfide complex resulted in the sulfidation of the host rocks. This alteration reduced the activity of the sulfur species (as H_2S or HS^-) in the hydrothermal fluids and this condition favors the incorporation of Au from solid solution to pyrite and arsenopyrite grains to form invisible gold, being undersaturated with respect to native gold (Simon et al., 1999; Reich et al., 2005). Then, the released H_2S-poor fluid produced by consumption of sulfur into sulfidation of host rocks and precipitation of auriferous sulfide minerals meets the fresh Au-bearing and H_2S-rich fluid causing the saturation of native gold produced by the reduction of H_2S activity in the hydrothermal fluid. Mixing of two different fluids brings about the destabilization of Au-bisulfide complexes and lead to the

precipitation of native gold grain (e.g., Seward, 1993). This gold mineralization process is consistent with an observation result in this study and paragenetic sequences of major ore minerals in the Gatsuurt and Boroo deposit, suggesting the multiple mineralization events. The earlier precipitation of major sulfide minerals than native gold, which is subsequently separated into non-auriferous and invisible Au-bearing pyrite and arsenopyrite.

The large variation of the $\delta^{34}S$ values from -2.6 ‰ to 17.2 ‰ in this study indicates the heterogeneity of S isotope composition of source materials. Because Fe-sulfidation, considered as main ore-forming mechanism in the study area, cause little S isotope fractionation during precipitation (e.g., Palin & Xu, 2000), the change of S isotope composition during migration in hydrothermal fluid and precipitation as sulfide minerals cannot be dominant mechanism to explain this variation. Therefore, the S isotope signature seems to be derived from a heterogeneous source. Because there are no outcrops of sulfate-bearing rocks in the study area (Fig. 2.3), a sediment-hosted pyrite with heterogeneous $\delta^{34}S$ values incorporated into metamorphic fluid during metamorphic event is more plausible for sulfur source in the Dzuunmod gold area.

Even though the calculated $\delta^{18}O_{water}$ values (from 6.3 to 9.3 ‰) of ore-forming fluid are not fully deviated from the area of primary magmatic water, these values suggest to indicate a metamorphic derivation of hydrothermal fluid due to the lack of coeval magmatic intrusion in the study area. In addition, Khishgee et al. (2014) reported the CO_2-rich and halite-bearing aqueous fluid inclusions in the Gatsuurt deposit, which is consistent characteristics of fluid inclusion type occurring in ore-forming fluid of the orogenic gold deposit (Goldfarb & Groves, 2015).

Based on these characteristics including alteration and ore mineral assemblages,

trace element data, stable isotope geochemistry, fluid inclusion and trapping temperature of fluid, and geochronological data in this and other studies (Cluer et al., 2005; Hendry et al., 2006; Goldfarb et al., 2014; Khishgee et al., 2014; Khishgee & Akasaka, 2015), the gold deposits in the Dzuunmod area has been classified into orogenic gold type where fluid and sulfur was originated from a metamorphic source. Hydrothermal fluid produced during metamorphic event was migrated to the Dzuunmod area through the NE-trending fault. Multiple gold and sulfide mineralization occurred by the sulfidation of host rocks and mixing of ore-forming fluids. Substantial difference of timing between intrusion and mineralization event suggests that mineralization is not directly associated with intrusion of granitoids (Boroo complex) to the existing metasedimentary rocks (Haraa Formation). However, the host rocks may influence not only the mineralization processes including paragenetic sequences and the form of Au-bearing minerals, but the trace element content of sulfide minerals.

References

Ahn, I., Lee, J. I., Kusakabe, M., & Choi, B.-G. (2012). Oxygen isotope measurements of terrestrial silicates using a CO 2-laser BrF 5 fluorination technique and the slope of terrestrial fractionation line. *Geosciences Journal, 16*(1), 7-16.

Badarch, G., Cunningham, W. D., & Windley, B. F. (2002). A new terrane subdivision for Mongolia: implications for the Phanerozoic crustal growth of Central Asia. *Journal of Asian Earth Sciences, 21*(1), 87-110.

Barton Jr, P. B. (1969). Thermochemical study of the system Fe-As-S. *Geochimica et Cosmochimica Acta, 33*(7), 841-857.

Bierlein, F., & Crowe, D. (2000). Phanerozoic orogenic lode gold deposits. *Gold in 2000, Reviews in Economic Geology, 13*, 103-139.

Blanchard, M., Alfredsson, M., Brodholt, J., Wright, K., & Catlow, C. R. A. (2007). Arsenic incorporation into FeS2 pyrite and its influence on dissolution: a DFT study. *Geochimica et Cosmochimica Acta, 71*(3), 624-630.

Bussien, D., Gombojav, N., Winkler, W., & Von Quadt, A. (2011). The Mongol–Okhotsk Belt in Mongolia—an appraisal of the geodynamic development by the study of sandstone provenance and detrital zircons. *Tectonophysics, 510*(1-2), 132-150.

Chang, Z., Large, R. R., & Maslennikov, V. (2008). Sulfur isotopes in sediment-hosted orogenic gold deposits: Evidence for an early timing and a seawater sulfur source. *Geology, 36*(12), 971-974.

Clark, C., Grguric, B., & Mumm, A. S. (2004). Genetic implications of pyrite chemistry from the Palaeoproterozoic Olary Domain and overlying Neoproterozoic Adelaidean sequences, northeastern South Australia. *Ore Geology Reviews, 25*(3-4), 237-257.

Clark, L. A. (1960). The Fe-As-S system--Phase relations and applications. *Economic Geology, 55*(7), 1345-1381.

Cluer, J., Kotlyar, B., Gantsetseg, O., Togtokh, D., Wood, G., & Ullrich, T. (2005). Geology of the Boroo gold deposit, northern Mongolia. *Seg-Iagod Guidbook Series, 11*, 105-117.

Dejidmaa, G. (1996). Gold metallogeny of Mongolia. *Mongolian geoscientist, 1*, 6-29.

Ding, C., Nie, F., Jiang, S., Liu, Y., & Cao, Y. (2016). Characteristics and origin of the Zhulazhaga gold deposit in Inner Mongolia, China. *Ore Geology Reviews,*

73, 211-221.

Donskaya, T., Gladkochub, D., Mazukabzov, A., & Ivanov, A. (2013). Late Paleozoic–Mesozoic subduction-related magmatism at the southern margin of the Siberian continent and the 150 million-year history of the Mongol-Okhotsk Ocean. *Journal of Asian Earth Sciences, 62*, 79-97.

Drummond, S., & Ohmoto, H. (1985). Chemical evolution and mineral deposition in boiling hydrothermal systems. *Economic Geology, 80*(1), 126-147.

Evans, K., Phillips, G., & Powell, R. (2006). Rock-buffering of auriferous fluids in altered rocks associated with the Golden Mile-style mineralization, Kalgoorlie gold field, Western Australia. *Economic Geology, 101*(4), 805-817.

Friedman, I., & O'Neil, J. R. (1977). *Data of geochemistry: Compilation of stable isotope fractionation factors of geochemical interest* (Vol. 440): US Government Printing Office.

Gerel, O., Kotlyar, B., Cluer, J., Enkhtuvshin, K., & Bold-Erdene, B. (1999). Geology and gold mineralization in the Khentei range. *Mongolian Geosci, 14*, 110-115.

Goldfarb, R. (1997). Gold deposits in metamorphic rocks of Alaska: Implications for ore genesis. *Econ. Geol. Monogr., 9*, 151-190.

Goldfarb, R., Baker, T., Dube, B., Groves, D. I., Hart, C. J., & Gosselin, P. (2005). Distribution, character and genesis of gold deposits in metamorphic terranes: Society of Economic Geologists.

Goldfarb, R., Groves, D., & Gardoll, S. (2001). Orogenic gold and geologic time: a global synthesis. *Ore Geology Reviews, 18*(1-2), 1-75.

Goldfarb, R. J., & Groves, D. I. (2015). Orogenic gold: Common or evolving fluid and metal sources through time. *Lithos, 233*, 2-26.

Goldfarb, R. J., Taylor, R. D., Collins, G. S., Goryachev, N. A., & Orlandini, O. F. (2014). Phanerozoic continental growth and gold metallogeny of Asia. *Gondwana Research, 25*(1), 48-102.

Groves, D., & Foster, R. (1991). Archaean lode gold deposits *Gold metallogeny and exploration* (pp. 63-103): Springer.

Hara, H., Kurihara, T., Tsukada, K., Kon, Y., Uchino, T., Suzuki, T., Takeuchi, M., Nakane, Y., Nuramkhaan, M., & Chuluun, M. (2013). Provenance and origins of a Late Paleozoic accretionary complex within the Khangai–Khentei belt in the Central Asian Orogenic Belt, central Mongolia. *Journal of Asian Earth Sciences, 75*, 141-157.

Hendry, J., Roscoe, W., & Ross, D. (2006). Technical report on the Gatsuurt gold project, Northern Mongolia, prepared for Centerra Gold Inc. *Roscoe Postle Associates Inc., Toronto*, 6-1.

Hodkiewicz, P., Groves, D., Davidson, G., Weinberg, R., & Hagemann, S. (2009). Influence of structural setting on sulphur isotopes in Archean orogenic gold deposits, Eastern Goldfields Province, Yilgarn, Western Australia. *Mineralium Deposita, 44*(2), 129.

Hoefs, J. (2018). *Stable Isotope Geochemistry*: Springer.

Hou, L., Peng, H., Ding, J., Zhang, J., Zhu, S., Wu, S., Wu, Y., & Ouyang, H. (2016). Textures and in situ chemical and isotopic analyses of pyrite, Huijiabao Trend, Youjiang Basin, China: Implications for paragenesis and source of sulfur. *Economic Geology, 111*(2), 331-353.

Hou, W.-R., Nie, F.-J., Jiang, S.-H., Bai, D.-M., Liu, Y., Yun, F., & Liu, Y.-F. (2010). SHRIMP zircon U-Pb dating of ore-bearing granite in the boroo large-size gold deposit, Mongolia and its geological significance. *Diqiu Xuebao(Acta*

Geoscientica Sinica), 31(3), 331-342.

Kelty, T. K., Yin, A., Dash, B., Gehrels, G. E., & Ribeiro, A. E. (2008). Detrital-zircon geochronology of Paleozoic sedimentary rocks in the Hangay–Hentey basin, north-central Mongolia: implications for the tectonic evolution of the Mongol–Okhotsk Ocean in central Asia. *Tectonophysics, 451*(1-4), 290-311.

Kerrich, R. (1987). The stable isotope geochemistry of Au-Ag vein deposits in metamorphic rocks. *Mineral. Assoc. Canada, Short Course Handbook, 13*, 287-336.

Khain, E., Bibikova, E., Salnikova, E., Kröner, A., Gibsher, A., Didenko, A., Degtyarev, K., & Fedotova, A. (2003). The Palaeo-Asian ocean in the Neoproterozoic and early Palaeozoic: new geochronologic data and palaeotectonic reconstructions. *Precambrian Research, 122*(1-4), 329-358.

Khishgee, C., & Akasaka, M. (2015). Mineralogy of the Boroo Gold Deposit in the North Khentei Gold Belt, Central Northern Mongolia. *Resource Geology, 65*(4), 311-327.

Khishgee, C., Akasaka, M., Ohira, H., & Sereenen, J. (2014). Gold Mineralization of the G atsuurt Deposit in the N orth K hentei Gold Belt, Central N orthern M ongolia. *Resource Geology, 64*(1), 1-16.

Koglin, N., Frimmel, H. E., Minter, W. L., & Brätz, H. (2010). Trace-element characteristics of different pyrite types in Mesoarchaean to Palaeoproterozoic placer deposits. *Mineralium Deposita, 45*(3), 259-280.

Kretschmar, U., & Scott, S. (1976). Phase relations involving arsenopyrite in the system Fe-As-S and their application. *Canadian mineralogist, 14*(3), 364-386.

Krouse, H. R., & Mayer, B. (2000). Sulphur and oxygen isotopes in sulphate *Environmental tracers in subsurface hydrology* (pp. 195-231): Springer.

LaFlamme, C., Jamieson, J. W., Fiorentini, M. L., Thébaud, N., Caruso, S., & Selvaraja, V. (2018a). Investigating sulfur pathways through the lithosphere by tracing mass independent fractionation of sulfur to the Lady Bountiful orogenic gold deposit, Yilgarn Craton. *Gondwana Research*.

LaFlamme, C., Sugiono, D., Thébaud, N., Caruso, S., Fiorentini, M., Selvaraja, V., Jeon, H., Voute, F., & Martin, L. (2018b). Multiple sulfur isotopes monitor fluid evolution of an Archean orogenic gold deposit. *Geochimica et Cosmochimica Acta, 222*, 436-446.

Li, S.-R., Santosh, M., Zhang, H.-F., Luo, J.-Y., Zhang, J.-Q., Li, C.-L., Song, J.-Y., & Zhang, X.-B. (2014). Metallogeny in response to lithospheric thinning and craton destruction: geochemistry and U–Pb zircon chronology of the Yixingzhai gold deposit, central North China Craton. *Ore Geology Reviews, 56*, 457-471.

Ma, Y., Jiang, S.-Y., & Li, H.-L. (2018). Isotope geochemistry and genesis of the Liyuan gold deposit, Shanxi, North China. *Ore Geology Reviews, 92*, 129-143.

Mango, H., & Ryan, P. (2015). Source of arsenic-bearing pyrite in southwestern Vermont, USA: sulfur isotope evidence. *Science of the total environment, 505*, 1331-1339.

McCuaig, T. C., & Kerrich, R. (1998). P—T—t—deformation—fluid characteristics of lode gold deposits: evidence from alteration systematics. *Ore Geology Reviews, 12*(6), 381-453.

Neumayr, P., Walshe, J., Hagemann, S., Petersen, K., Roache, A., Frikken, P., Horn, L., & Halley, S. (2008). Oxidized and reduced mineral assemblages in greenstone belt rocks of the St. Ives gold camp, Western Australia: vectors to high-grade ore bodies in Archaean gold deposits? *Mineralium Deposita, 43*(3), 363-371.

Niu, S.-D., Li, S.-R., Santosh, M., Zhang, D.-H., Li, Z.-D., Shan, M.-J., Lan, Y.-X., Gao, D.-R., & Zhao, W.-B. (2016). Mineralogical and isotopic studies of base metal sulfides from the Jiawula Ag–Pb–Zn deposit, Inner Mongolia, NE China. *Journal of Asian Earth Sciences, 115*, 480-491.

Ohmoto, H. (1972). Systematics of sulfur and carbon isotopes in hydrothermal ore deposits. *Economic Geology, 67*(5), 551-578.

Ohmoto, H., & Rye, R. O. (1979). *Isotopes of sulfur and carbon* (H. Barnes Ed.). New York: Wiley.

Palin, J., & Xu, Y. (2000). Gilt by association? Origins of pyritic gold ores in the Victory mesothermal gold deposit, Western Australia. *Economic Geology, 95*(8), 1627-1634.

Parfenov, L., Popeko, L., & Tomurtogoo, O. (2001). Problems of tectonics of the Mongol-Okhotsk orogenic belt. *Russian Journal of Pacific Geology, 16*(5), 797-830.

Phillips, G., & Powell, R. (2010). Formation of gold deposits: a metamorphic devolatilization model. *Journal of Metamorphic Geology, 28*(6), 689-718.

Phillips, G. N., & Groves, D. I. (1983). The nature of Archaean gold-bearing fluids as deduced from gold deposits of Western Australia. *Journal of the Geological Society of Australia, 30*(1-2), 25-39.

Phillips, G. N., Groves, D. I., Neall, F., Donnelly, T., & Lambert, I. (1986). Anomalous sulfur isotope compositions in the Golden Mile, Kalgoorlie. *Economic Geology, 81*(8), 2008-2015.

Pokrovski, G. S., Kokh, M. A., Guillaume, D., Borisova, A. Y., Gisquet, P., Hazemann, J.-L., Lahera, E., Del Net, W., Proux, O., & Testemale, D. (2015). Sulfur radical species form gold deposits on Earth. *Proceedings of the National*

Academy of Sciences, 112(44), 13484-13489.

Reich, M., Kesler, S. E., Utsunomiya, S., Palenik, C. S., Chryssoulis, S. L., & Ewing, R. C. (2005). Solubility of gold in arsenian pyrite. *Geochimica et Cosmochimica Acta, 69*(11), 2781-2796.

Ridley, J., & Diamond, L. (2000). Fluid chemistry of orogenic lode gold deposits and implications for genetic models. *Reviews in Economic Geology, 13*, 141-162.

Rye, R. O. (2005). A review of the stable-isotope geochemistry of sulfate minerals in selected igneous environments and related hydrothermal systems. *Chemical Geology, 215*(1-4), 5-36.

Seal, R. R. (2006). Sulfur isotope geochemistry of sulfide minerals. *Reviews in mineralogy and geochemistry, 61*(1), 633-677.

Sengor, A., & Natal'In, B. (1996). Paleotectonics of Asia: fragments of a synthesis. In: Yin A. & Harrison, M. (eds). *The tectonic evolution of Asia. Cambridge University Press, Cambridge*, 486-640.

Şengör, A., Natal'In, B., & Burtman, V. (1993). Evolution of the Altaid tectonic collage and Palaeozoic crustal growth in Eurasia. *Nature, 364*(6435), 299.

Seward, T. (1993). The hydrothermal geochemistry of gold *Gold metallogeny and exploration* (pp. 37-62): Springer.

Sheppard, S. M. (1986). Characterization and isotopic variations in natural waters. *Reviews in mineralogy and geochemistry, 16*(1), 165-183.

Simon, G., Kesler, S. E., & Chryssoulis, S. (1999). Geochemistry and textures of gold-bearing arsenian pyrite, Twin Creeks, Nevada; implications for deposition of gold in Carlin-type deposits. *Economic Geology, 94*(3), 405-421.

Su, W., Xia, B., Zhang, H., Zhang, X., & Hu, R. (2008). Visible gold in arsenian

pyrite at the Shuiyindong Carlin-type gold deposit, Guizhou, China: Implications for the environment and processes of ore formation. *Ore Geology Reviews, 33*(3-4), 667-679.

Sung, Y.-H., Brugger, J., Ciobanu, C., Pring, A., Skinner, W., & Nugus, M. (2009). Invisible gold in arsenian pyrite and arsenopyrite from a multistage Archaean gold deposit: Sunrise Dam, Eastern Goldfields Province, Western Australia. *Mineralium Deposita, 44*(7), 765.

Taylor, B. (1987). Stable isotope geochemistry of oreforming fluids. *Short course in stable isotope geochemistry of low temperature fluids*, 337-445.

Tomurtogoo, O., Windley, B., Kröner, A., Badarch, G., & Liu, D. (2005). Zircon age and occurrence of the Adaatsag ophiolite and Muron shear zone, central Mongolia: constraints on the evolution of the Mongol–Okhotsk ocean, suture and orogen. *Journal of the Geological Society, 162*(1), 125-134.

Tumur, S., Lkhagvasuren, J., & Gerelmaa, N. (1995). Report of 1: 50000 scale geological mapping and general prospecting carried out in the Noyon Uul Area of the Boroo and Zuunmod District. *Geological Information Center, Ulaanbaatar, Report*(4859).

Uemoto, T., Ridley, J., Mikucki, E., Groves, D. I., & Kusakabe, M. (2002). Fluid chemical evolution as a factor in controlling the distribution of gold at the Archean Golden Crown lode gold deposit, Murchison province, Western Australia. *Economic Geology, 97*(6), 1227-1248.

Vallance, J., Boiron, M.-C., Cathelineau, M., Fourcade, S., Varlet, M., & Marignac, C. (2004). The granite hosted gold deposit of Moulin de Cheni (Saint-Yrieix district, Massif Central, France): petrographic, structural, fluid inclusion and oxygen isotope constraints. *Mineralium Deposita, 39*(3), 265-281.

Ward, J., Mavrogenes, J., Murray, A., & Holden, P. (2017). Trace element and sulfur isotopic evidence for redox changes during formation of the Wallaby Gold Deposit, Western Australia. *Ore Geology Reviews, 82*, 31-48.

Wen, B.-J., Fan, H.-R., Santosh, M., Hu, F.-F., Pirajno, F., & Yang, K.-F. (2015). Genesis of two different types of gold mineralization in the Linglong gold field, China: Constrains from geology, fluid inclusions and stable isotope. *Ore Geology Reviews, 65*, 643-658.

Windley, B. F., Alexeiev, D., Xiao, W., Kröner, A., & Badarch, G. (2007). Tectonic models for accretion of the Central Asian Orogenic Belt. *Journal of the Geological Society, 164*(1), 31-47.

Xiao, W., Windley, B., Badarch, G., Sun, S., Li, J., Qin, K., & Wang, Z. (2004). Palaeozoic accretionary and convergent tectonics of the southern Altaids: implications for the growth of Central Asia. *Journal of the Geological Society, 161*(3), 339-342.

Xiao, W., Windley, B. F., Hao, J., & Zhai, M. (2003). Accretion leading to collision and the Permian Solonker suture, Inner Mongolia, China: termination of the central Asian orogenic belt. *Tectonics, 22*(6).

Xu, D., Deng, T., Chi, G., Wang, Z., Zou, F., Zhang, J., & Zou, S. (2017). Gold mineralization in the Jiangnan Orogenic Belt of South China: geological, geochemical and geochronological characteristics, ore deposit-type and geodynamic setting. *Ore Geology Reviews, 88*, 565-618.

Yakubchuk, A. (2001). The Altaids: tectonic evolution and metallogeny. *Soc. Econ. Geol. Newsl., 46*, 7-14.

Yin, A., & Nie, S. (1996). *20 A Phanerozoic Palinspastic Reconstruction of China and its Neighboring Regions*. New York: Cambridge Univ. Press.

Yuan, M.-W., Li, S.-R., Li, C.-L., Santosh, M., Alam, M., & Zeng, Y.-J. (2018). Geochemical and isotopic composition of auriferous pyrite from the Yongxin gold deposit, Central Asian Orogenic Belt: Implication for ore genesis. *Ore Geology Reviews, 93*, 255-267.

Zhang, L., Yang, L.-Q., Groves, D. I., Liu, Y., Sun, S.-C., Qi, P., Wu, S.-G., & Peng, J.-S. (2018). Geological and H–O–S–Pb isotopic constraints on ore genesis, Huangjindong gold deposit, Jiangnan Orogen, southern China. *Ore Geology Reviews*.

Zhu, Y., An, F., & Tan, J. (2011). Geochemistry of hydrothermal gold deposits: a review. *Geoscience Frontiers, 2*(3), 367-374.

Zonenshain, L., Kuzmin, M., & Natapov, L. (1990). *Geology of the USSR: A Plate-Tectonic Synthesis, Geodyn.* Paper presented at the Ser.

Zorin, Y. A. (1999). Geodynamics of the western part of the Mongolia–Okhotsk collisional belt, Trans-Baikal region (Russia) and Mongolia. *Tectonophysics, 306*(1), 33-56.

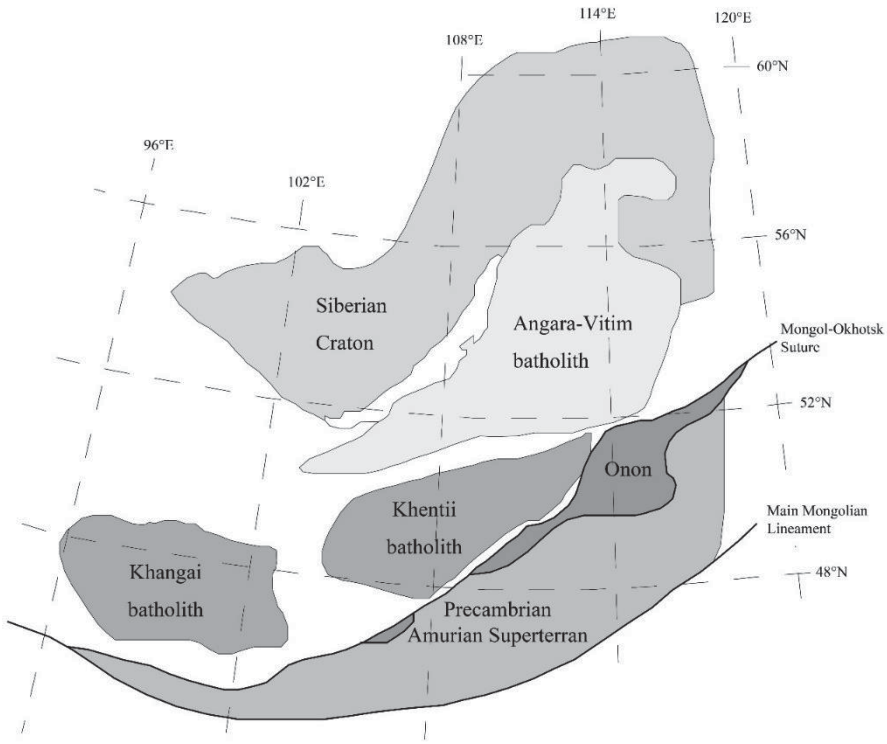

Figure 2.1. Distribution of the Late Paleozoic to Early Mesozoic batholiths and belts in Mongolia and Russia (modified fromDonskaya et al., 2013).

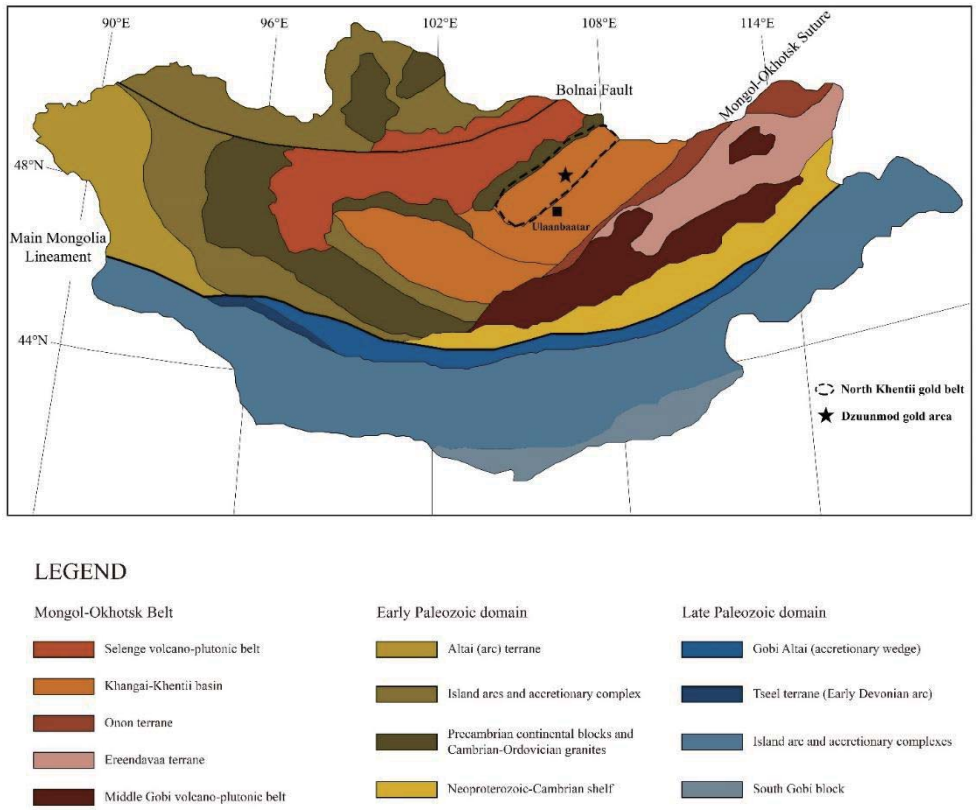

Figure 2.2. Simplified tectonostratigraphic map of Mongolia (modified after Badarch et al., 2002; Bussien et al., 2011).

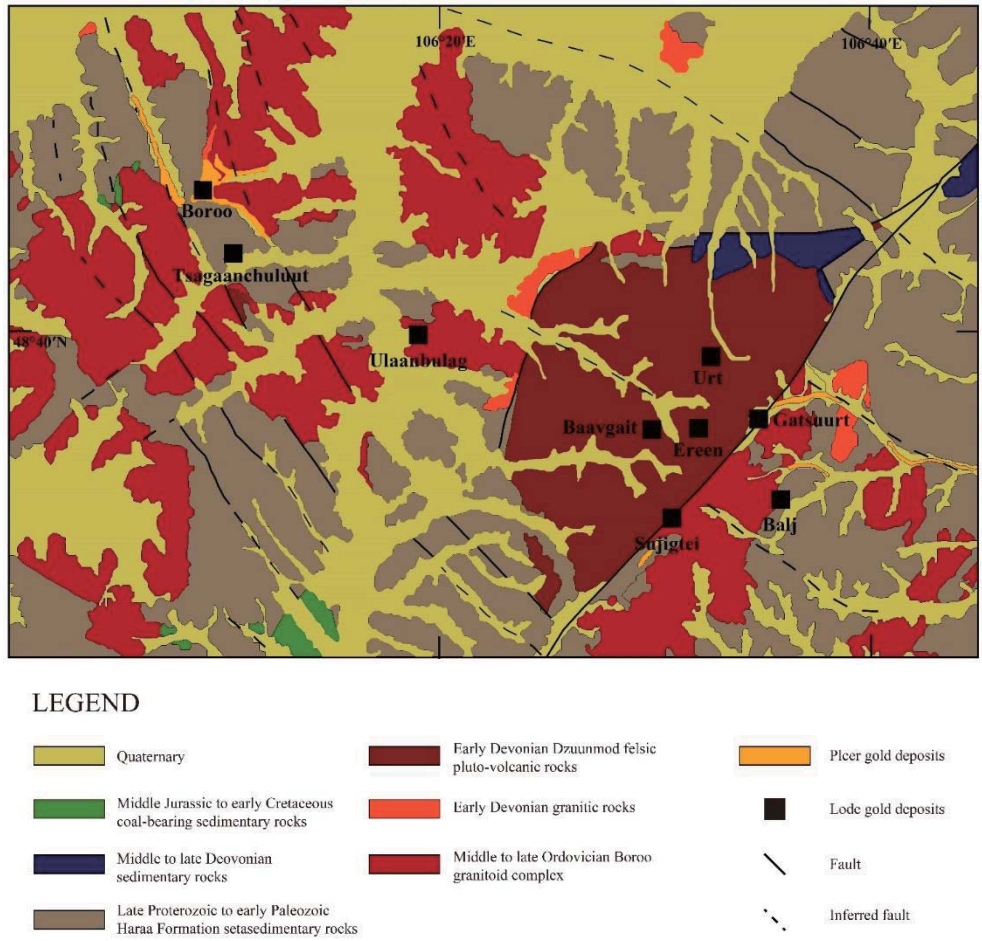

Figure 2.3. Geological map of the North Khentii Gold Belt (NKGB) in northern Mongolia and the distribution of major lode deposit in the area (modified from Khishgee & Akasaka, 2015).

Figure 2.4. Field photographs of ore deposits in the study area. (a) view of Gatsuurt deposit with Sujigtei fault, (b) & (c) host rocks, tectonic clay and siliceous rocks in the Gatsuurt deposit, (d) view of Ereen deposit with gateway of old underground mine, (e) fault-controlled gold mineralization within quartz vein in Ereen deposit, (f) view of open-pit mine in Boroo deposit, (g) view of Ulaanbulag deposit, (h) & (i) host rocks and NE-trending fault in Balj occurrence.

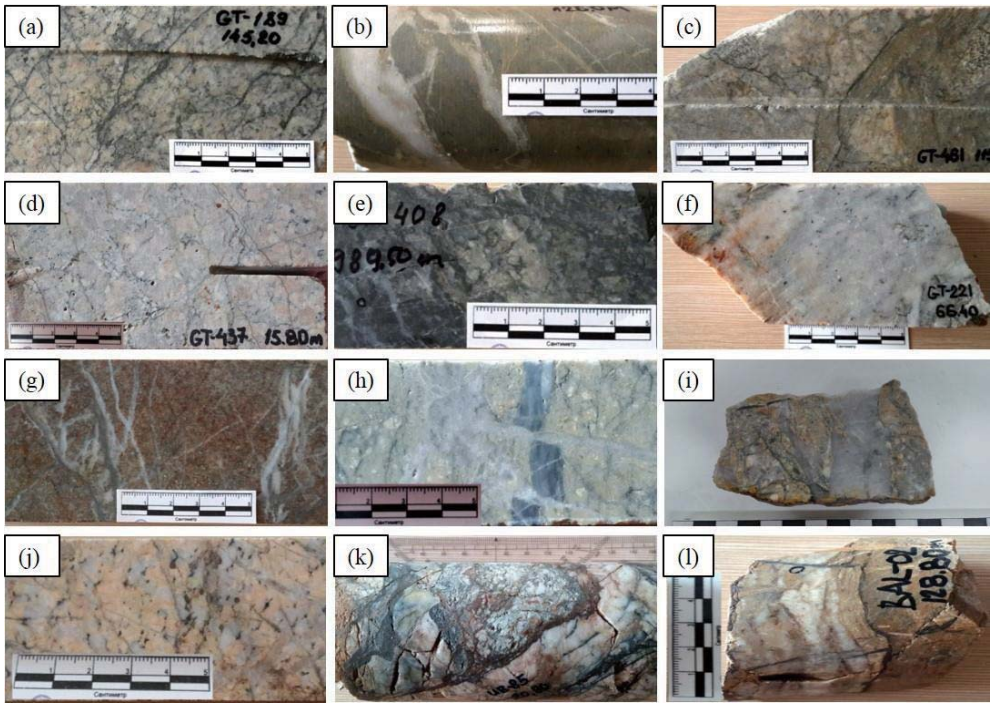

Figure 2.5. Photographs of drill cores and hand specimens. (a) sulfidized granite in the Central zone, (b) rhyolite dike with quartz veins in the Main zone, (c) diorite influenced by siliceous alteration, (d) sulfidized sandstone, (e) silicified granite & (f) quartz vein in granite in Gatsuurt deposit, (g) sulfidized rhyolite & (h) quartz veins in Sujigtei deposit, (i) altered rhyolite with quartz vein in Ereen deposit, (j) silicified granite in Boroo deposit, (k) quartz veinlet with sulfide grain in granite in Ulaanbulag deposit, (l) quartz veins in sandstone in Balj occurrence.

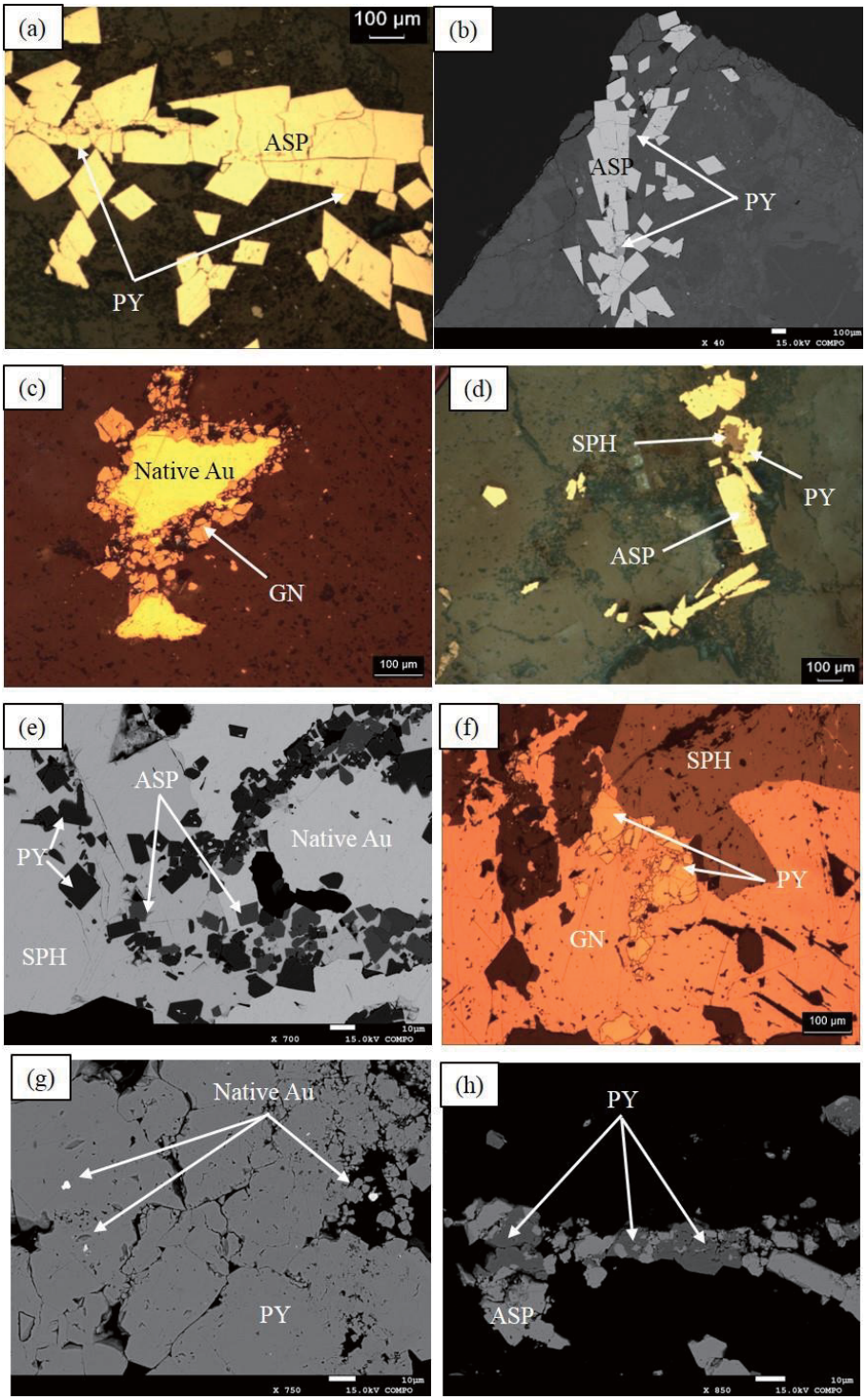

Figure 2.6. Representative reflected-light photomicrographs and BSE images of

sulfide minerals and native gold in Dzuunmod gold area. (a) & (b) pyrite and arsenopyrite in disseminated and stockwork type, (c) native gold with galena, (d) pyrite and arsenopyrite with sphalerite & (e) native gold, pyrite, arsenopyrite and sphalerite in quartz vein type in Gatsuurt deposit, (f) pyrite, galena and sphalerite & (g) native gold grain within pyrite grain in Sujigtei deposit, (h) pyrite and arsenopyrite in Boroo deposit. PY: pyrite, ASP: arsenopyrite, SPH: sphalerite, GN: galena.

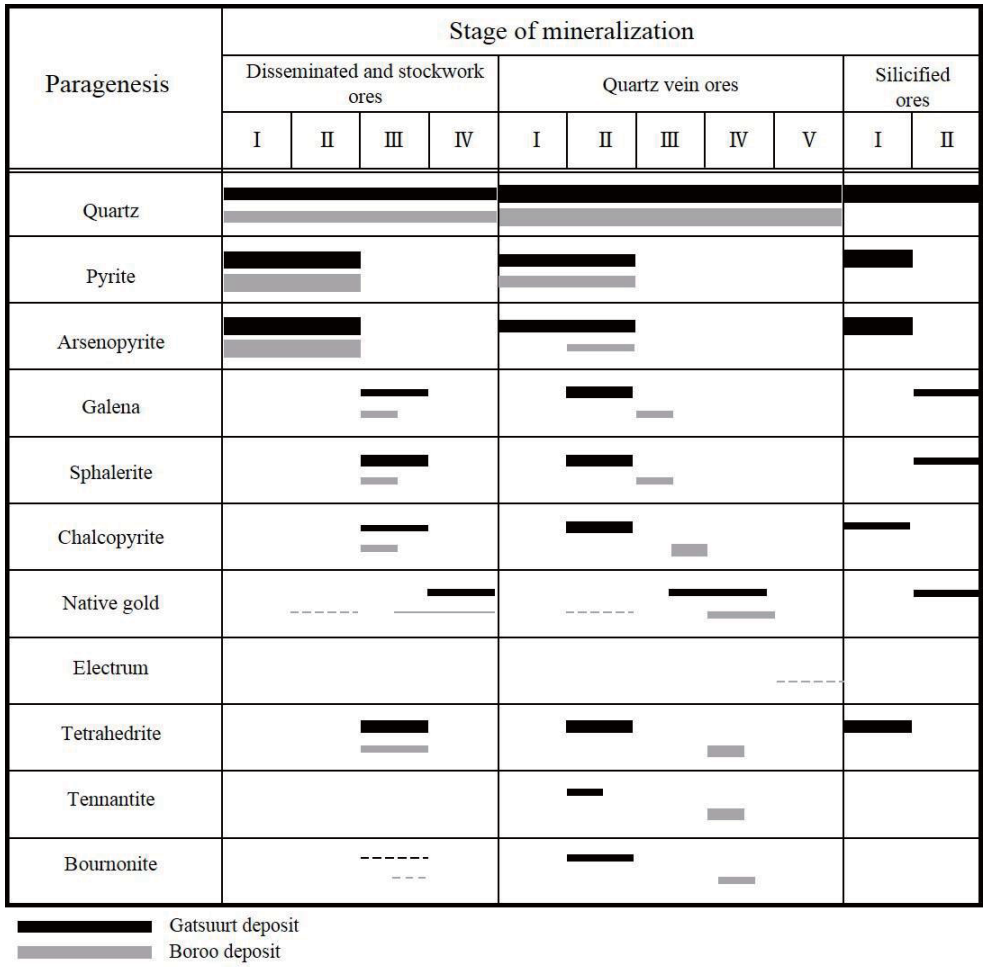

Figure 2.7. Mineral paragenetic sequences of the Gatsuurt deposit and Boroo deposit modified from Khishgee et al. (2014) and Khishgee and Akasaka (2015).

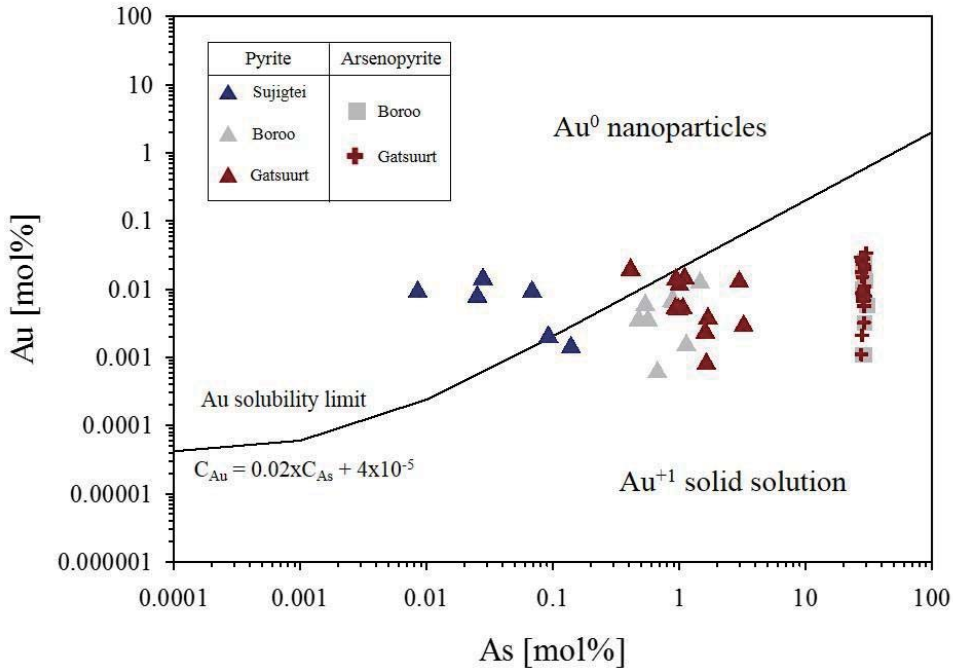

Figure 2.8. Au-As diagram with Au solubility line defined by Reich et al. (2005) and plots of pyrite and arsenopyrite from Gatsuurt, Boroo and Sujigtei deposit.

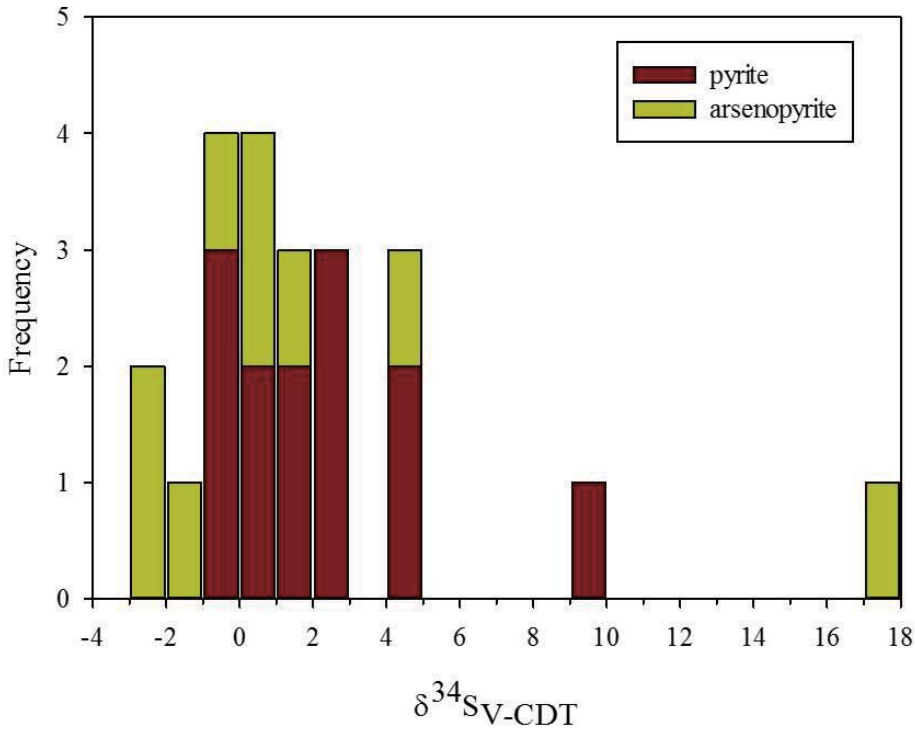

Figure 2.9. Histogram of sulfur isotope composition ($\delta^{34}S$) of pyrite and arsenopyrite in the Dzuunmod gold area.

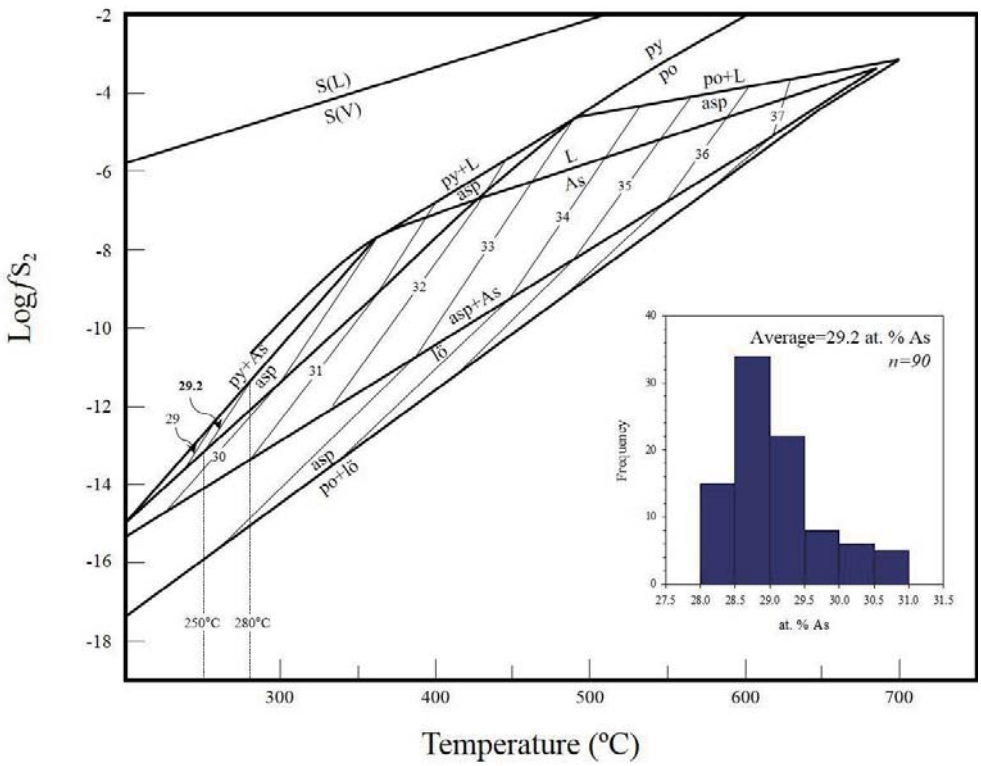

Figure 2.10. Temperature – logfS_2 diagram presenting arsenopyrite and pyrite stability field with at. % As in the Fe-As-S system (after Kretschmar and Scott, 1976). The average As content of arsenopyrite in quartz vein samples (29.2 at. % As) is plotted in the diagram. Asp: arsenpyrite, Py: pyrite, Lö: Loellingite, Po: Pyrrhotite, As: arsenic, L: sulfur-arsenic liquid.

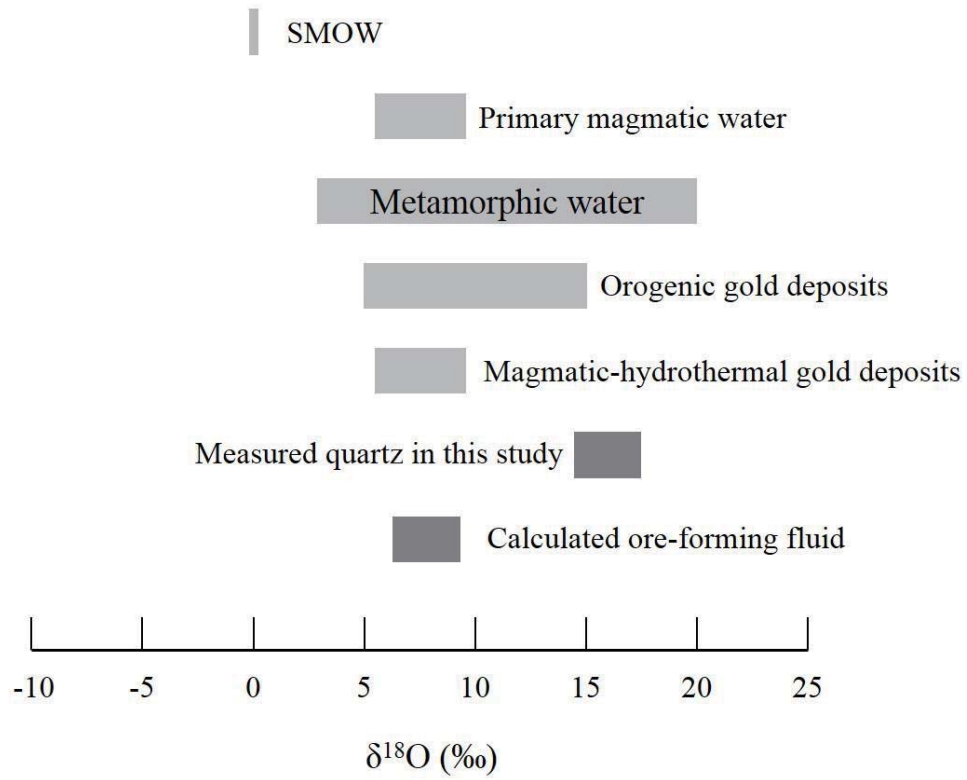

Figure 2.11. $\delta^{18}O$ values of several geologically important fluid sources (Sheppard, 1986), typical orogenic and magmatic-hydrothermal gold deposits (Taylor, 1987; McCuaig & Kerrich, 1998; Goldfarb et al., 2005; Goldfarb & Groves, 2015; Ding et al., 2016; Zhang et al., 2018) and calculated ore-forming fluids from measured $\delta^{18}O$ of quartz in this study.

Table 2.1. Summary of geological characteristics of gold deposits and occurrences in the Dzuunmod area.

Deposit	Host rocks	Structure	Alteration Assemblage	Ore type	Major sulfide ore minerals
Gatsuurt	Granite, Sandstone, Diorite, Rhyolite	Sujigtei fault-steep	Silica, potassic, sericitic, carbonatic	sulfide zone, quartz vein, silica	Py, Asp, Cpy, Sph, Gal
Sujigtei	Rhyolite	Sujigtei fault-steep	Silica, sericitic, potassic	Quartz vein	Py, Asp, Gal, Cpy
Ereen	Rhyolite	Gentle dipping	Silica, sericitic, potassic	Quartz vein	Py, Asp, Cgal, Cpy
Boroo	Granite, Sandstone, Diorite	Boroo fault-gentle dipping	Silica, potassic, sericitic, carbonatic	sulfide zone, quartz vein	Py, Asp, Cpy, Sph, Gal
Ulaanbulag	Granite, Sandstone, Diorite	Ulaanbulag fault-gentle dipping	Silica, potassic, sericitic, carbonatic	sulfide zone, quartz vein	Py, Asp, Gal, Sph
Balj	Sandstone	Balj fault-gentle dipping	Silica, sericitic, carbonatic	Quartz vein	Py, Asp
Biluut	Rhyolite	Gentle dipping	Silica, sericitic, potassic	quartz vein, sulfide zone	Py, Asp
Urt	Rhyolite	Gentle dipping	Silica, sericitic, potassic	quartz vein	Py, Asp
Baavgait	Rhyolite	Gentle dipping	Silica, sericitic, potassic	quartz vein	Py, Asp

Table 2.2. Sulfur isotope compositions of pyrite and arsenopyrite with mineralization type and host rock in the Dzuunmod gold area.

Deposit	Sample	Mineral*	Mineralization type	Host rock	$\delta^{34}S$		
					I	II	mean
Gatsuurt	GT-189_145.20m	py	disseminated sulfide	sulfidized granite	-0.2	0.2	0.0
	GT-280_104.50m	py		sulfidized rhyolite with porphyry texture	2.6	3.1	2.8
	GT-437_89.20m	py		sulfidized granite with stockwork and quartz-sulfide veins	-0.7		-0.7
	GT-461_115.80m	py		altered diorite with quartz-sulfide veins	2.6	2.8	2.7
	GT-461_130.30m	py		sulfidized granite with stockwork and quartz-sulfide veins	1.1		1.1
	GT-490_170.80m	asp		diorite with quartz-carbonate veins	-2.2		-2.2
	GT-95_80.80m	asp	quartz vein	altered sandstone	0.3		0.3
	GT-376_203.20m	asp		sulfidized rhyolite porphyry	17.0	17.4	17.2
	GT-461_108.60m	asp		quartz vein with sulfide in granite	-0.2		-0.2
	GT-221_66.40m	py	silica	siliceous altered granite with VG	0.9		0.9
	GT-49_43.50m	asp		silica zone with sulfide VG and breccia texture	-1.5		-1.5
	GT-189_22.45m	py		silica zone in granite with veinlets	1.0	0.5	0.7
	GT-408_989.50m	asp		Pervasive Quartz Silica zone	1.3		1.3
	GZ	asp		altered rhyolite	-2.6		-2.6
Sujigtei	SJ-006_165.50m	py	quartz vein	sulfidized rhyolite with weak siliceous and sericite alteration	2.7		2.7
Ereen	ER-10/1	asp	quartz vein	quartz vein in sulfidized rhyolite porphyry	4.4	4.2	4.3

Table 2.2. *(Continued)*

Deposit	Sample	Mineral*	Mineralization type	Host rock	$\delta^{34}S$		
					Ⅰ	Ⅱ	mean
Boroo	BR-P-6	py	disseminated sulfide	sulfidized sandstone	-0.1	-0.9	-0.5
	MDD-008	py		granite with stockwork and quart veinlets	4.1	4.3	4.2
Ulaanbulag	UB-79_62.20m	py	disseminated sulfide	quartz vein with sulfide in granite	1.7		1.7
Khargana	KH-P-1	py	quartz vein	sulfidized rhyolite porphyry	9.0	9.6	9.3
Biluut	Bi-07_109.60m	asp	quartz vein	rhyolite porphyry to stockwork or breccia with potassic alteration	0.3		0.3
	Bi-07_113.90m	py	disseminated sulfide	brecciated rhyolite porphyry	4.7	4.9	4.8

Table 2.3. Oxygen isotope composition ($\delta^{18}O$) of quartz samples from Au-bearing quartz veins, disseminated and stockwork, and silica type ores and calculated $\delta^{18}O$ values of ore-forming fluid in the Dzuunmod gold deposits.

Deposit	Sample	Mineralization type	$\delta^{18}O_{V\text{-}SMOW}$ (‰)	
			Quartz	Fluid*
Gatsuurt	GT-372_99.60m	Quartz vein	16.5	8.2
	GT-172_357.80m	Quartz vein	15.0	6.7
	GT-93_38.40m	Quartz vein	15.2	6.8
	GT-462_126.0m	Quartz vein	16.1	7.7
	GT-408_989.30m	silica	14.7	6.3
	GT-94_96.40m	silica	15.4	7.0
	GT-339_138.40m	silica	16.7	8.3
Sujigtei	SJ-08_49.0m	Quartz vein	15.5	7.2
Ereen	ER-7-q	Quartz vein	16.0	7.7
Boroo	BDD-105_40.60m	Quartz vein	16.2	7.9
	KH-BOR-4_136.0m	Quartz vein	16.2	7.9
Ulaanbulag	UB-79_60.85m	Quartz vein	17.0	8.6
Biluut	BI-07_114.30m	Quartz vein	17.4	9.1
Balj	BAL-02_136.75m	Disseminated	17.7	9.3

Supplementary Table 2.1. EPMA data of sulfides in the Dzuunmod gold area. The '-' indicates the below detection limit.

Sample	Fe	Co	Ni	Cu	S	Ag	Pb	Au	Mo	Bi	Sb	Zn	As	Total
Gatsuurt														
GT-49	35.40	0.03	-	-	22.46	0.03	0.07	0.01	0.22	-	0.01	0.04	41.10	99.36
	35.14	0.04	-	-	22.37	0.01	-	0.03	0.22	-	0.01	0.03	40.99	98.83
	0.04	-	-	-	13.26	-	85.92	-	-	-	-	0.11	-	99.33
	0.46	-	-	-	32.91	-	-	-	0.36	-	-	64.78	-	98.52
	35.70	0.06	-	-	22.78	0.01	-	0.10	0.19	-	0.06	0.02	40.47	99.39
	35.57	0.07	0.03	-	22.89	0.03	0.07	0.09	0.22	-	0.03	-	40.47	99.46
	35.42	0.02	0.00	0.05	22.71	0.01	0.02	0.03	0.21	-	0.01	0.02	41.01	99.50
	35.59	0.01	0.03	0.03	22.88	-	0.07	-	0.15	-	-	0.10	40.28	99.14
	35.86	0.03	-	-	22.52	0.02	-	0.04	0.19	-	-	-	40.99	99.64
	35.09	0.02	-	-	21.57	0.01	0.06	0.12	0.16	-	0.04	0.01	42.24	99.30
	35.06	0.03	0.05	-	22.31	0.03	-	0.08	0.21	-	-	-	41.15	98.91
	35.05	0.03	-	0.02	22.03	-	-	0.03	0.19	-	-	0.02	41.59	98.96
	35.27	0.14	0.23	-	23.56	0.02	-	0.07	0.19	-	0.05	0.01	39.74	99.27
	35.15	0.05	0.09	0.01	21.47	-	-	-	0.22	-	-	-	42.53	99.52
GT-189	36.00	0.05	0.01	-	23.55	-	0.01	0.01	0.16	-	-	-	40.23	100.0
	35.87	0.06	0.01	0.02	23.43	-	0.01	0.03	0.20	0.01	0.03	0.01	40.31	99.98
	45.69	0.08	-	0.05	52.30	0.02	-	-	0.45	-	-	0.01	1.16	99.76
	35.83	0.05	0.02	0.00	23.53	0.01	0.03	-	0.18	-	0.00	-	39.98	99.62
	36.42	0.04	0.00	0.04	23.96	0.02	-	-	0.22	-	0.02	-	39.50	100.2
	45.86	0.05	-	0.04	52.79	-	-	-	0.47	-	0.01	-	0.67	99.88
	36.00	0.04	-	-	23.58	-	0.02	-	0.19	-	-	0.00	39.98	99.80
	36.09	0.05	0.02	-	23.67	-	0.04	0.00	0.25	-	0.03	0.05	39.76	99.96
	35.81	0.01	-	0.03	24.01	0.01	-	0.11	0.22	-	0.05	0.03	39.43	99.69
	45.38	0.08	0.04	0.01	52.15	-	-	-	0.47	-	0.01	0.07	0.98	99.17
	45.34	0.03	-	0.02	52.26	-	-	-	0.41	-	-	0.04	0.60	98.69
	45.90	0.04	-	0.03	53.32	0.02	-	-	0.42	-	-	0.04	-	99.77
	46.25	0.06	-	-	52.12	-	-	0.09	0.47	-	-	0.03	0.76	99.78
	45.67	0.02	0.04	0.02	52.85	0.01	-	-	0.46	-	0.01	0.02	0.57	99.67
	45.69	0.05	-	0.01	51.79	-	-	-	0.37	-	-	-	1.12	99.02
	46.01	0.03	0.00	0.00	52.61	0.01	-	-	0.42	-	-	-	0.56	99.65
	36.03	0.08	-	0.03	23.57	0.02	0.01	0.10	0.18	-	-	-	39.91	99.93
	36.13	0.03	0.01	-	23.31	-	-	0.03	0.20	-	0.02	0.03	40.06	99.83
	35.52	0.04	-	0.03	22.68	-	0.00	-	0.15	-	0.01	0.01	41.10	99.53
	35.96	0.04	-	0.00	23.11	0.00	0.01	0.03	0.21	-	-	-	40.46	99.83
	45.77	0.06	-	0.05	51.81	-	-	-	0.52	-	0.01	-	1.47	99.68
	35.68	0.06	-	-	22.52	-	-	-	0.20	-	0.01	0.08	41.47	100.0
	45.58	0.07	0.00	-	51.76	-	-	-	0.45	-	-	0.05	0.98	98.89
	35.66	0.03	-	-	23.43	0.01	-	-	0.24	-	0.01	-	39.85	99.22
	45.72	0.04	0.02	-	52.25	0.02	-	-	0.44	-	-	-	0.70	99.18
	35.92	0.02	0.02	-	22.63	-	-	0.01	0.18	-	-	0.05	41.21	100.1
GT-252	35.63	0.01	-	0.00	23.01	0.01	-	-	0.22	-	0.06	0.06	41.08	100.1
	35.74	0.04	-	-	22.97	0.02	-	-	0.17	-	-	-	41.40	100.3
	45.72	0.00	0.01	0.02	51.20	-	-	-	0.41	-	-	-	2.46	99.83
	45.31	0.02	-	0.04	51.37	-	-	-	0.43	-	0.03	0.03	2.25	99.48
	45.57	0.07	-	0.04	51.94	-	-	0.03	0.45	-	-	0.00	1.82	99.90
	45.55	0.07	-	0.01	51.49	0.02	0.00	0.03	0.43	-	-	-	1.96	99.56
	35.39	0.07	-	-	22.78	-	0.04	0.02	0.22	-	0.01	-	41.33	99.87
	45.01	0.03	-	0.02	51.68	0.02	-	-	0.44	-	-	-	2.24	99.45

Supplementary Table 2.1. *(Continued)*

Sample	Fe	Co	Ni	Cu	S	Ag	Pb	Au	Mo	Bi	Sb	Zn	As	Total
	45.02	0.09	0.07	0.01	51.35	-	-	0.02	0.54	-	-	0.02	3.10	100.2
	44.77	0.06	-	0.04	50.91	-	0.00	-	0.44	-	0.01	0.01	2.90	99.13
	45.04	0.04	0.01	-	50.99	-	-	0.00	0.45	-	0.01	-	3.00	99.54
	45.16	0.07	0.01	-	51.33	0.00	-	-	0.40	-	-	-	2.40	99.36
	45.08	0.06	0.01	0.01	50.60	-	-	-	0.48	-	-	-	3.00	99.23
	45.31	0.07	-	0.03	50.72	-	-	0.01	0.41	-	-	0.01	2.94	99.49
	35.50	0.05	-	-	22.41	-	0.01	0.04	0.18	0.02	0.02	0.01	41.58	99.83
	44.80	0.04	-	0.02	51.32	-	-	-	0.42	-	-	-	2.62	99.22
	44.88	0.04	-	0.02	51.32	-	-	-	0.40	-	0.01	-	2.07	98.73
	45.20	0.07	0.02	0.01	51.51	-	-	-	0.43	-	0.03	0.01	2.45	99.71
	45.22	0.06	-	-	51.30	0.00	-	-	0.45	-	0.01	-	2.09	99.13
	45.28	0.05	-	0.03	51.62	0.01	-	0.07	0.41	-	0.02	-	2.02	99.50
	34.97	0.04	0.03	-	22.07	0.02	0.03	-	0.17	-	0.05	-	42.01	99.39
	45.21	0.04	-	0.02	50.59	0.04	0.00	-	0.44	-	-	-	3.14	99.48
	45.48	0.05	0.03	0.01	51.28	-	-	-	0.41	-	0.01	0.06	2.32	99.66
	44.41	0.06	0.04	0.02	51.75	0.00	-	0.07	0.46	-	-	-	1.72	98.51
	44.94	0.01	0.01	-	51.08	0.01	-	-	0.44	-	0.04	-	2.96	99.49
	45.42	0.01	0.01	0.00	51.18	0.01	-	-	0.46	-	0.02	-	2.79	99.89
	45.58	0.03	-	0.01	51.76	0.01	-	0.06	0.44	-	0.02	0.04	1.84	99.79
	35.73	0.04	-	-	23.09	0.00	-	0.03	0.20	-	-	0.01	41.05	100.2
	45.46	0.02	-	0.00	51.50	-	-	0.03	0.42	-	0.02	0.03	1.71	99.19
	45.55	0.03	0.01	-	51.72	0.01	0.00	-	0.47	-	0.01	-	1.71	99.51
	43.64	0.68	0.02	0.02	49.39	-	-	0.06	0.43	-	0.02	-	5.38	99.64
	35.30	0.03	-	0.06	22.40	0.03	-	0.07	0.17	-	0.06	-	41.61	99.74
	44.17	0.06	-	-	49.62	0.01	0.03	0.01	0.39	-	0.07	-	5.87	100.2
	44.97	0.10	0.04	0.03	51.85	0.02	-	-	0.46	-	0.02	-	1.51	98.99
	46.15	0.03	0.01	0.00	53.17	0.01	-	0.00	0.52	-	0.00	0.07	-	99.96
	46.06	0.07	-	0.02	53.21	0.01	-	0.01	0.54	-	0.02	0.00	-	99.94
	45.98	0.08	0.01	-	53.18	-	-	-	0.40	-	0.04	0.08	0.18	99.95
	45.25	0.03	-	-	51.25	0.01	-	0.03	0.47	-	-	0.09	2.92	100.1
GT-408	45.67	0.09	0.03	0.01	52.23	0.01	-	-	0.48	-	-	-	1.17	99.69
	45.82	0.04	-	0.02	52.88	-	-	-	0.44	-	-	0.01	0.09	99.29
	45.31	0.05	0.03	-	50.91	-	-	-	0.40	-	-	0.05	2.18	98.93
	45.78	0.06	0.01	-	51.42	0.04	-	-	0.45	-	-	-	1.43	99.19
	45.77	0.05	-	-	51.57	0.03	-	-	0.42	-	0.01	0.03	1.39	99.26
	45.54	0.06	-	0.03	51.02	0.02	0.02	0.01	0.44	-	-	-	1.50	98.63
	45.74	0.04	-	-	51.65	0.00	-	-	0.43	-	-	0.02	1.06	98.95
	35.79	0.03	0.02	0.05	22.91	0.02	-	-	0.21	-	0.02	0.01	40.19	99.25
	35.67	0.06	0.03	-	22.93	-	0.11	0.03	0.12	-	0.07	0.02	40.62	99.66
	45.18	0.06	0.01	0.01	51.83	0.01	-	-	0.48	-	0.04	-	1.32	98.94
	35.77	0.05	-	-	23.48	0.02	0.01	0.06	0.22	-	-	-	40.18	99.77
	45.35	0.04	-	0.05	51.67	-	-	-	0.46	-	0.03	-	1.95	99.54
	35.05	0.02	-	-	22.84	0.01	-	0.04	0.18	-	0.02	-	40.44	98.59
	45.25	0.04	-	-	51.79	-	-	0.03	0.48	-	-	0.02	1.30	98.91
	45.45	0.03	-	-	51.83	0.00	-	-	0.42	-	0.00	-	1.31	99.04
	45.13	0.05	-	0.00	50.99	0.00	-	0.01	0.39	-	0.02	-	2.74	99.33
	45.65	0.05	-	0.01	52.02	-	-	-	0.43	-	0.01	0.00	0.60	98.76
	45.74	0.02	-	0.01	51.78	-	-	-	0.50	-	-	-	1.29	99.33
	45.79	0.05	-	-	52.63	-	0.03	0.02	0.48	-	0.03	-	0.21	99.24
	45.88	0.04	0.04	-	53.05	-	-	-	0.46	-	-	-	0.92	100.4
	38.44	0.05	0.00	0.02	31.28	0.02	-	0.01	0.23	-	0.00	0.02	30.42	100.5

Supplementary Table 2.1. *(Continued)*

Sample	Fe	Co	Ni	Cu	S	Ag	Pb	Au	Mo	Bi	Sb	Zn	As	Total
	45.15	0.05	0.02	0.03	51.42	-	-	0.04	0.49	-	-	-	1.94	99.14
	45.49	0.05	0.01	-	52.14	0.02	0.11	-	0.43	-	0.02	0.05	1.37	99.68
	45.38	0.04	0.03	-	53.01	-	0.01	0.06	0.46	-	-	0.06	0.67	99.70
	45.10	0.03	-	0.00	51.65	-	0.02	0.01	0.41	-	0.01	0.06	1.64	98.92
	45.91	0.07	-	-	52.51	-	-	-	0.46	-	0.03	-	0.57	99.54
	45.90	0.02	0.01	0.06	52.58	-	0.03	0.00	0.48	-	-	-	1.37	100.4
	45.99	0.04	-	0.02	52.61	-	-	-	0.48	-	-	-	0.70	99.83
	45.66	0.05	0.00	0.01	51.63	0.01	-	-	0.44	-	-	-	1.83	99.63
	45.07	0.03	-	0.03	51.27	-	0.01	-	0.40	-	-	-	2.29	99.10
	45.81	0.11	0.01	0.01	52.52	0.03	-	-	0.45	-	-	-	0.80	99.72
	46.02	0.06	-	-	52.67	-	-	0.03	0.43	-	-	0.01	0.50	99.73
	45.44	0.01	0.00	0.07	51.53	0.02	-	-	0.42	-	-	-	1.81	99.29
	45.48	0.03	0.00	-	52.71	-	-	-	0.42	-	-	-	0.64	99.28
	45.82	0.03	0.00	-	52.18	0.03	-	-	0.41	-	-	-	1.08	99.55
GT-461	44.99	0.09	0.01	0.05	52.49	-	0.00	0.02	0.47	-	0.03	-	0.79	98.95
	0.10	0.02	-	0.01	13.21	-	85.46	-	-	-	-	0.01	-	98.81
	44.50	0.09	-	0.01	52.28	0.01	0.01	0.02	0.43	-	-	0.03	1.55	98.94
GT-172	45.95	0.05	-	0.01	52.80	0.01	-	0.04	0.42	-	0.01	-	1.17	100.4
	45.02	0.07	0.08	0.04	52.12	0.02	-	0.01	0.46	-	-	0.02	1.74	99.58
	35.65	0.05	0.02	0.01	22.69	-	-	0.07	0.17	-	0.00	-	41.47	100.1
	35.54	0.02	-	0.04	23.09	0.01	0.01	0.01	0.25	-	0.00	0.02	40.56	99.55
	35.25	0.05	0.16	0.02	22.66	0.01	-	0.02	0.21	-	0.00	-	41.02	99.40
GT-372	35.75	0.05	-	0.04	22.62	-	-	0.07	0.16	-	0.01	-	40.75	99.44
	35.49	0.02	-	-	22.64	-	0.03	-	0.20	-	0.00	-	40.90	99.27
	35.97	0.04	0.01	0.00	22.28	0.03	0.01	0.07	0.18	-	-	0.02	41.19	99.80
	35.83	0.04	-	-	22.57	0.00	-	-	0.24	-	0.03	-	41.10	99.81
	35.83	0.06	-	0.03	22.31	0.01	-	-	0.18	-	0.01	0.04	40.89	99.35
	35.29	0.02	0.02	0.01	22.44	-	-	0.04	0.17	-	-	-	41.42	99.40
	35.25	0.03	-	-	22.20	-	-	-	0.25	-	-	0.01	41.54	99.27
	35.96	0.05	0.00	-	22.99	-	-	0.01	0.16	-	0.05	-	41.06	100.3
	35.54	0.05	-	0.01	22.68	0.02	0.02	0.05	0.20	-	0.04	-	40.94	99.53
	35.63	0.07	0.01	-	22.37	0.03	0.05	0.00	0.23	-	0.05	-	41.30	99.75
	35.70	0.02	-	0.05	22.98	-	-	-	0.18	-	-	0.01	40.52	99.44
	35.52	0.28	-	0.02	23.08	-	0.05	0.06	0.24	-	0.00	-	41.28	100.5
	35.23	0.01	0.01	-	22.86	-	-	0.10	0.22	-	0.00	0.01	41.01	99.46
	35.69	0.03	-	-	22.92	-	0.02	0.02	0.21	-	-	-	41.15	100.0
	35.63	0.05	0.00	0.04	22.79	-	-	0.05	0.17	-	0.00	0.02	41.22	99.96
	35.51	0.05	-	0.02	23.15	0.01	-	0.11	0.16	0.00	0.01	0.06	41.25	100.3
	35.57	0.02	-	0.00	22.58	-	-	-	0.13	-	-	0.01	41.12	99.43
	35.94	0.04	-	-	23.07	-	-	0.06	0.20	-	-	0.01	40.99	100.3
	35.88	0.01	-	-	22.54	0.06	-	-	0.22	-	-	0.02	41.52	100.2
	35.52	0.01	0.00	-	22.65	0.01	0.07	0.06	0.20	-	0.05	0.02	41.17	99.77
	35.67	0.04	-	0.00	22.64	0.01	-	-	0.17	-	0.01	0.04	40.97	99.55
	35.55	0.02	-	-	22.77	-	-	0.04	0.19	-	0.02	0.03	41.49	100.1
	35.52	0.05	-	0.03	22.77	-	-	-	0.18	-	-	0.00	41.16	99.71
	35.37	0.07	-	-	22.09	-	-	-	0.14	-	0.01	-	42.25	99.93
	35.78	0.01	-	-	22.51	-	-	0.10	0.15	-	-	-	41.26	99.82
	35.62	0.02	-	-	22.70	0.01	0.03	-	0.19	-	0.02	0.03	41.27	99.88
	35.38	0.02	-	0.04	21.57	-	-	-	0.14	-	0.04	0.01	43.24	100.4
	35.51	0.02	-	-	22.34	0.01	-	-	0.21	-	0.02	-	41.42	99.53
	35.86	0.03	-	-	22.84	0.02	0.02	0.02	0.17	-	-	-	40.80	99.74
	35.63	0.03	-	0.05	22.48	-	-	-	0.17	-	-	-	41.11	99.47

Supplementary Table 2.1. *(Continued)*

Sample	Fe	Co	Ni	Cu	S	Ag	Pb	Au	Mo	Bi	Sb	Zn	As	Total
GT-462	45.24	0.05	0.00	0.01	52.37	0.00	-	0.02	0.42	-	0.01	0.02	1.75	99.89
	36.01	0.06	-	-	22.72	0.01	-	-	0.17	-	0.02	-	41.14	100.1
	36.10	0.03	0.01	-	22.65	-	-	0.03	0.26	-	-	-	41.44	100.5
	35.80	0.02	-	-	22.99	0.02	-	0.05	0.21	-	0.00	0.02	40.70	99.80
	35.42	0.05	0.01	-	23.23	-	-	0.02	0.19	-	0.01	0.06	40.86	99.84
	36.03	0.05	-	-	22.84	0.02	0.08	0.03	0.28	-	-	-	40.89	100.2
Sujigtei														
SJ-006	46.05	0.04	0.01	-	52.99	-	-	-	0.52	-	-	-	-	99.61
	45.63	0.05	0.03	-	53.23	-	-	0.07	0.55	-	-	-	0.05	99.60
	46.06	0.06	0.03	-	53.34	0.05	-	-	0.43	-	-	0.01	0.16	100.1
	46.09	0.07	0.03	-	53.45	0.01	-	-	0.42	-	-	-	0.17	100.2
	46.05	0.03	-	0.02	53.56	0.03	0.00	-	0.46	-	-	-	-	100.1
	45.86	0.03	0.03	0.02	53.41	-	-	0.03	0.44	-	0.01	0.04	-	99.85
	46.23	0.07	-	-	53.18	-	-	-	0.43	-	-	-	0.52	100.4
	46.13	-	-	-	52.82	-	0.01	-	0.42	-	0.00	-	0.24	99.60
	45.90	0.02	-	-	52.97	-	0.01	0.05	0.48	-	0.01	0.01	0.13	99.56
	45.90	0.05	0.01	0.06	52.69	0.01	-	-	0.44	-	0.00	0.04	0.48	99.66
	46.27	0.04	0.00	-	52.88	0.01	-	-	0.48	-	-	0.03	0.34	100.0
	45.99	0.05	0.01	-	53.33	-	-	0.01	0.52	-	-	-	0.17	100.1
	46.28	0.03	-	0.02	53.32	-	-	-	0.48	-	-	0.07	0.09	100.3
	46.22	0.06	-	0.01	53.09	-	-	0.04	0.45	-	-	0.01	0.05	99.93
	46.32	0.02	-	-	53.12	0.02	-	-	0.45	-	0.02	0.02	0.11	100.1
	46.44	0.05	-	0.02	53.23	0.01	-	0.01	0.40	-	0.02	0.03	0.26	100.5
	46.39	0.07	-	-	53.36	0.02	-	-	0.50	-	-	-	-	100.3
	46.43	0.05	-	0.03	53.49	-	-	0.05	0.43	-	-	0.00	0.02	100.5
	46.35	0.07	0.02	-	52.97	0.02	-	-	0.50	-	0.00	-	0.37	100.3
	46.26	0.08	-	-	52.74	-	0.01	-	0.44	-	0.01	-	-	99.53
	46.22	0.03	-	-	53.22	0.00	-	-	0.46	-	-	-	0.26	100.2
	46.59	0.03	0.01	-	53.80	-	-	0.13	0.44	-	-	-	-	101.0
SJ-008	45.51	0.08	-	0.03	52.76	0.01	0.02	-	0.49	-	0.01	0.18	-	99.07
	46.30	0.04	-	0.00	52.58	-	-	-	0.43	-	-	-	-	99.35
	45.45	0.06	-	0.00	52.66	-	-	-	0.43	-	-	-	-	98.60
	0.00	-	-	0.04	13.48	-	86.86	-	-	-	-	0.03	-	100.4
	1.37	0.02	-	37.51	25.27	0.02	-	0.00	0.22	-	28.85	6.03	0.87	100.2
	45.93	0.07	-	-	53.68	0.02	-	-	0.43	-	-	0.14	0.08	100.3
	46.06	0.03	0.01	0.01	53.79	-	-	-	0.53	-	0.04	-	-	100.5
Ereen														
ER-10/1	46.19	0.05	0.01	0.01	53.56	0.00	-	0.04	0.44	-	0.01	-	0.11	100.4
	45.48	0.07	-	0.04	52.92	-	-	-	0.40	-	0.01	0.03	0.85	99.80
	45.71	0.06	-	-	53.30	-	-	0.02	0.43	-	-	-	0.19	99.71
	45.68	0.06	0.01	0.04	52.79	-	-	-	0.49	-	-	-	0.84	99.91
	45.86	0.06	0.01	0.01	52.93	-	-	-	0.52	-	-	-	0.70	100.1
	44.62	0.03	-	0.03	51.69	0.02	-	-	0.43	-	-	0.10	1.73	98.64
	45.61	0.02	-	0.03	53.03	-	-	-	0.41	-	-	-	0.51	99.61
Boroo														
BR-P-6	35.94	0.03	0.01	-	22.26	-	-	0.06	0.16	-	0.04	0.00	41.91	100.4
	35.07	0.09	0.08	-	21.12	0.01	-	-	0.22	-	0.01	0.02	43.29	99.92
	35.30	0.03	-	-	21.99	-	0.01	-	0.16	-	-	0.01	41.58	99.07
	35.02	0.05	-	-	21.41	-	0.02	0.02	0.19	-	0.03	-	43.17	99.90
	35.39	0.05	0.05	0.05	21.87	-	-	-	0.14	-	0.01	-	41.38	98.94
	45.23	0.09	0.00	0.03	51.34	0.02	-	-	0.48	-	0.01	0.04	1.83	99.07
	35.43	0.03	-	-	22.43	-	0.04	0.07	0.16	-	0.13	0.01	41.42	99.62

Supplementary Table 2.1. *(Continued)*

Sample	Fe	Co	Ni	Cu	S	Ag	Pb	Au	Mo	Bi	Sb	Zn	As	Total
	45.47	0.02	0.02	0.05	52.18	0.02	-	0.03	0.47	-	-	-	1.61	99.86
	35.41	0.03	-	0.03	22.64	-	-	0.01	0.18	-	-	-	41.63	99.93
	45.76	0.07	-	0.02	52.28	-	-	0.02	0.38	-	-	0.01	0.88	99.41
	45.33	0.03	-	0.01	51.71	-	-	0.06	0.40	-	0.02	-	2.70	100.3
	45.36	0.05	0.01	0.02	52.19	-	-	0.03	0.42	-	0.01	-	0.99	99.06
	35.79	0.05	0.03	0.01	22.21	-	0.02	0.05	0.18	-	-	0.02	41.77	100.1
	35.73	0.01	0.02	-	23.00	-	0.01	0.08	0.20	-	0.00	-	40.98	100.0
	35.58	0.04	-	-	22.54	0.02	0.02	-	0.23	-	-	-	41.23	99.66
	35.23	0.03	0.06	0.04	22.03	0.00	-	0.05	0.22	-	0.01	-	42.51	100.2
	34.74	0.04	0.02	0.03	21.82	-	-	-	0.15	-	0.01	0.02	42.45	99.29
	45.25	0.06	0.02	0.02	51.82	-	-	0.00	0.49	-	-	-	1.23	98.90
	35.19	0.05	-	-	22.40	0.01	-	0.10	0.21	-	-	0.06	41.66	99.67
	35.77	0.04	-	0.05	22.89	0.00	0.02	0.08	0.15	-	0.04	0.04	40.59	99.67
	45.49	0.05	0.02	0.02	51.49	0.05	0.03	-	0.44	-	0.03	-	1.10	98.72
	35.42	0.10	0.13	0.04	22.22	-	-	0.06	0.20	-	0.02	-	41.71	99.90
	35.39	0.03	-	0.04	23.20	-	-	0.04	0.22	-	-	-	40.38	99.29
	35.58	0.02	-	0.03	23.08	0.00	-	0.07	0.17	-	0.00	0.03	40.78	99.77
	35.50	0.03	0.01	-	22.14	-	0.00	-	0.19	-	0.02	-	42.00	99.90
	45.24	0.03	0.06	0.01	52.12	0.02	-	-	0.43	-	-	-	1.09	99.02
	45.28	0.06	0.02	-	52.25	-	-	-	0.37	-	0.04	-	1.02	99.03
	45.25	0.04	-	0.04	51.22	-	0.01	0.01	0.43	-	0.03	0.01	2.08	99.11
	35.93	0.05	0.01	0.03	23.16	-	0.04	0.00	0.20	-	-	-	40.88	100.3
	45.58	0.04	0.00	0.04	51.93	0.02	-	-	0.37	-	-	0.02	0.95	98.95
	45.64	0.04	-	0.02	51.43	-	-	0.02	0.41	-	0.02	-	1.03	98.59
	45.40	0.09	-	0.02	51.95	-	-	-	0.48	-	0.01	-	0.73	98.68
	45.27	0.04	0.00	-	51.32	0.01	-	-	0.48	-	0.03	0.02	1.63	98.79
	45.24	0.05	-	0.03	51.22	0.02	-	0.03	0.47	-	-	0.05	1.66	98.76
	45.38	0.05	-	-	52.10	-	-	-	0.46	-	-	-	0.99	98.97
	45.15	0.05	0.01	0.06	51.86	0.02	-	-	0.43	-	0.00	-	1.50	99.08
	45.18	0.06	-	0.03	51.61	0.02	-	-	0.48	-	-	-	1.47	98.86
	35.39	0.03	0.02	0.01	23.05	-	-	-	0.18	-	-	-	40.80	99.49
	45.33	0.05	0.02	0.06	51.71	0.00	-	-	0.43	-	-	-	1.20	98.80
	34.27	0.01	-	-	21.65	-	0.00	-	0.20	-	0.02	0.01	43.27	99.42
	35.47	-	0.01	0.00	22.59	-	-	0.01	0.24	-	-	0.03	41.46	99.82
Ulaanbulag														
UB-85	35.84	0.04	-	-	23.59	-	-	-	0.17	-	-	0.04	40.20	99.88
	35.52	0.04	0.03	-	23.40	0.01	-	0.03	0.19	-	0.00	-	40.56	99.79
	35.17	0.04	-	-	21.48	-	-	0.08	0.12	-	-	0.02	42.64	99.54
	35.52	0.04	-	-	22.61	-	-	0.18	0.20	-	-	-	40.89	99.43
	35.76	0.05	-	-	22.99	0.01	-	-	0.16	-	0.01	-	40.67	99.64
	35.91	0.05	-	-	23.26	-	-	0.01	0.18	-	-	0.02	40.17	99.60
	35.85	0.02	-	-	22.78	0.01	-	0.03	0.15	-	0.00	0.02	41.05	99.91
	35.68	0.05	-	-	23.56	-	-	0.05	0.24	-	0.00	0.02	40.12	99.72
	35.28	0.03	0.06	-	22.61	-	0.04	-	0.18	-	-	-	41.01	99.22
	35.90	0.01	-	-	22.63	0.04	0.02	0.03	0.19	-	-	-	41.19	100.0
	35.98	0.01	-	-	23.23	-	-	-	0.15	-	-	-	40.07	99.45
	36.11	0.07	-	-	23.35	0.02	-	-	0.18	-	0.01	-	40.29	100.0
	35.82	0.03	0.00	0.00	22.90	0.01	-	0.03	0.21	-	0.00	-	41.25	100.3
	35.97	0.05	0.01	0.01	23.47	-	0.05	-	0.22	-	-	-	40.50	100.3
	36.19	0.02	0.01	0.00	23.08	-	-	-	0.17	-	0.02	0.00	40.78	100.3
	35.36	0.05	-	0.01	22.63	0.00	-	0.06	0.18	-	0.00	0.02	41.31	99.62

Supplementary Table 2.1. *(Continued)*

Sample	Fe	Co	Ni	Cu	S	Ag	Pb	Au	Mo	Bi	Sb	Zn	As	Total
Balj														
BAL-02	45.61	0.02	0.03	-	52.65	0.02	-	0.09	0.46	-	0.01	0.01	1.37	100.3
	45.19	0.01	-	0.04	52.92	0.00	-	0.05	0.47	-	0.03	-	1.43	100.1
	45.12	0.07	0.04	-	52.41	-	-	-	0.42	-	0.01	0.03	2.36	100.5
	45.11	0.05	-	0.01	52.35	-	0.00	-	0.46	-	0.01	-	1.64	99.63
	45.15	0.07	0.05	0.01	53.42	-	-	0.03	0.46	-	-	0.04	0.44	99.66
	45.64	0.05	0.01	0.01	53.46	-	-	-	0.46	-	-	-	0.23	99.87
	45.33	0.05	-	0.01	52.65	0.00	-	-	0.42	-	-	-	1.60	100.1
Biluut														
Bi-07	35.60	0.05	-	0.00	22.50	0.01	-	0.05	0.17	-	0.04	0.05	41.51	99.97
	34.82	0.05	-	-	21.15	-	-	-	0.23	-	0.01	0.01	43.12	99.38
	35.25	0.03	-	-	22.44	0.02	-	-	0.19	-	0.07	0.03	41.61	99.63
	34.49	0.03	-	-	21.78	-	0.02	0.00	0.19	-	0.04	-	42.27	98.81
	34.64	0.03	0.01	-	21.53	-	-	-	0.26	-	0.03	-	42.17	98.68
	34.47	0.03	-	-	21.47	0.01	0.02	0.12	0.23	-	0.03	0.00	42.58	98.96
	34.63	-	0.01	0.02	21.95	-	0.00	-	0.17	-	0.05	0.05	42.10	98.98
	35.22	0.04	-	0.02	22.02	-	-	0.03	0.19	-	-	0.02	42.23	99.78
	35.35	0.07	0.02	-	22.19	0.02	0.10	-	0.20	-	0.05	0.04	41.93	99.97
	34.69	0.03	0.01	0.02	22.08	-	-	-	0.19	-	0.06	-	41.76	98.85
	45.43	0.03	-	0.04	53.50	0.02	-	0.03	0.56	-	0.00	0.03	-	99.64
	45.14	0.10	-	-	52.83	0.00	-	-	0.52	-	0.01	-	-	98.61
	45.23	0.06	-	0.05	53.23	0.01	0.12	-	0.51	-	0.09	0.03	0.01	99.34
	35.49	0.00	-	-	22.56	0.01	-	-	0.18	-	0.05	0.01	41.18	99.48
	34.09	0.04	0.01	-	21.97	-	0.02	0.10	0.19	-	0.03	-	42.15	98.60
	45.50	0.02	-	0.02	53.64	0.03	-	0.02	0.46	-	-	0.08	-	99.77

Concluding Remarks

In this Ph.D. thesis, I reported the geological, mineralogical and stable isotope geochemical characteristics of the Erdenetiin Ovoo porphyry Cu-Mo deposit and the Dzuunmod orogenic gold deposits in northern Mongolia to understand the ore genesis and sources. These deposits were chosen for this study due to (1) a representative ore deposit type for Cu and Au, (2) many interesting geological issues and (3) high potential for Cu and Au resources.

In chapter 1, the $\delta^{65}Cu$ values of the Cu ore minerals from the Erdenetiin Ovoo porphyry Cu-Mo deposit (-1.01 ‰ to 10.0 ‰) were measured to trace the Cu sources and understand the Cu isotope fractionation during mineralization processes. The $\delta^{65}Cu$ values of the Cu sulfide minerals (0.14 ‰ to 2.69 ‰) indicate a magmatic source as the Cu origin and little effect of Cu isotope fractionation during formation of secondary Cu sulfide minerals. This is considered to be attributed to marge mass transportation and/or the involvement of biogenic activities. The positive $\Delta_{Cu\ (II)\ mineral\ -\ Cu\ (I)\ mineral}$ values in the study area indicate that an approximate mass balance is satisfied and that quick redox reactions did not allow sufficient time for Cu transport. The $\delta^{34}S$ values of the primary sulfide minerals range from -2 ‰ to 1.3 ‰, with an average value of -0.1 ‰, indicating that sulfur is mainly originated from the homogeneous magmatic source. By contrast, the slightly lower $\delta^{34}S$ values of the secondary sulfide minerals show a wider and more negative range from -3.2 ‰ to -0.3 ‰ with an average of -1.6 ‰. This is regarded as the result of either S isotope fractionation processes or input of sulfur species with different S isotope compositions. The little gap of $\delta^{65}Cu$ values between primary and secondary Cu sulfide minerals and the positive $\Delta_{Cu\ (II)\ mineral\ -\ Cu\ (I)\ mineral}$ values indicate the signals of

insignificant Cu transport in the study area. It is suggested that little possibility of the formation of an exotic Cu occurrence in the Erdenetiin Ovoo porphyry Cu-Mo deposit.

In chapter 2, geological, mineralogical and geochemical characteristics of the orogenic gold deposits and occurrences were studied to understand the deposit formation processes and trace the sources of sulfur and ore-forming fluid. The deposits such as Gatsuurt, Boroo, Ereen, Sujigtei, and Khargana and occurrecnes such as Biluut and Balj represent the similar host rocks (metasedimentary rocks, volcanic rocks and granitoids complex), alteration types associated with gold mineralization (sericitic, potassic and siliceous) and major ore mineralogy (pyrite, arsenopyrite and gold). This implies that they were formed by consistent ore-forming processes with similar sulfur and fluid sources. The large variation of the $\delta^{34}S$ values from -2.6 ‰ to 17.2 ‰ indicates the heterogeneous sulfur isotope composition of its sources. Because the Fe-sulfidation cannot cause a significant sulfur isotope fractionation during mineralization processes and there is no outcrops of sulfate-bearing rocks in the deposit area, a sediment-hosted pyrite incorporated into hydrothermal fluid during metamorphic event is most plausible sulfur source. The measured $\delta^{18}O_{quartz}$ values (from 14.7 ‰ to 17.7 ‰) and the calculated $\delta^{18}O_{water}$ values indicate metamorphic derivation of ore-forming fluids. Based on these results, the gold deposits in the Dzuunmod area can be classified into orogenic gold type where fluid and sulfur was derived from a metamorphic source. Hydrothermal fluid produced during metamorphic event was migrated to the Dzuunmod area through the NE-trending fault and multiple mineralization processes occurred by the sulfidation of host rocks and mixing of ore-forming fluids.